Balanced Multiresolution in Multilevel Focus+Context Visualization

Hasan, Mahmudul

Hasan, M. (2018). Balanced Multiresolution in Multilevel Focus+Context Visualization (Unpublished doctoral thesis). University of Calgary, Calgary, AB. doi:10.11575/PRISM/32845
http://hdl.handle.net/1880/107665
doctoral thesis

UNIVERSITY OF CALGARY

Balanced Multiresolution in Multilevel Focus+Context Visualization

by

Mahmudul Hasan

A THESIS

SUBMITTED TO THE FACULTY OF GRADUATE STUDIES

IN PARTIAL FULFILLMENT OF THE REQUIREMENTS FOR THE

DEGREE OF DOCTOR OF PHILOSOPHY

GRADUATE PROGRAM IN COMPUTER SCIENCE

CALGARY, ALBERTA

AUGUST, 2018

Abstract

Given a set of symmetric/antisymmetric filter vectors containing only regular multiresolution filters, the method we present in this thesis can establish a balanced multiresolution (BMR) scheme for images, allowing their balanced decomposition and subsequent perfect reconstruction without the use of any extraordinary boundary filters. We define balanced multiresolution such that it allows balanced decomposition i.e. decomposition of a high-resolution image into a low-resolution image and corresponding details of equal size. Several applications of such a decomposition result in a balanced wavelet transform (BWT) that makes on-demand reconstruction of regions of interest (ROIs) efficient in both computational load and implementation aspects. We find such decomposition and perfect reconstruction based on an appropriate combination of symmetric/antisymmetric extensions near the image and detail boundaries. In our method, exploiting such extensions correlates to performing sample (pixel/voxel) split operations. We demonstrate our general approach for some commonly used symmetric/antisymmetric multiresolution filters. We also show the application of such a balanced multiresolution scheme in constructing an interactive multilevel focus+context visualization framework for the navigation and exploration of large-scale 2D and 3D images.

Typically, the given filters are floating-point values, so our BWTs reversibly map integers to floating-point i.e. real values. We extend our balanced multiresolution framework further to construct reversible integer-to-integer BWTs from a given symmetric/antisymmetric decomposition filter vector of width less or equal to four. In our approach, we adjust the linear combination of fine samples suggested by the given decomposition vector using optimal sample split operations in combination with a rounding operation. Such adjustments translate an affine integer combination of fine samples to obtain an integer coarse sample, which closely approximates the floating-point coarse sample suggested by the given decomposition filter vector. The associated translation vectors give us the detail samples. Furthermore, when

necessary, we construct every other detail sample differently in order to ensure local perfect reconstruction. Compared to their integer-to-real counterparts, the resulting reversible integer-to-integer BWTs occupy less memory, offer better compressibility, and do not require sample quantization for rendering purposes.

Acknowledgements

First and foremost, I would like to express my honest gratitude to my supervisor, Prof. Faramarz Samavati for his instrumental mentorship and tremendous support throughout the entire duration of my doctoral study. The work presented in this thesis is predominantly inspired by the numerous brainstorming sessions I held with Prof. Samavati, in which he shared his invaluable insights, innovative ideas, and constructively critical feedback. Additionally, I am immensely thankful for the professional development opportunities he helped me avail during the course of my doctoral study in the Graphics Jungle Lab.

I would also like to thank my co-supervisor, Prof. Mario Costa Sousa, and supervisory committee members, Prof. Christian Jacob and Prof. Marina Gavrilova for their insightful feedback in improving the quality of the work presented in this thesis. My special thanks go to Prof. Lisa Higham and Prof. Jalal Kawash for their mentorship that greatly improved my teaching, communication, and leadership skills.

Furthermore, I am profoundly grateful to my wife, Shahnewaz A. Jolly, and my parents, Anowara Begum and Muhammad A. Mannan, for their unconditional support and encouragement throughout my entire graduate student life and most importantly, to never stop believing in me, even during my darkest hours.

Last but not the least, I would like to extend my sincere appreciation to my fellow labmates – Dr. Javad Sadeghi, Dr. Luke Olsen, Dr. Ali Mahdavi-Amiri, Dr. Adam Runions, Dr. Elisa Amorim, Dr. Ronan Amorim, Troy Alderson, Erika Harrison, Mark Sherlock, and Jeffrey Packer to name a few, for being there to patiently attend my research presentations, often review my research manuscripts, and provide their useful feedback.

This thesis is dedicated to the four people who kept me going even when I felt like giving up –

my best friend and beloved wife, Shahnewaz Jolly;

my uncompromisingly supportive parents, Anowara Begum and Muhammad Mannan;

and my exceptionally knowledgeable and kind supervisor, Prof. Faramarz Samavati.

Table of Contents

List of Tables

List of Figures and Illustrations

List of Acronyms

Acronym	Elaboration
BIWT	Balanced Integer Wavelet Transform
BMR	Balanced Multiresolution
BWT	Balanced Wavelet Transform
DE	Digital Earth
DGGS	Discrete Global Grid System
ELASF	Even-Length Analysis/Synthesis Filter
FPS	Frames Per Second
GPU	Graphics Processing Unit
GRITIT	Generalized Reversible Integer-to-Integer Transform
LC-RS	Left-Child Right-Sibling
OLASF	Odd-Length Analysis/Synthesis Filter
ORT	Overlapping Rounding Transform
ROI	Region of Interest
S	Sequential
S+P	Sequential plus Prediction
WTSP	Wavelet-based Time-Space Partitioning

Chapter 1

Introduction

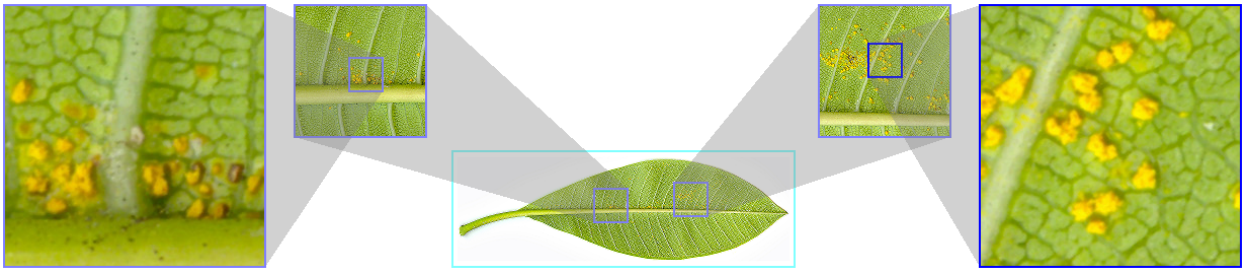

Figure 1.1: Multilevel focus+context visualization of a Plumeria rubra leaf with frangipani rust. Source image dimensions: 10496×3328.

The continuous growth of 2D/3D image size in various application domains and the prolific use of handheld devices mandate the ability to visualize and explore large-scale images within the physical and ergonomic limitations of the screen space available on such devices. To address this issue, we present a multilevel focus+context visualization framework for large-scale 2D and 3D images. The advantages of such a visualization framework are manifold. It allows for more manageable utilization of screen space by the creation of a multilevel visualization hierarchy. In such a multilevel hierarchy, enlarged *regions of interest* (ROIs) can also serve as contexts to further increase the depth of the hierarchy, if required (see Fig. 1.1; data source: S. Fraser-Smith, Wikipedia; used under the Creative Commons Attribution 2.0 Generic license). Therefore, such a hierarchy permits the visualization of contexts with higher *degrees of interest* [CN02] in higher resolutions, while maintaining interactive frame rates. The ability to have multiple ROIs at different desired resolutions at the same or different levels of the visualization hierarchy also enables comparative analyses, highlighting their discontinuities, similarities, and relationships.

Such a visualization framework can be supported by a multiresolution approach, allowing different levels of detail of the data to be properly retrieved, scaled, and rendered at different

resolutions on demand. Wavelet transform representations can be exploited to produce coarse approximations of data while retaining the ability to recover the original data when more detail is desired. This can enhance the overall visualization throughput by removing excessive details unless required. Additionally, wavelet transformation ensures a linear runtime for decomposition and reconstruction with no additional storage requirements. In order to support the proposed visualization framework, we additionally present the construction of *balanced wavelet transforms* (BWTs) and *balanced integer wavelet transforms* (BIWTs) using our novel *balanced multiresolution* (BMR) framework.

The operations we specify for pixels in this thesis are readily applicable to voxels; so from this point forward, we generally refer to pixels and voxels as *samples*. In the next three sections, we introduce our balanced multiresolution and multilevel focus+context visualization frameworks while summarizing the contributions of this thesis.

1.1 Balanced Multiresolution

Context. Applications that facilitate multiscale 2D and 3D image visualization and exploration (see [LHJ99, WS05, SBO07], for example) benefit from multiresolution schemes that decompose high-resolution images into low-resolution approximations and corresponding *details* (usually, wavelet coefficients). Several subsequent applications of such a decomposition constructs the corresponding *wavelet transform*. This wavelet transform can then be used to derive low-resolution approximations of the entire image, as well as high-resolution approximations of a *region of interest* (ROI), on demand. Reconstructing the high-resolution approximation of a ROI involves locating the corresponding details from a hierarchy of details within the wavelet transform. One such hierarchy of details resulting from only two levels of decomposition of an Earth image (data source: Visible Earth, NASA) is shown in Fig. 1.2.

For the purpose of demonstration, we created the wavelet transform in Fig. 1.2 using the *short* filters of quadratic B-spline presented by Samavati *et al.* [SB04, SBO07]. In practice,

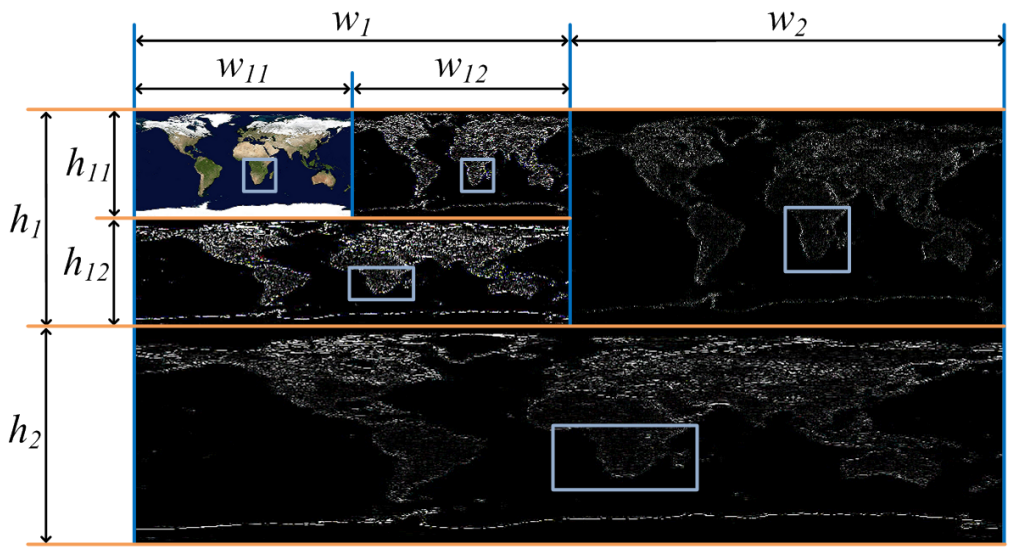

Figure 1.2: Hierarchy of details in a wavelet transform resulting from two levels of decomposition of a 1024×512 Earth image. The coarse image (at the top left corner) contains a rectangular ROI and the details corresponding to that ROI are enclosed by rectangles within all levels of details.

images that require multiscale visualization are larger in size and may require more levels of decomposition. For each level of decomposition in this particular example, the image was first decomposed heightwise and then widthwise.

Problem. Sequences of samples along each image dimension can be treated as finite-length signals. It is well-known that decomposition and reconstruction of finite-length signals require special treatments at the boundaries [AW03], which often involves the use of extraordinary boundary filters. The use of extraordinary boundary filters (as opposed to regular filters) for handling image and detail boundaries lead to irregular reconstruction near image boundaries.

From a hierarchy of details, such as the one in Fig. 1.2, if we need to reconstruct the high-resolution approximation of a ROI located in the low-resolution (coarse) image shown in the top-left rectangle in Fig. 1.2, we have to locate the corresponding details in some or all of the rectangles that contain details depending on the expected level of resolution. Locating these details will be straightforward if each of the heightwise and widthwise decomposition steps decomposes an image into two halves of equal size – one half corresponding to the coarse image and the other half corresponding to the details. Among B-spline wavelets, only the

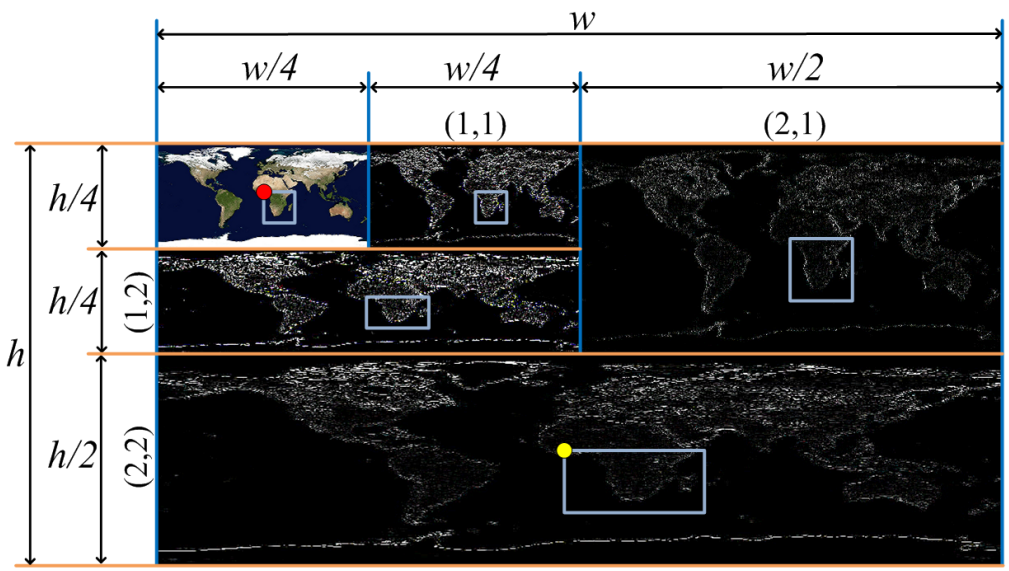

Figure 1.3: A ROI in a balanced wavelet transform after two levels of balanced decompositions of a 1024×512 Earth image is shown. The location of the coarse sample highlighted with a red circle at top-left corner of the ROI rectangle in the coarse image is denoted (x, y). Due to balanced decompositions, the detail rectangles (four here) corresponding to the ROI can be found with simple dyadic operations. For example, the location of the detail sample highlighted with a yellow circle at top-left corner of the detail rectangle corresponding to the ROI is $\left(2^l x, 2^{l-1}(h/4 + y)\right)$, where the level of resolution $l = 2$.

filters obtained from Haar wavelets provide such a balanced decomposition [Haa10, SDS96]. However, because Haar wavelets and the associated B-spline functions are not continuous, it would be beneficial to achieve such a balanced decomposition for the filters obtained from B-splines with higher continuity.

Existing multiresolution schemes for the local filters of second or higher order scaling functions and their wavelets (see [SBO07, CDF92, Dau92, Mey90], for example) result in unequal numbers of coarse and detail samples after decomposition (i.e. $w_1 \neq w_2, w_{11} \neq w_{12}, h_1 \neq h_2$, and $h_{11} \neq h_{12}$ in Fig. 1.2). Such inequalities resulting from decomposition make locating the details corresponding to a ROI for reconstruction a cumbersome task (which involves keeping track of level-wise offsets from boundaries), specially when an interactive multilevel visualization hierarchy (see Fig. 1.1, for example) is concerned. Creation of a such an interactive visualization hierarchy requires efficient on-demand access to details.

In contrast, balanced decompositions can construct BWTs, such as the one shown in

Fig. 1.3 (data source: Visible Earth, NASA). In Fig. 1.3, the rectangles containing different levels of details for the entire image are numbered with $(l, 1)$ tuples for widthwise and $(l, 2)$ tuples for heightwise decompositions, where l represents the level of resolution. Locating the details corresponding to a ROI on demand in a BWT includes a number of simple dyadic operations, which are known to perform significantly faster than non-dyadic operations in both hardware and software implementations. Such efficient access to details is demonstrated by means of an example in Fig. 1.3. In general, if $c_{x,y}$ is the coarse sample at the top-left corner of a ROI rectangle, then $d^{(l,1)}_{2^{l-1}(w_c+x),2^{l-1}y}$ and $d^{(l,2)}_{2^l x,2^{l-1}(h_c+y)}$ are the detail samples at the top-left corners of the detail rectangles corresponding to the ROI for widthwise and heightwise balanced decompositions, respectively. Here, $w_c \times h_c$, which is $\frac{w}{4} \times \frac{h}{4}$ in Fig. 1.3, is the resolution of the coarse image containing the ROI.

Proposed approach. In order to address the issues discussed above, in this thesis, we introduce a technique for devising *balanced multiresolution* (BMR) schemes for the local filters of second or higher order scaling functions and their wavelets. Our technique uses an appropriate combination of symmetric/antisymmetric extensions near the image and detail boundaries, which correlate to sample split operations. To guarantee a perfect (lossless) reconstruction without the use of any extraordinary boundary filters, our method requires each of the given decomposition and reconstruction filter vectors (kernels) to be either symmetric or antisymmetric about their centers. Many existing sets of local regular multiresolution filters, such as those associated with the B-spline wavelets [SBO07], biorthogonal and reverse biorthogonal wavelets [CDF92, Dau92], and Meyer wavelets [Mey90, Dau92], exhibit such symmetric/antisymmetric structures.

Contributions. We present a novel method to devise a BMR scheme for a given set of symmetric/antisymmetric multiresolution filter vectors containing regular filters. Devised BMR schemes allow balanced decomposition and perfect reconstruction without the use of extraordinary boundary filters. A BWT representation of an image resulting from balanced

decompositions provides straightforward and efficient access to previously extracted details corresponding to a ROI on demand. We also provide ready-to-use BMR schemes devised using our proposed method for eleven commonly used sets of symmetric/antisymmetric multiresolution filter vectors (see Table A.1).

1.2 Reversible Integer-to-Integer Balanced Wavelet Transform

Context and motivation. BMR schemes resulting from our BMR framework introduced in section 1.1 can efficiently support a framework for interactive multilevel focus+context visualization of large-scale 2D and 3D images that provides an effective technique for the navigation and exploration of such imagery within the ergonomic and physical confines of limited screen space. That visualization framework allows for improved visualization throughput by on-demand reconstruction of ROIs at desired resolutions from an underlying BWT. However, the underlying BWT constructed utilizing our BMR framework referred to in section 1.1 may occupy more memory compared to that of the original image, while containing the same number of samples. One desired property for a wavelet transform is to have its storage requirement not more than that of the original image [SBO07]. Our original BMR framework could not achieve this property when working with integer samples because the decomposition filters that are typically applied to the integer samples in images for the construction of BWTs are floating-point values. As a result, the constructed BWTs contain floating-point values that must be stored to ensure reversibility (i.e. perfect reconstruction). For instance, the BWT constructed from a 32-bit RGBA image will occupy sixteen bytes of per sample in single-precision floating-point format as opposed to just four bytes for that of the original image.

Therefore, as another goal for this thesis, we aim to construct reversible BWTs that map integers to integers. The samples in such *balanced integer wavelet transforms* (BIWTs) i.e. the transform coefficients can be stored occupying less memory compared to their floating-

point counterparts. This enables large-scale image visualization applications, such as those supporting multilevel focus+context visualization, to handle comparatively larger imagery, while potentially reducing the computation time. For instance, rendering coarse images reconstructed from BIWTs does not require the sample quantization step, leading to higher frame rates. Furthermore, integer wavelet transforms, in general, are known to be useful for image compression [AK00], while their floating-point counterparts lead to poor compression efficiency [Ada02].

Problems and challenges. Our original BMR framework for symmetric/antisymmetric multiresolution filters introduced in section 1.1 holds a set of useful properties to efficiently support interactive multilevel focus+context visualization. First, the *balanced decomposition* offered by the BMR framework, which by definition is the decomposition of $2n$ fine samples into n coarse and n detail samples (wavelet coefficients) where $n \in \mathbb{Z}^+$, enables efficient and straightforward, on-demand, random-access to details within the hierarchy of details in a BWT by means of simple dyadic operations. Such dyadic operations are known to have more efficient software as well as hardware implementations compared to their non-dyadic counterparts. Second, the BMR framework allows *local* perfect reconstruction, which is crucial for on-demand reconstruction of high-resolution approximations of ROIs from a BWT to support multilevel focus+context visualization. Last but not the least, the BMR framework only makes use of the given set of regular multiresolution filters and avoids the use of any extraordinary boundary filters by exploiting symmetric/antisymmetric extensions at image and detail boundaries. Therefore, our primary set of challenges while extending the existing BMR framework for the construction of BIWTs is associated to retraining the three properties listed above such that the resulting framework still efficiently supports interactive multilevel focus+context visualization.

In addition to making the resulting coarse and detail samples integers, yet further constraints in the construction of the intended BIWTs come from what constitute the

resulting coarse and detail values. Our proposed framework starts from a given symmetric/antisymmetric decomposition filter vector that generally produces a floating-point coarse value. In order to respect the choice of symmetric/antisymmetric decomposition filter vector, it is important for the resulting coarse integer samples to closely approximate the corresponding coarse floating-point samples. On the other hand, the detail samples should mostly constitute close to zero, low-magnitude values like that in conventional wavelet transforms. This property leads to better compression efficiency by reducing the number of unique detail sample values in wavelet transforms.

Contributions and methodology. The primary contribution of this part the thesis lies in presenting an extended BMR framework that can devise a novel BMR scheme to construct reversible BIWTs based on a given symmetric/antisymmetric decomposition filter vector of width less or equal to four. Furthermore, we show how a BMR scheme devised by the proposed framework can be used to support an application allowing interactive multilevel focus+context visualization of large-scale imagery.

To obtain an integer coarse sample under our proposed framework, we start by applying optimal sample split operations to rewrite the linear combination of fine samples suggested by the given symmetric/antisymmetric decomposition filter vector. The rewritten form yields a translation of an affine integer combination of fine samples i.e. an intermediate integer sample. The optimality of the applied sample split operations rely on minimizing the length of the associated translation vector, which is used to form a detail sample in our presented framework. Next, we perform a rounding operation on the translation vector and use the resulting vector to translate the previously obtained intermediate integer sample to obtain the expected integer coarse sample. Ensuring local perfect reconstruction under this framework may require alternating definitions of detail integer samples, implied by the use of alternating sets of optimal sample split operations employed in the initial rewriting step. To avoid the use of extraordinary boundary filters and rounding operators during balanced decomposition and

perfect reconstruction, we make use of symmetric/antisymmetric extensions at fine image, coarse image, and detail boundaries like that in our original BMR framework introduced in section 1.1.

1.3 Application in Multilevel Focus+Context Visualization

Query window-based focus+context visualization is useful for the visualization and exploration of large-scale 2D and 3D images. It allows simultaneous visualization of both the local and global views of the data, possibly at varying scales. Facilitating such visualization involves rendering a low-resolution approximation of data providing the context and a high-resolution approximation of an enclosed ROI selected by a query window, defining the focus. The work presented in this thesis extends this mode of focus+context visualization to construct a multilevel focus+context visualization framework.

In order to support the presented visualization framework by an underlying wavelet transform, on-demand reconstruction of high-resolution approximations of the ROIs from low-resolution approximations of data and their corresponding details is required. Here we exploit either a BWT or a BIWT resulting from our work referred to in sections 1.1 and 1.2, respectively.

Such a framework can be used to efficiently support web-based visualization and exploration of complex large-scale imagery on handheld devices with limited screen spaces. This is possible due to the use of either BWT or BIWT, which needs only be constructed once (for each image) on the server-side in a preprocessing phase and allows robust on-demand reconstruction queries to be performed via progressive transmission with minimal communication overhead, exploiting the *L-updating* technique described later in this thesis. We additionally discuss the performance characteristics of our framework with respect to time and space complexities, achieved frame rates, and implications of using different sets of multiresolution filters. Furthermore, *scalability and multilevel hierarchy* was highlighted as one of the top

ten challenges regarding *interaction and user interfaces* in extreme-scale visual analytics by Wong *et al.* [WSJ*12]. We envision that our presented framework for large-scale image visualization and exploration will provide insights toward developing similar visualization frameworks suitable for extreme-scale visual analytics.

1.4 Summary and Thesis Roadmap

In this chapter, we introduced our balanced multiresolution (BMR) framework for contrstructing balanced wavelet transforms (BWTs) and balanced integer wavelet transforms (BIWTs) from images, as well as their application in multilevel focus+context visualization, while highlighting the contributions of this thesis. Our work on BMR and multilevel focus+context visualization frameworks, referred to in sections 1.1 and 1.3, respectively, have been published in [HSJ14, HSJ15, HSS15].

This thesis is organized as follows. In chapter 2, we present a review of existing related work, discuss some preliminaries, and introduce the notations used throughout the thesis. Next, we present how our BMR framework constructs BWTs in chapter 3 and BIWTs in chapter 4, accompanied by several examples. We demonstrate the application of balanced multiresolution in real-time multilevel focus+context visualization with experimental results in chapter 5. Finally, chapter 6 concludes the thesis. We also provide four appendices with additional examples of balanced multiresolution schemes devised by our BMR framework.

Chapter 2

Background and Preliminaries

In this chapter, we primarily review existing related work within the following four categories: multiresolution, reversible integer-to-integer wavelet transform, symmetric and antisymmetric extensions, and focus+context visualization. We conclude the chapter by discussing some preliminaries that pertain to the multiresolution frameworks we propose in the thesis, while introducing the relevant notations. Some parts of our presented survey of previous work in this chapter have been published in [HSJ14, HSJ15, HSS15].

2.1 Multiresolution

In the next two subsections, we review relevant background literature on multiresolution for regular meshes and images.

2.1.1 Multiresolution for Regular Meshes

Here we review the multiresolution methods applicable to curves and tensor-product meshes (surfaces and volumes) given their applicability to multidimensional images due to their regular structure.

Hierarchical representation of multiresolution tensor-product surfaces was made possible due to the pioneering work of Forsey and Bartels [FB88]. They localized the editing effect in a desired manner on tensor-product surfaces through hierarchically controlled subdivisions. This was done by adding finer sets of B-splines onto existing coarse sets. However, it resulted in an over-representation because the union of the sets of basis functions from different resolutions did not form a set of basis functions. Adding complementary basis functions to the coarse set of basis functions is a possible way to resolve the problem of over-representation.

This means of supporting multiresolution is closely aligned to the wavelet theory approach to multiresolution [SDS96]. Wavelet representations of details may, however, introduce undesired undulations, as pointed out by Gortler and Cohen [GC95]. Furthermore, under this approach, optimizing the behaviour of the analysis (decomposition) using least squares is difficult due to the need to support interactive mesh manipulations [ZSS97].

Samavati and Bartels pioneered in their work on a mathematically clean and efficient approach to multiresolution based on reverse subdivision [SB99, BS00, BGS06, BS11]. Under this approach, during the analysis, each coarse vertex is obtained by efficiently solving a local least squares optimization problem. The use of least squares optimization reduces the undesired undulations. Additionally, the resulting wavelets provide a much more compact support compared to the conventional wavelets for curves and regular surfaces. Some of the examples demonstrating the application of our proposed method use multiresolution filters resulting from this approach (see the examples in section 3.2, for instance).

2.1.2 Multiresolution for Images

Notable existing approaches obtaining a multiresolution representation supporting context-aware visualization of 3D images include the wavelet tree [WS05], segmentation of texture-space into an octree [LHJ99, PTCF02, PHF07], octree-based tensor approximation hierarchy [SGM*11], and trilinear resampling on the Graphics Processing Unit (GPU) coupled with the deformation of regularly partitioned image regions [WWLM11]. For 4D images, the wavelet-based time-space partitioning (WTSP) tree was used in [WS05]. In [WS05], Haar [Haa10, SDS96] and Daubechies' D4 [Dau88] wavelets were used to construct the wavelet transforms in each node of the wavelet and WTSP trees.

2.2 Reversible Integer-to-Integer Wavelet Transform

From a historical perspective, reversible integer-to-integer wavelet transforms have been remarkably instrumental in image and signal coding applications [DC97, CDSY98, JP98a, Ada02, XYZ*05, LYK07], more specifically, in the domain of image compression [SP96, GSK*97, AK00]. As the name suggests, reversible integer-to-integer wavelet transforms map integers to integers and they are reversible i.e. invertible exploiting finite-precision arithmetic that can be performed using smaller word size, reducing memory requirements and prospectively, the associated computational complexity. Furthermore, they are nonlinear approximations of conventional, linear wavelet transforms [CK96]. The nonlinearity generally come from the use of various rounding operators during decomposition and reconstruction, such as, floor, biased floor, ceiling, biased ceiling, truncation, biased truncation, round-away-from-zero (RAFZ), etc. [Ada02]. These properties of reversible integer-to-integer wavelet transforms make them extraordinarily suitable for developing lossless, hybrid lossy/lossless, and strictly lossy image coding systems [ZASB95, SP96, AK00]. Lossless (perfect) reconstruction of RIOs while exploiting lossy compression is addressed in [NC98, AF98].

The next six subsections review a specific example of reversible integer-to-integer wavelet transform, namely the *sequential* (S) transform [Wen87, BF89, RJ91], followed by the evolution of noteworthy frameworks for devising reversible integer-to-integer wavelet transforms, namely the *sequential plus prediction* (S+P) transform framework [SP96], the *lifting* framework [CDSY98], the *overlapping rounding transform* (ORT) framework [JP97, JP98a, JP98b], the *generalized reversible integer-to-integer transform* (GRITIT) framework [Ada02, Ada03], and symmetric-extension-compatible, nonexpansive reversible integer-to-integer wavelet transforms [Ada02, AW03].

2.2.1 Sequential (S) Transform

S transform [Wen87, BF89, RJ91] is the simplest known reversible integer-to-integer wavelet transform, which approximates the linear Haar wavelet transform [Haa10]. From implementation standpoint, a number of slightly varying constructions for S transform can be found in the literature. Here, we include a commonly used construction like that in [SP96], where the general recipe for decomposition is

$$\begin{cases} c_i = \left\lfloor \frac{f_{2i-1}+f_{2i}}{2} \right\rfloor, \\ d_i = f_{2i-1} - f_{2i}, \end{cases} \tag{2.1}$$

and that for a perfect reconstruction is

$$\begin{cases} f_{2i-1} = c_i + \left\lfloor \frac{d_i+1}{2} \right\rfloor, \\ f_{2i} = f_{2i-1} - d_i. \end{cases} \tag{2.2}$$

In equations (2.1) and (2.2), f_{2i-1} and f_{2i} represent fine integer samples and c_i and d_i represent a coarse integer sample and a detail integer sample, respectively, where $i \in \{1 \dots n\}$ for a suitably large $n \in \mathbb{Z}^+$.

As pointed out in [Ada02], the reversibility of S transform is based on the observations one can unambiguously recover two numbers for their sum and difference, both of which have the same parity. Like its real-to-real counterpart [Haa10], S transform readily supports balanced decomposition i.e. from a sequence of $2n$ fine samples, it produces n coarse and n detail samples for a suitably large $n \in \mathbb{Z}^+$.

2.2.2 Sequential plus Prediction (S+P) Transform Framework

The decomposition process under the S+P transform framework [SP96] differs from that of S transform in the generation of detail samples (see the second equation in (2.1)). In the S+P transform framework, the detail sample generated by S transform is adjusted by a predictor term defined on a local neighbourhood of constructed coarse integer samples. The predictor term can be different based on embedded predictor coefficients and the considered width of

the local neighbourhood of constructed coarse samples — resulting in different reversible integer-to-integer wavelet transforms under the S+P transform framework. The well-known two-six transform [ZASB95] is one such example; furthermore, the S+P transform framework produces S transform when the predictor term is zero.

2.2.3 Lifting Framework

The lifting framework for constructing reversible integer-to-integer wavelet transforms was first proposed by Calderbank *et al.* [CDSY98], based on Sweldens' lifting scheme [Swe95, Swe96, Swe98]. Lifting scheme uses reversible ladder-based polyphase networks [BvdE92] to perform polyphase filtering. As described in [Ada02], to construct a reversible integer-to-integer wavelet transform for a given linear wavelet transform, the lifting framework devises the forward transform (i.e. decomposition) such that it constitutes one or more reversible integer-to-integer lifting steps followed by a reversible integer-to-integer scaling step. Each lifting step is defined by the application of corresponding filter and a rounding operator. The inverse transform (i.e. reconstruction) inverts the scaling step first and then the series of lifting steps from the forward transform process in the reverse order.

2.2.4 Overlapping Rounding Transform (ORT) Framework

The ORT framework [JP97, JP98a, JP98a] is a special case of the lifting framework [CDSY98] with minor extensions as shown by Adams [Ada02, Ada03]. With the help of GRITIT framework [Ada02, Ada03], Adams showed that when the applicable operations under the ORT framework are decomposed into lifting and scaling steps, unlike the lifting framework, the ORT framework allows lifting and scaling steps to be intermixed. In addition, it allows intermixing those with any number of shifts in the subband signals. The ORT framework may not allow the wavelet transforms to be calculated in-place based on the choice of allowed filtering steps during polyphase filtering, which makes the resulting reversible integer-to-integer wavelet transforms less practical for use in applications handling large-scape multidimensional

images.

2.2.5 Generalized Reversible Integer-to-Integer Transform (GRITIT) Framework

In addition to constructing reversible integer-to-integer wavelet transforms, the GRITIT framework proposed by Adams [Ada02, Ada03], can describe preexisting frameworks, such as, the S+P framework [SP96], the lifting framework [CDSY98], and the ORT framework [JP97, JP98a, JP98b], allowing for comparative analyses of multiple frameworks. Under the GRITIT framework, the forward transform (i.e. decomposition) constitutes a split operation followed by polyphase filtering, comprising one or more displace, exchange, shift, and scale operations in any order. The employed split, displace, exchange, shift, and scale operations are reversible integer-to-integer operations. The inverse transform (i.e. reconstruction) inverts the sequence of operations from the forward transform in the reverse order.

2.2.6 Nonexpansive Reversible Integer-to-Integer Wavelet Transforms

Adams *et al.* [Ada02, AW03] introduced two families of reversible integer-to-integer wavelet transforms, namely *odd-length analysis/synthesis filter* (OLASF) and *even-length analysis/synthesis filter* (ELASF) families and proved that they are compatible with symmetric/antisymmetric extensions to form nonexpansive transforms for finite-length signals. In other words, given n fine integer samples for a suitably large $n \in \mathbb{Z}^+$, the forward transform will produce n_1 coarse integer samples and n_2 detail integer samples, where $n_1 + n_2 = n$. Our proposed framework in chapter 4 also uses symmetric/antisymmetric extensions but employs a geometric approach for the forward transform to ensure a balanced decomposition i.e. $n_1 = n_2$ and $n_1 + n_2 = n$ for a suitably large $n \in 2\mathbb{Z}^+$.

2.3 Symmetric and Antisymmetric Extensions

As mentioned earlier, we achieve balanced decomposition and subsequent perfect reconstruction based on the use of an appropriate combination of symmetric and antisymmetric extensions near the image and detail boundaries. In the literature, symmetric and antisymmetric extensions were used in the context of various types of wavelet transforms [LL00, KZT02, AW03, LS08]. In contrast, our proposed method allows the construction of a *balanced wavelet transform*.

For end point and boundary interpolations, extraordinary filters (as opposed to regular filters) are used in multiresolution methods for curves and regular meshes, respectively. However, the use of extraordinary filters at image boundaries for boundary interpolation assigns incongruous importance to the image boundaries. Therefore, for 2D or 3D image decomposition, the general practice is to use symmetric extensions near the image boundaries to avoid boundary case evaluations using extraordinary filters [SBO07]. However, an arbitrary choice of symmetric extension for decomposition while using a given set of multiresolution filters may eventually lead to the use of extraordinary boundary filters for a perfect reconstruction (see section 3.3, for example). This can also make on-demand reconstruction of image parts corresponding to a ROI computationally untidy near the image boundaries. Therefore, a careful setup of symmetric/antisymmetric extensions for both decomposition and reconstruction is required, which can be obtained by our presented method.

2.4 Focus+Context Visualization

Because we chose to demonstrate the use of a balanced multiresolution scheme resulting from our method in a real-time focus+context visualization application, here we review some of the notable related work.

In many visualization tasks, it is useful to simultaneously visualize both the local and global views of the data, *possibly at different scales*, which is known as focus+context

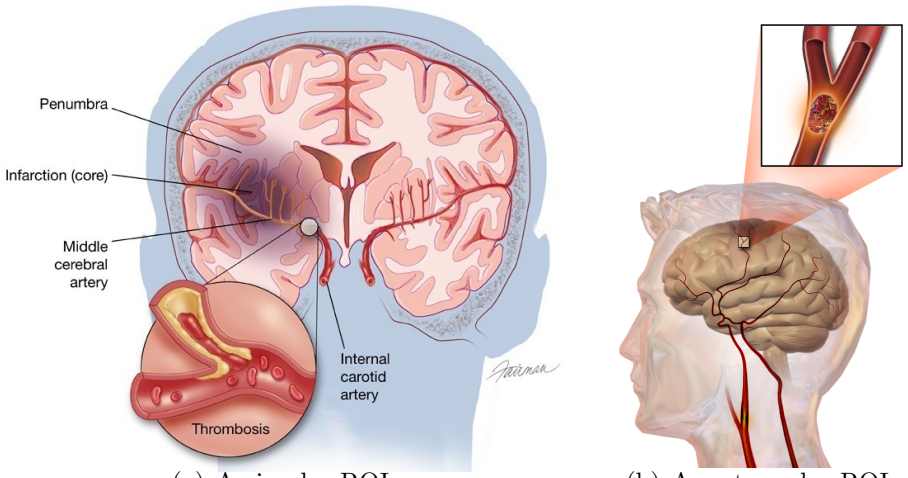

(a) A circular ROI. (b) A rectangular ROI.

Figure 2.1: Traditional focus+context visualization in medical illustrations. (a) Thrombosis in human brain. Copyright Fairman Studios, LLC. Used with permission. (b) An embolic stroke, showing a blockage lodged in a blood vessel. Blausen Medical Communications, Inc. Used under the Creative Commons Attribution 3.0 Unported license.

visualization. One approach to implement focus+context is to use the metaphor of lenses [TSS*06, WWLM11, HMC11]. This metaphor is inspired by techniques used in traditional medical (see Fig. 2.1), technical, and scientific illustrations [Hod03].

Our implemented approach to focus+context visualization of multidimensional images is closest to the technique presented by Taerum *et al.* for the visualization of small-scale clinical volumetric datasets [TSS*06]. In their approach, the resolution of a given 3D image is reduced by one level using reverse subdivision [SB99, BS00], which is rendered during user interactions to achieve interactive frame rates. The 3D image is rendered in the original resolution while there is no user-interaction. The ROI identified by a query window is enlarged by the application of B-spline subdivision to allow different levels of smoothness. Therefore, the authors used only three different levels of resolution. In contrast, our implementation for multiresolution visualization of images provides a true multiresolution framework, where the resolutions of both the coarse image (providing context information) and the enlarged ROI (providing focus information) can be controlled by the user.

Hauser generalized focus+context visualization across the fields of information and

scientific visualizations based on the various methods (such as graphics resource allocation) used to discriminate between data subsets corresponding to focus and context [Hau06]. Using a metaphor of lenses is a prominent way of supporting focus+context visualization [TSS*06, HMC11, WWLM11]. This technique is influenced by traditional handcrafted medical, technical, and scientific illustrations [Hod03]. According to the categorization by Cohen and Brodlie [CB04], our implemented multiresolution approach to this metaphor of lenses is discontinuous and undistorted like that in [TSS*06], as opposed to continuous and distorted techniques in [HMC11, WWLM11].

Multifocal and/or multicontext visualization techniques have been used in the literature for various types of data. Cossalter *et al.* used a multifocal multilevel technique for network visualizations [CMS13]. Tu and Shen presented a multifocal technique applicable to treemap visualizations for hierarchical data [TS08]. Mendez *et al.* used a multifocal [MKS06] and Kalkofen *et al.* a multicontext [KMS07] approach to focus+context visualization in augmented reality applications. Ropinski *et al.* made use of a multifocal approach, utilizing multiple interactive closeups for the visualization of multiple modalities of medical data [RVB*09]. Beyond the scope of this thesis work, we collaborated with Packer *et al.* [Pac13, PHS17] to present a technique for illustrative multifocal multicontext visualization of layered tubular volumes (for instance, human muscle tissue) along a snaking path in a perspective view. In contrast to this body of work, in this thesis, we take a multiresolution approach to interactive multilevel focus+context visualization, supported by an underlying BWT. Sherlock *et al.* [She17, SHS16] adapted our present interactive multilevel focus+context visualization approach for a Digital Earth (DE) supported by an underlying *discrete global grid system* (DGGS).

2.5 Preliminaries & Notations

The thesis adopts and extends the notations for denoting multiresolution operations used by Samavati *et al.* in [SBO07].

2.5.1 Decomposition

Given a column vector of fine samples C^k, a column vector of coarse samples C^{k-1} is obtained by downsampling C^k using the matrix equation

$$C^{k-1} = \mathbf{A}^k C^k, \tag{2.3}$$

and the *details* lost due to downsampling, denoted by D^{k-1} are captured using the matrix equation

$$D^{k-1} = \mathbf{B}^k C^k. \tag{2.4}$$

$\mathbf{A}^k$ and $\mathbf{B}^k$ used in equations (2.3) and (2.4) are decomposition (analysis) filter matrices. This process of deriving C^{k-1} and D^{k-1} from C^k is referred to as *decomposition*. Note that for image decomposition, the sequences of samples along each dimension can be treated independently, allowing any such sequence to form C^k for decomposition.

2.5.2 Reconstruction

The *reconstruction* process involves recovering the column vector of fine samples C^k from the column vectors of coarse sample C^{k-1} and corresponding details D^{k-1}. Reconstruction (synthesis) filter matrices $\mathbf{P}^k$ and $\mathbf{Q}^k$ respectively refine C^{k-1} and D^{k-1} to recover C^k as follows:

$$C^k = \mathbf{P}^k C^{k-1} + \mathbf{Q}^k D^{k-1}. \tag{2.5}$$

Equation (2.5) reverses the application of decomposition filter matrices $\mathbf{A}^k$ and $\mathbf{B}^k$ on the original column vector of fine samples C^k. Therefore, decomposition and reconstruction are

inverse processes that satisfy

$$\begin{bmatrix} \mathbf{A}^k \\ \mathbf{B}^k \end{bmatrix} \begin{bmatrix} \mathbf{P}^k & \mathbf{Q}^k \end{bmatrix} = \begin{bmatrix} \mathbf{I} & \mathbf{0} \\ \mathbf{0} & \mathbf{I} \end{bmatrix}.$$

2.5.3 Wavelet Transform

Recursive decompositions of a column vector of fine samples C^k into column vectors of coarse samples

$$C^l, C^{l+1}, \ldots, C^{k-1}$$

and corresponding details

$$D^l, D^{l+1}, \ldots, D^{k-1}$$

construct the *wavelet transform* of C^k, denoted by

$$C^l, D^l, D^{l+1}, \ldots, D^{k-1},$$

where $l < k$. From this wavelet transform, we can fully or partially reconstruct each of $C^{l+1}, \ldots, C^{k-1}, C^k$.

2.5.4 Simplified Notations

For the rest of the thesis, we simplify the notations by omitting the superscript k for the kth level of resolution with the following assumptions: $F = C^k$, $C = C^{k-1}$, $D = D^{k-1}$, $\mathbf{A} = \mathbf{A}^k$, and $\mathbf{B} = \mathbf{B}^k$, $\mathbf{P} = \mathbf{P}^k$, and $\mathbf{Q} = \mathbf{Q}^k$. Also, the decomposition and reconstruction filter matrices are assumed to have appropriate sizes to satisfy the equations

$$C = \mathbf{A}F, \tag{2.6}$$

$$D = \mathbf{B}F, \tag{2.7}$$

$$F = \mathbf{P}C + \mathbf{Q}D. \tag{2.8}$$

The filter matrices $\mathbf{A}$, $\mathbf{B}$, $\mathbf{P}$ and $\mathbf{Q}$ we consider are of banded, repetitive, and slanted structure. Therefore, let the nonzero entries in a representative row of $\mathbf{A}$ and $\mathbf{B}$ be represented

by decomposition filter vectors **a** and **b**, respectively. In a similar manner, let the nonzero entries in a representative column of **P** and **Q** be denoted by reconstruction filter vectors **p** and **q**, respectively.

Furthermore, let $sizeof(V)$ represent the number of elements in vector V and the widths of filter vectors **a** and **b** be represented by w_{a} and w_{b}, respectively, i.e. $sizeof(\mathbf{a}) = w_{\mathrm{a}}$ and $sizeof(\mathbf{b}) = w_{\mathrm{b}}$.

2.5.5 Symmetric and Antisymmetric Extensions

Fig. 2.2 shows three types of extensions as defined in [KNI94]. Consider a sequence of n samples $(f_1, f_2, \ldots, f_n)$, corresponding to a column vector of samples $\begin{bmatrix} f_1 & f_2 & \ldots & f_n \end{bmatrix}^T$, where $n \in \mathbb{N}$ and $n \geq 3$. Fig. 2.2(a), 2.2(b), and 2.2(c) show the extended sequences obtained through half-sample symmetric, whole-sample symmetric, and half-sample antisymmetric extensions, respectively, at both ends of $(f_1, f_2, \ldots, f_n)$. Whole-sample antisymmetry, not shown in Fig. 2.2, can be obtained by negating the samples in the extensions of Fig. 2.2(b). Note that the types of extensions at both ends of a sequence do not necessarily have to be the same (as used in Fig. 3.8, for example).

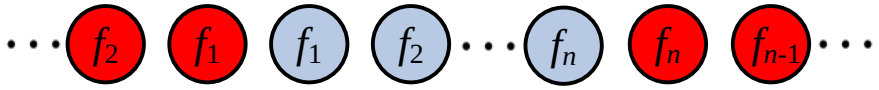

(a) Half-sample symmetry.

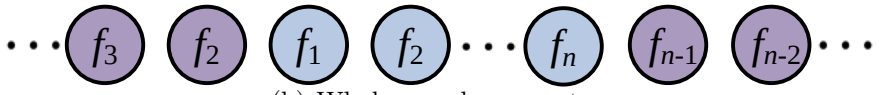

(b) Whole-sample symmetry.

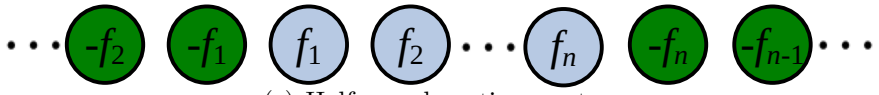

(c) Half-sample antisymmetry.

Figure 2.2: Symmetric and antisymmetric extensions.

To be consistent with the coloring used in Fig. 2.2, from this point forward in this thesis, notations and figures may use red, purple, and green to denote the samples introduced by

half-sample symmetric, whole-sample symmetric, and half-sample antisymmetric extensions, respectively.

2.6 Summary

In this chapter, we presented a survey of existing related work on multiresolution for regular meshes and images, a specific example of reversible integer-to-integer wavelet transform followed by five noteworthy frameworks for devising such wavelet transforms, symmetric and antisymmetric extensions, and focus+context visualization. This chapter also discussed relevant preliminaries and introduced the notations used throughout the thesis.

Chapter 3

Balanced Multiresolution

In this chapter, we present the construction of balanced wavelet transforms (BWTs) using our novel balanced multiresolution (BMR) framework. Our work presented in this chapter has been published in [HSS15].

3.1 Problem Definition

Given a set of regular multiresolution filters in the form of symmetric/antisymmetric filter vectors **a**, **b**, **p**, and **q**, devise a balanced multiresolution scheme applicable to a high-resolution column vector of samples F that satisfies:

(i) $C = \mathbf{A}F'$ and $D = \mathbf{B}F'$, analogous to equations (2.6) and (2.7), where $F \rightarrow F'$ by the use of symmetric extensions at its boundaries and the nonzero entries in each row of $\mathbf{A}$ and $\mathbf{B}$ correspond to the regular filters in the given filter vectors **a** and **b**, respectively;

(ii) $sizeof(C) = sizeof(D)$ i.e. a balanced decomposition;

(iii) $sizeof(C) + sizeof(D) = sizeof(F)$ i.e. a compact representation of the resulting balanced wavelet transform; and

(iv) $F = \mathbf{P}C' + \mathbf{Q}D'$, analogous to equation (2.8), where $C \rightarrow C'$ and $D \rightarrow D'$ through symmetric/antisymmetric extensions at their boundaries and the nonzero entries in each column of $\mathbf{P}$ and $\mathbf{Q}$ correspond to the regular filters in the given filter vectors **p** and **q**, respectively.

3.2 Methodology

In this section, we explain and demonstrate by examples how our method achieves balanced decomposition and subsequent perfect reconstruction by choosing an appropriate combination of symmetric and antisymmetric extensions near the image and detail boundaries.

3.2.1 Balanced Decomposition

We defined balanced decomposition as the task of decomposing a high-resolution image into a low-resolution image and corresponding details of equal size. Balanced decomposition of a 3D image of dimensions $2w \times 2h \times 2s$ results in an image of dimensions $w \times h \times s$ after one level of widthwise, heightwise, and depthwise decomposition. To allow l levels of balanced decomposition, we need the following conditions to be satisfied: $2w = 2^l m$, $2h = 2^l n$, and $2s = 2^l z$, where $m, n, z \in \mathbb{Z}^+$. Disregarding the third dimension infers the same idea for a 2D image. Once the ideal dimensions are known, the high-resolution image should be uniformly resampled to those dimensions before the application of our balanced decomposition procedure.

Given the decomposition filter vectors **a** and **b**, to achieve a balanced decomposition of a column vector containing an even number of fine samples F, we first decide on the type of symmetric extension to use for decomposition based on the parity of w_{a} and w_{b}. Then an extended column vector of fine samples F' is obtained from F, through the chosen type of symmetric extension, such that $sizeof(F')$ ensures the generation of $sizeof(F)/2$ coarse samples and $sizeof(F)/2$ detail samples by a subsequent application of filter vectors **a** and **b** on F', respectively.

Demonstration by example. Before we outline the general construction for the balanced decomposition process, here we demonstrate how it works for a given set of decomposition filter vectors. In this example, we consider the decomposition filter vectors **a** and **b** from

following set of local regular multiresolution filters [SB04, SBO07]:

$$\begin{cases} \mathbf{a} &= \begin{bmatrix} -\frac{1}{4} & \frac{3}{4} & \frac{3}{4} & -\frac{1}{4} \end{bmatrix}, \\ \mathbf{b} &= \begin{bmatrix} \frac{1}{4} & -\frac{3}{4} & \frac{3}{4} & -\frac{1}{4} \end{bmatrix}, \\ \mathbf{p} &= \begin{bmatrix} \frac{1}{4} & \frac{3}{4} & \frac{3}{4} & \frac{1}{4} \end{bmatrix}, \\ \mathbf{q} &= \begin{bmatrix} -\frac{1}{4} & -\frac{3}{4} & \frac{3}{4} & \frac{1}{4} \end{bmatrix}. \end{cases} \tag{3.1}$$

The filter vectors in equation (3.1) are known as the *short* filters of quadratic (third order) B-spline [SBO07] and were constructed by reversing Chaikin subdivision [Cha74]. Recall from section 2.5 that filter vectors $\mathbf{a}$ and $\mathbf{b}$ contain the nonzero entries in a representative row of analysis filter matrices $\mathbf{A}$ and $\mathbf{B}$, respectively.

For the purpose of demonstration, assume that we are given a fine column vector of 8 samples $F = \begin{bmatrix} f_1 & f_2 & \dots & f_8 \end{bmatrix}^T$, on which we have to perform a balanced decomposition. Provided $sizeof(F) = 8$, a balanced decomposition should result in column vectors of coarse samples $C = \begin{bmatrix} c_1 & c_2 & c_3 & c_4 \end{bmatrix}^T$ and detail samples $D = \begin{bmatrix} d_1 & d_2 & d_3 & d_4 \end{bmatrix}^T$.

In Fig. 3.1, we present one possible setup to obtain such a balanced decomposition. It shows the application of equations $C = \mathbf{A}F'$ and $D = \mathbf{B}F'$, analogous to equations (2.6) and (2.7), where $F' = \begin{bmatrix} f_1 & f_1 & f_2 & \dots & f_8 & f_8 \end{bmatrix}^T$. First, note that F' was obtained by extending the given sample vector F by 2 extra samples. In general, when the dilation factor is 2, a given column vector of fine samples F, with $sizeof(F) = 2n$ for $n \in \mathbb{Z}^+$, does not have enough samples to accommodate n shifts of both $\mathbf{a}$ and $\mathbf{b}$ for generating n coarse and n detail samples, respectively. The number of extra samples x, required for a balanced decomposition can be obtained by the general formula:

$$x = max(w_\mathrm{a}, w_\mathrm{b}) + 2(n-1) - 2n \tag{3.2}$$

$$\Rightarrow x = max(w_\mathrm{a}, w_\mathrm{b}) - 2. \tag{3.3}$$

Here we explain how equation 3.2 evaluates x. We need at least $max(w_\mathrm{a}, w_\mathrm{b})$ fine samples to

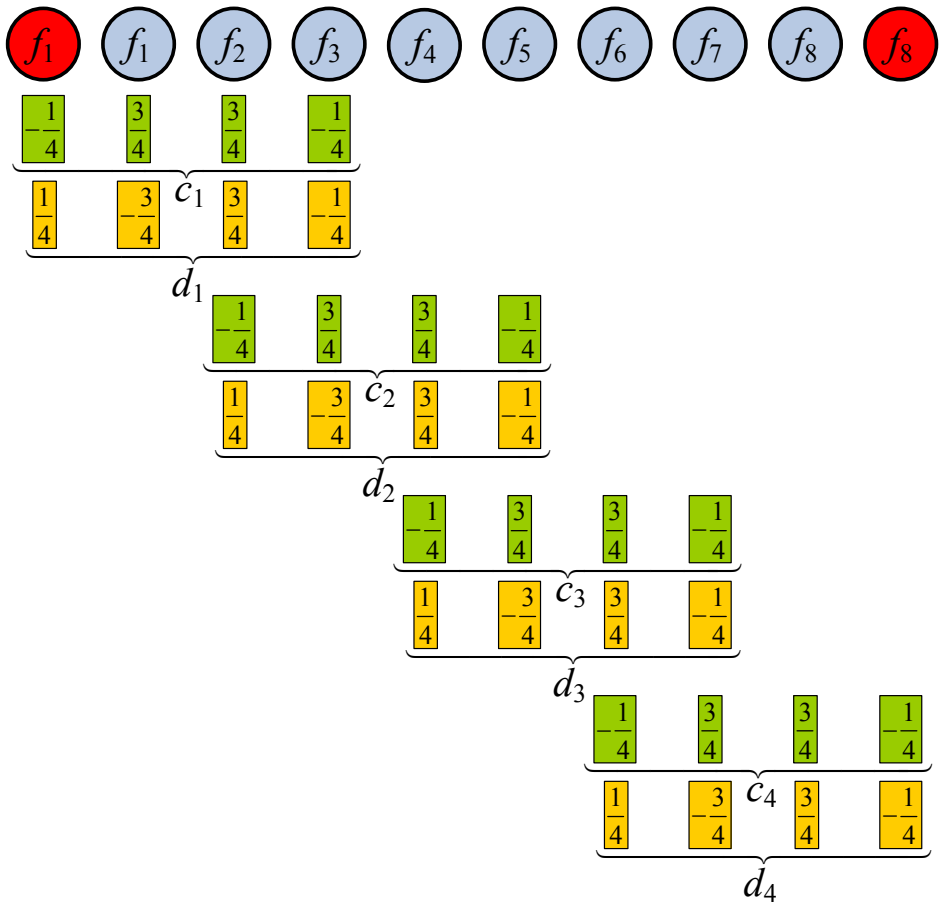

Figure 3.1: Balanced decomposition of 8 fine samples using the decomposition filter vectors **a** and **b** from equation (3.1).

obtain both c_1 and d_1, which explains the first term on the right-hand side of equation 3.2. Next, because the dilation factor is 2, every 2 additional samples will guarantee the generation of an additional pair of c_i and d_i. Here, $i \in \{2, \ldots, n\}$ because we want to generate $|\{2, \ldots, n\}| = n - 1$ more coarse samples and $n - 1$ more detail samples to achieve a balanced decomposition. This indicates the need for an additional $2(n - 1)$ fine samples, justifying the addition of the second term on the right-hand side of equation 3.2. Therefore, subtracting $2n$ i.e. the $sizeof(F)$ in the third term gives us the required number of extra samples.

For the families of multiresolution filters we consider in this thesis, w_{a} and w_{b} are either both even or both odd. For example, see the decomposition filter vectors obtained from B-spline wavelets [SBO07], biorthogonal and reverse biorthogonal wavelets [CDF92, Dau92], and

Meyer wavelets [Mey90, Dau92]. The multiresolution filter vectors obtained from most such wavelets and their scaling functions are available in commonly used mathematical software packages such as MATLAB [MAT14]. For the given filter vectors **a** and **b** in equation (3.1), because both w_{a} and w_{b} are even, observe that the extension of F by 2 extra samples to obtain F' was achieved by half-sample symmetric extension at both ends of F. Here we would have used whole-sample symmetric extension instead if both w_{a} and w_{b} were odd. Use of an appropriate type of symmetric extension is required to avoid the use of any extraordinary boundary filters for a perfect reconstruction. We justify our choice of symmetric extension for a balanced decomposition later in section 3.2.3.

Finally, as shown in Fig. 3.1, the filter vectors **a** and **b** in equation (3.1) are applied to the samples in F' to obtain C and D in order to complete the balanced decomposition process. For instance, the coarse sample c_1 and the detail sample d_1 are computed from the first 4 samples in F' as follows:

$$\begin{cases} c_1 &= -\frac{1}{4}f_1 + \frac{3}{4}f_1 + \frac{3}{4}f_2 - \frac{1}{4}f_3, \\ d_1 &= \ \ \frac{1}{4}f_1 - \frac{3}{4}f_1 + \frac{3}{4}f_2 - \frac{1}{4}f_3. \end{cases} \tag{3.4}$$

Note that the total contribution of f_1 in the construction of c_1 is $\frac{1}{2}f_1$, written as $-\frac{1}{4}f_1 + \frac{3}{4}f_1$ in equation (3.4) through an implicit sample split operation. A similar sample split is observed in the construction of d_1, as shown in equation (3.4). Therefore, the symmetric extensions at both ends of F implicitly lead to a number of sample split operations during decomposition.

Therefore, for $n \in \mathbb{Z}^+$, a balanced multiresolution scheme based on the *short* filters of

quadratic B-spline given in equation (3.1) can make use of the matrix equations

$$\begin{bmatrix} c_1 \\ c_2 \\ \vdots \\ c_n \end{bmatrix} = \begin{bmatrix} -\frac{1}{4} & \frac{3}{4} & \frac{3}{4} & -\frac{1}{4} & 0 & 0 & 0 & \cdots \\ 0 & 0 & -\frac{1}{4} & \frac{3}{4} & \frac{3}{4} & -\frac{1}{4} & 0 & \cdots \\ \vdots & \vdots & \vdots & \vdots & \vdots & \vdots & \vdots & \ddots \end{bmatrix} \begin{bmatrix} f_1 \\ f_1 \\ f_2 \\ \vdots \\ f_{2n-1} \\ f_{2n} \\ f_{2n} \end{bmatrix}$$

and

$$\begin{bmatrix} d_1 \\ d_2 \\ \vdots \\ d_n \end{bmatrix} = \begin{bmatrix} \frac{1}{4} & -\frac{3}{4} & \frac{3}{4} & -\frac{1}{4} & 0 & 0 & 0 & \cdots \\ 0 & 0 & \frac{1}{4} & -\frac{3}{4} & \frac{3}{4} & -\frac{1}{4} & 0 & \cdots \\ \vdots & \vdots & \vdots & \vdots & \vdots & \vdots & \vdots & \ddots \end{bmatrix} \begin{bmatrix} f_1 \\ f_1 \\ f_2 \\ \vdots \\ f_{2n-1} \\ f_{2n} \\ f_{2n} \end{bmatrix}$$

for the decomposition process, analogous to equations (2.6) and (2.7).

General construction. Now we present our general approach for achieving a balanced decomposition. Given the symmetric/antisymmetric decomposition filter vectors **a** and **b** containing only regular filters, carry out the following steps to achieve a balanced decomposition of a fine column vector of samples F, where $sizeof(F) = 2n$ for a suitably large $n \in \mathbb{Z}^+$.

1. Determine x, the number of extra samples required for a balanced decomposition using equation (3.3).

2. If both w_{a} and w_{b} are even, extend F with x extra samples using half-sample symmetric extension to obtain F'. Use whole-sample symmetric extension instead if both w_{a} and w_{b}

are odd. Justification for our choice of symmetric extension can be found in section 3.2.3. To avoid giving inconsistent importance to any end (boundary) of F:

(a) If x is even, introduce $x/2$ samples at each end of F.

(b) If x is odd, introduce $\lfloor x/2 \rfloor$ samples at one end and $\lfloor x/2 \rfloor + 1$ samples at the other end of F. Let us refer to the end at which $\lfloor x/2 \rfloor + 1$ samples are introduced as the *odd end*. Alternate between the ends of F as the choice of the odd end during multiple levels of decomposition.

3. To obtain C and D such that $sizeof(C) = sizeof(D)$, use equations $C = \mathbf{A}F'$ and $D = \mathbf{B}F'$, analogous to equations (2.6) and (2.7).

3.2.2 Perfect Reconstruction

Given the reconstruction filter vectors $\mathbf{p}$ and $\mathbf{q}$ that can reverse the application of the decomposition filter vectors $\mathbf{a}$ and $\mathbf{b}$, to achieve a perfect reconstruction of the column vector of fine samples F from its prior balanced decomposition into C and D, we first reconstruct as many interior samples of F as possible by the application of $\mathbf{p}$ and $\mathbf{q}$ on C and D, using equation (2.8). To evaluate the samples near each boundary (end) of F, we form a square system of linear equations based on the prior construction of corresponding boundary samples in C and D, where the unknowns constitute the boundary samples of F yet to be reconstructed. Symbolically solving two such square systems for the two boundaries of F reveals the extended versions of C and D (denoted by C' and D', respectively) required for a perfect reconstruction by the application of $\mathbf{p}$ and $\mathbf{q}$ using equation $F = \mathbf{P}C' + \mathbf{Q}D'$, analogous to equation (2.8).

Demonstration by example. Here we demonstrate how we perform a perfect reconstruction of F following its balanced decomposition to C and D by means of an example, before giving the general construction for our perfect reconstruction process. In this example, we consider the reconstruction filter vectors $\mathbf{p}$ and $\mathbf{q}$ given in equation (3.1). Recall from section 2.5 that

filter vectors $\mathbf{p}$ and $\mathbf{q}$ contain the nonzero entries in a representative column of synthesis filter matrices $\mathbf{P}$ and $\mathbf{Q}$, respectively.

This example to demonstrate our perfect reconstruction process is an extension of the example shown in Fig. 3.1. Therefore, from the resulting column vectors of coarse samples $C = \begin{bmatrix} c_1 & c_2 & c_3 & c_4 \end{bmatrix}^T$ and detail samples $D = \begin{bmatrix} d_1 & d_2 & d_3 & d_4 \end{bmatrix}^T$ in section 3.2.1, we now want to reconstruct the corresponding column vector of fine samples $F = \begin{bmatrix} f_1 & f_2 & \dots & f_8 \end{bmatrix}^T$.

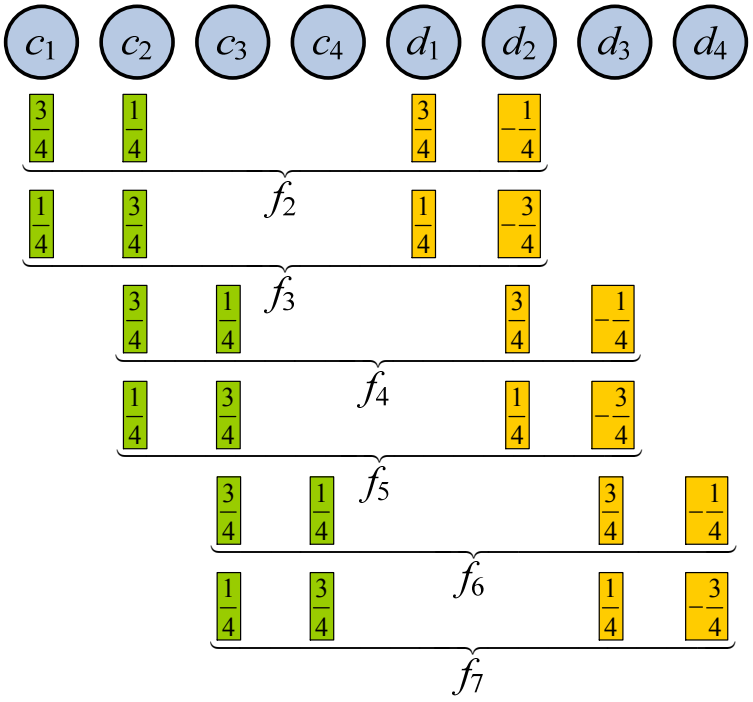

Figure 3.2: Perfect reconstruction of 6 of the 8 fine samples using the reconstruction filter vectors $\mathbf{p}$ and $\mathbf{q}$ from equation (3.1).

In Fig. 3.2, we show the application of the filter vectors $\mathbf{p}$ and $\mathbf{q}$ to the samples in C and D, respectively. For instance, the fine sample f_2 is reconstructed from the first two coarse samples and the first two detail samples as follows:

$$f_2 = \frac{3}{4}c_1 + \frac{1}{4}c_2 + \frac{3}{4}d_1 - \frac{1}{4}d_2.$$

Note that the application of the filter vectors $\mathbf{p}$ and $\mathbf{q}$ to the samples in C and D in Fig. 3.2 left two samples, f_1 and f_8, near the two ends of F not reconstructed. Note that having two

samples near the boundaries of F yet to reconstruct is specific to this example. The example in section 3.2.4 receives 5 samples yet to reconstruct at this stage. Now, to reconstruct f_1, we form the following 1×1 system of linear equations based on the prior construction of c_1 (as shown in Fig. 3.1) to which f_1 made some contribution during decomposition:

$$c_1 = -\frac{1}{4}f_1 + \frac{3}{4}f_1 + \frac{3}{4}f_2 - \frac{1}{4}f_3 \tag{3.5}$$

$$\begin{aligned}
\Rightarrow f_1 &= 2c_1 - \frac{3}{2}f_2 + \frac{1}{2}f_3 \\
\Rightarrow f_1 &= 2c_1 - \frac{3}{2}\left(\frac{3}{4}c_1 + \frac{1}{4}c_2 + \frac{3}{4}d_1 - \frac{1}{4}d_2\right) \\
&\quad + \frac{1}{2}\left(\frac{1}{4}c_1 + \frac{3}{4}c_2 + \frac{1}{4}d_1 - \frac{3}{4}d_2\right) \\
\Rightarrow f_1 &= c_1 - d_1.
\end{aligned} \tag{3.6}$$

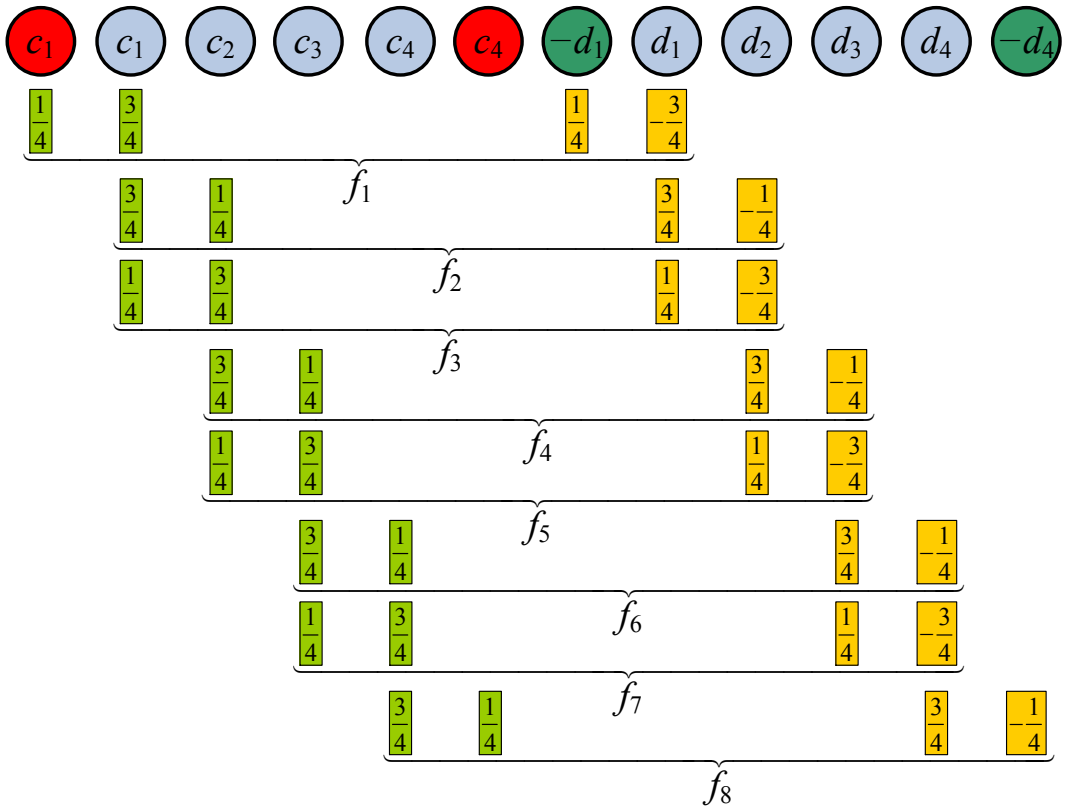

Figure 3.3: Perfect reconstruction of 8 fine samples using the reconstruction filter vectors $\mathbf{p}$ and $\mathbf{q}$ from equation (3.1).

Although it appears from equation (3.6) that f_1 is not reconstructed using *regular filters*,

our prior appropriate choice of symmetric extension to obtain F' from F (justified later in section 3.2.3) guarantees that we can rewrite f_1 using the regular filter values from $\mathbf{p}$ and $\mathbf{q}$ in equation (3.1). This is achieved by a rearrangement of the right-hand side of equation (3.6), which is implicitly equivalent to performing two sample split operations:

$$f_1 \;=\; \tfrac{1}{4}c_1 + \tfrac{3}{4}c_1 + \tfrac{1}{4}(-d_1) - \tfrac{3}{4}d_1. \tag{3.7}$$

This rewriting step is important because it allows the reconstruction of fine samples near the boundaries of F without the use of any extraordinary boundary filters. Equation (3.7) now yields the introduction of one extra coarse sample through half-sample symmetric extension and one extra detail sample through half-sample antisymmetric extension for the reconstruction of f_1, as shown in Fig. 3.3. We use a similar approach to determine how to reconstruct the boundary sample f_8, resulting in

$$f_8 \;=\; \tfrac{3}{4}c_4 + \tfrac{1}{4}c_4 + \tfrac{3}{4}d_1 - \tfrac{1}{4}(-d_4), \tag{3.8}$$

as reflected in Fig. 3.3. This concludes the perfect reconstruction process.

Therefore, based on our findings from equations (3.7) and (3.8), for a given column vector of $2n$ fine samples for a suitably large $n \in \mathbb{Z}^+$, we get

$$\begin{cases} f_1 \;=\; \tfrac{1}{4}c_1 + \tfrac{3}{4}c_1 + \tfrac{1}{4}(-d_1) - \tfrac{3}{4}d_1, \\ \\ f_{2n} \;=\; \tfrac{3}{4}c_n + \tfrac{1}{4}c_n + \tfrac{3}{4}d_n - \tfrac{1}{4}(-d_n). \end{cases}$$

As a result, a balanced multiresolution scheme based on the *short* filters of quadratic B-spline

given in equation (3.1) will make use of the matrix equation

$$\begin{bmatrix} f_1 \\ f_2 \\ \vdots \\ f_{2n} \end{bmatrix} = \begin{bmatrix} \frac{1}{4} & \frac{3}{4} & 0 & 0 & \cdots & 0 & 0 & 0 \\ 0 & \frac{3}{4} & \frac{1}{4} & 0 & \cdots & 0 & 0 & 0 \\ 0 & \frac{1}{4} & \frac{3}{4} & 0 & \cdots & 0 & 0 & 0 \\ 0 & 0 & \frac{3}{4} & \frac{1}{4} & \cdots & 0 & 0 & 0 \\ 0 & 0 & \frac{1}{4} & \frac{3}{4} & \cdots & 0 & 0 & 0 \\ \vdots & \vdots & \vdots & \vdots & \ddots & \vdots & \vdots & \vdots \\ 0 & 0 & 0 & 0 & \cdots & \frac{3}{4} & \frac{1}{4} & 0 \\ 0 & 0 & 0 & 0 & \cdots & \frac{1}{4} & \frac{3}{4} & 0 \\ 0 & 0 & 0 & 0 & \cdots & 0 & \frac{3}{4} & \frac{1}{4} \end{bmatrix} \begin{bmatrix} c_1 \\ c_1 \\ c_2 \\ \vdots \\ c_n \\ c_n \end{bmatrix} + \begin{bmatrix} \frac{1}{4} & -\frac{3}{4} & 0 & 0 & \cdots & 0 & 0 & 0 \\ 0 & \frac{3}{4} & -\frac{1}{4} & 0 & \cdots & 0 & 0 & 0 \\ 0 & \frac{1}{4} & -\frac{3}{4} & 0 & \cdots & 0 & 0 & 0 \\ 0 & 0 & \frac{3}{4} & -\frac{1}{4} & \cdots & 0 & 0 & 0 \\ 0 & 0 & \frac{1}{4} & -\frac{3}{4} & \cdots & 0 & 0 & 0 \\ \vdots & \vdots & \vdots & \vdots & \ddots & \vdots & \vdots & \vdots \\ 0 & 0 & 0 & 0 & \cdots & \frac{3}{4} & -\frac{1}{4} & 0 \\ 0 & 0 & 0 & 0 & \cdots & \frac{1}{4} & -\frac{3}{4} & 0 \\ 0 & 0 & 0 & 0 & \cdots & 0 & \frac{3}{4} & -\frac{1}{4} \end{bmatrix} \begin{bmatrix} -d_1 \\ d_1 \\ d_2 \\ \vdots \\ d_n \\ -d_n \end{bmatrix}$$

for the reconstruction process, analogous to equation (2.8).

General construction. Now we describe our general approach to achieve perfect reconstruction. Given the symmetric/antisymmetric reconstruction filter vectors **p** and **q** containing only regular filters that can reverse the application of the decomposition filter vectors **a** and **b**, carry out the following steps to perfectly reconstruct the column vector of fine samples F from its prior balanced decomposition into C and D.

1. Assume that $F = \begin{bmatrix} {F_l}^T & {F_m}^T & {F_r}^T \end{bmatrix}^T$, where ${F_l}^T$ and ${F_r}^T$ respectively contain some samples at the left and right boundaries of F^T, and F_m contains the remaining interior samples of F. To reconstruct the samples in F_m, use the equation $F_m = \mathbf{P}C + \mathbf{Q}D$, analogous to equation (2.8). The samples in F_l and F_r are yet to be reconstructed.
   (In the example above, we had $F_l = [f_1]$, $F_m = \begin{bmatrix} f_2 & f_3 & \ldots & f_7 \end{bmatrix}^T$, and $F_r = [f_8]$. Note that F_l and F_r may contain more samples; for instance, the F_l and F_r encountered in 3.2.4 have 2 and 3 samples, respectively.)

2. To reconstruct the samples in F_l:

   (a) Form a system of linear equations based on the prior construction of some coarse and detail boundary samples, to which the fine samples in F_l made some contributions during the decomposition process. It should be a $m \times m$ system, where $m = sizeof(F_l)$ and the unknowns are the samples of F_l.

   (For example, see the 1×1 system formed by equation (3.5) and the 2×2 system formed by the two equations in (3.16).)

   (b) Solving the system formed in step 2(a) symbolically will evaluate each sample in F_l as a linear combination of some samples from C and D.

   (For example, see equation (3.6) and the two equations in (3.17).)

   (c) Rewrite the linear combination(s) of coarse and detail samples on the right-hand side(s) of the equation(s) obtained in step 2(b) using the regular filter values from the filter vectors **p** and **q** as coefficients. Such rewriting here correlates to performing sample split operations. This will reveal the following two pieces of information applicable to the left boundaries of C and D for a perfect reconstruction: (i) the type of symmetric/antisymmetric extension that must be used and (ii) the number of extra samples that must be to introduced.

   (For example, see equation (3.7) and the two equations in (3.18).)

3. Use an approach similar to that in step 2 to reconstruct the samples in F_r.

Note that steps 2-3 above allow the generation of C' and D' respectively from C and D, such that condition (iv) of the problem definition given in section 3.1 is satisfied.

3.2.3 Choice of Symmetric Extension for Decomposition

Claim. For a given set of symmetric/antisymmetric multiresolution filter vectors **a**, **b**, **p**, and **q**, even values of w_{a} and w_{b} imply the use of half-sample symmetric extensions at the

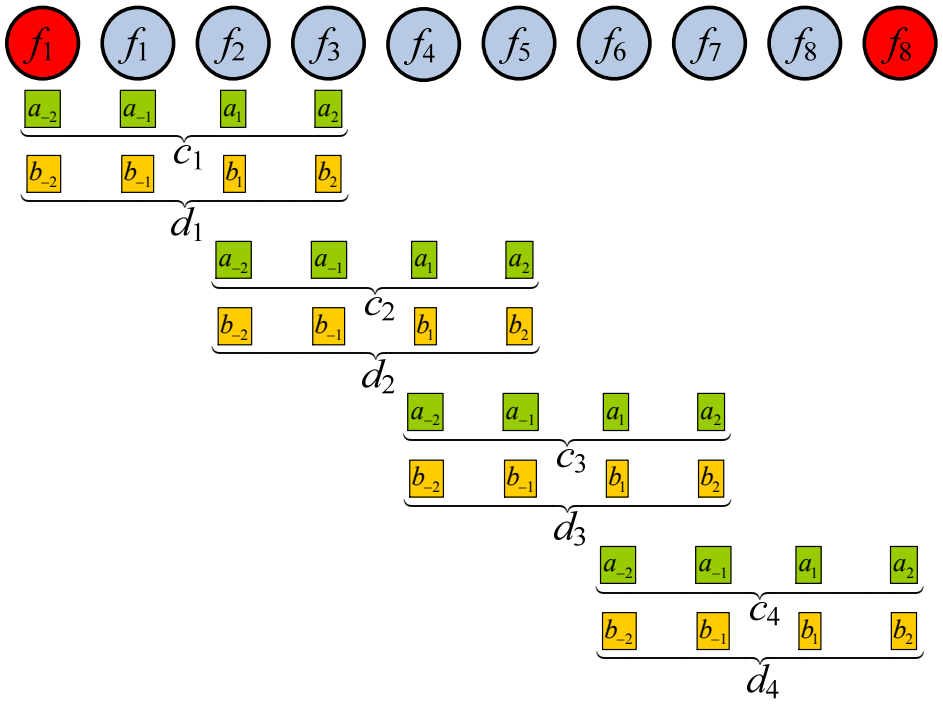

(a) Balanced decomposition using half-sample symmetric extension.

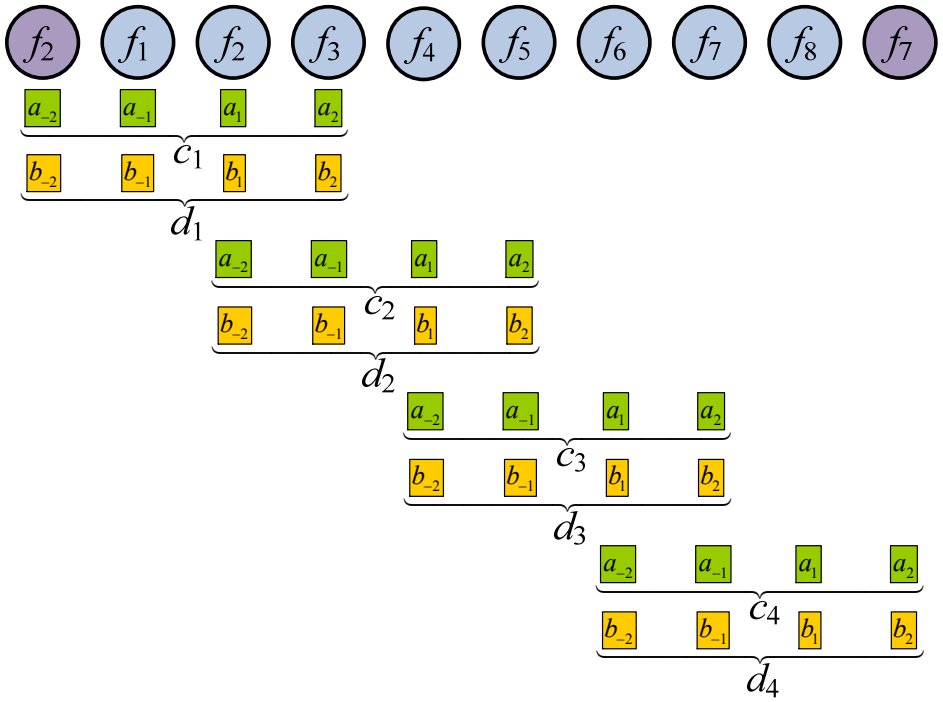

(b) Balanced decomposition using whole-sample symmetric extension.

Figure 3.4: Balanced decomposition of 8 fine samples using the decomposition filter vectors **a** and **b** from equation (3.9).

image boundaries during a balanced decomposition to ensure a perfect reconstruction only using the regular reconstruction filters from **p** and **q**. On the other hand, odd values of w_{a} and w_{b} imply the use of whole-sample symmetric extensions instead.

Proof outline. We outline the proof by means of an example that makes use of the filter vectors containing only regular filters,

$$\begin{cases} \mathbf{a} &= \begin{bmatrix} a_{-2} & a_{-1} & a_1 & a_2 \end{bmatrix}, \\ \mathbf{b} &= \begin{bmatrix} b_{-2} & b_{-1} & b_1 & b_2 \end{bmatrix}, \\ \mathbf{p} &= \begin{bmatrix} p_{-2} & p_{-1} & p_1 & p_2 \end{bmatrix}, \\ \mathbf{q} &= \begin{bmatrix} q_{-2} & q_{-1} & q_1 & q_2 \end{bmatrix}. \end{cases} \tag{3.9}$$

The widths of the filter vectors **a**, **b**, **p**, and **q** in equation (3.9) are assumed to be 4 as in the case of the filter vectors containing the *short* filters of quadratic B-spline in equation (3.1). Therefore, here w_{a} and w_{b} are even. Next, two possible balanced decompositions of a fine column vector of 8 samples $F = \begin{bmatrix} f_1 & f_2 & \dots & f_8 \end{bmatrix}^T$ are shown by the use of half-sample and whole-sample symmetric extensions at its boundaries in Fig. 3.4(a) and 3.4(b), respectively.

Now, our goal is to perfectly reconstruct F from the column vectors of coarse samples $C = \begin{bmatrix} c_1 & c_2 & c_3 & c_4 \end{bmatrix}^T$ and detail samples $D = \begin{bmatrix} d_1 & d_2 & d_3 & d_4 \end{bmatrix}^T$ using only the regular reconstruction filters vectors **p** and **q** from equation (3.9) as shown in Fig. 3.5.

We intend to evaluate the unknowns in Fig. 3.5, which are $\alpha c_i \in \{-c_1, c_1, -c_2, c_2\}$, $\beta c_j \in \{-c_3, c_3, -c_4, c_4\}$, $\gamma d_k \in \{-d_1, d_1, -d_2, d_2\}$, and $\delta d_l \in \{-d_3, d_3, -d_4, d_4\}$ near the boundaries of C and D. Once evaluated, these will reveal the type of symmetric/antisymmetric extensions to be used at the boundaries of C and D to ensure a perfect reconstruction using only the regular reconstruction filters. Here $\alpha, \beta, \gamma, \delta \in \{+, -\}$ represent the signs of c_i, c_j, d_k and d_l, respectively. When negative, they allow the representation of antisymmetric extensions.

Now, let us try to evaluate αc_i. As shown in Fig. 3.5, αc_i contributes to the reconstruction of f_1. If we consider the balanced decomposition shown in Fig. 3.4(a) and try to evaluate f_1

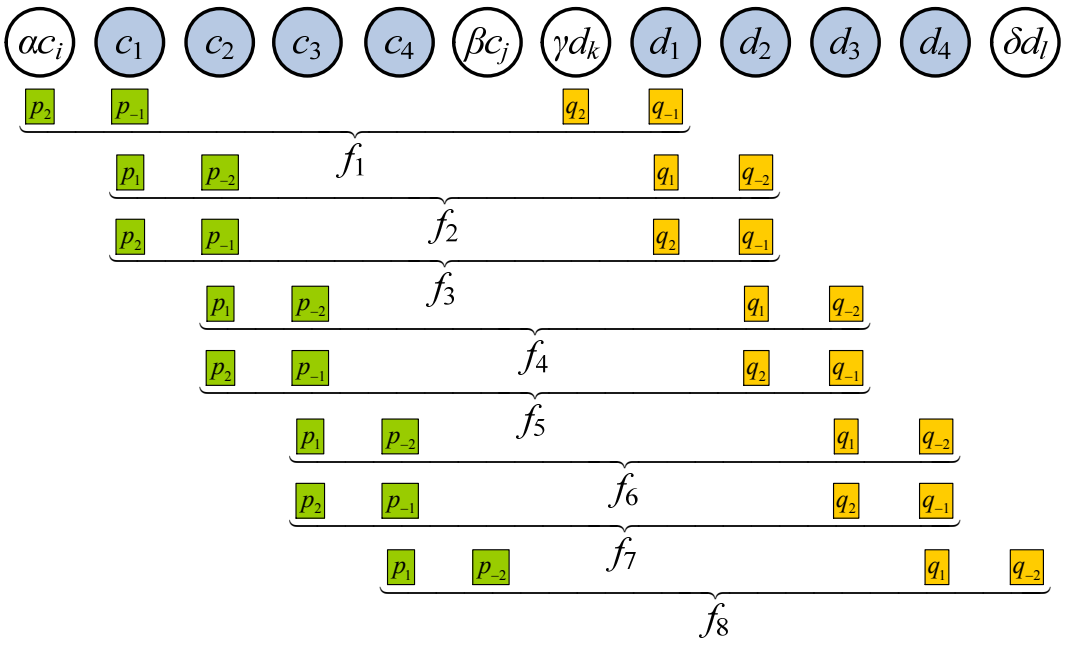

Figure 3.5: Perfect reconstruction of 8 fine samples using the reconstruction filter vectors $\mathbf{p}$ and $\mathbf{q}$ from equation (3.9).

following our general approach from section 3.2.2, we get

$$
\begin{aligned}
c_1 &= a_{-2}f_1 + a_{-1}f_1 + a_1 f_2 + a_2 f_3 \\
\Rightarrow f_1 &= \frac{1}{a_{-2}+a_{-1}}c_1 - \frac{a_1}{a_{-2}+a_{-1}}f_2 - \frac{a_2}{a_{-2}+a_{-1}}f_3 \\
\Rightarrow f_1 &= \frac{1}{a_{-2}+a_{-1}}c_1 \\
&\quad -\frac{a_1}{a_{-2}+a_{-1}}\left(p_1c_1 + p_{-2}c_2 + q_1d_1 + q_{-2}d_2\right) \\
&\quad -\frac{a_2}{a_{-2}+a_{-1}}\left(p_2c_1 + p_{-1}c_2 + q_2d_1 + q_{-1}d_2\right) \\
\Rightarrow f_1 &= \left(\frac{1-a_1p_1-a_2p_2}{a_{-2}+a_{-1}}\right)c_1 + \left(\frac{-a_1p_{-2}-a_2p_{-1}}{a_{-2}+a_{-1}}\right)c_2 \\
&\quad + \left(\frac{-a_1q_1-a_2q_2}{a_{-2}+a_{-1}}\right)d_1 + \left(\frac{-a_1q_{-2}-a_2q_{-1}}{a_{-2}+a_{-1}}\right)d_2. \qquad (3.10)
\end{aligned}
$$

Next, if we consider the balanced decomposition shown in Fig. 3.4(b) and try to evaluate f_1

following our general approach from section 3.2.2, we get

$$\begin{aligned}
c_1 &= a_{-2}f_2 + a_{-1}f_1 + a_1 f_2 + a_2 f_3 \\
\Rightarrow f_1 &= \frac{1}{a_{-1}}c_1 - \frac{a_{-2}+a_1}{a_{-1}}f_2 - \frac{a_2}{a_{-1}}f_3 \\
\Rightarrow f_1 &= \frac{1}{a_{-1}}c_1 - \frac{a_{-2}+a_1}{a_{-1}}\left(p_1 c_1 + p_{-2}c_2 + q_1 d_1 + q_{-2}d_2\right) \\
&\quad + \frac{a_2}{a_{-1}}\left(p_2 c_1 + p_{-1}c_2 + q_2 d_1 + q_{-1}d_2\right) \\
\Rightarrow f_1 &= \left(\frac{1 - a_{-2}p_1 - a_1 p_1 - a_2 p_2}{a_{-1}}\right)c_1 \\
&\quad + \left(\frac{-a_{-2}p_2 - a_1 p_2 - a_2 p_{-1}}{a_{-1}}\right)c_2 \\
&\quad + \left(\frac{-a_{-2}q_1 - a_1 q_1 - a_2 q_2}{a_{-1}}\right)d_1 \\
&\quad + \left(\frac{-a_{-2}q_2 - a_1 q_2 - a_2 q_{-1}}{a_{-1}}\right)d_2. \qquad (3.11)
\end{aligned}$$

Let the filter values multiplied to c_1 and c_2 in the reconstruction of f_1 be denoted by $w(c_1)$ and $w(c_2)$, respectively. In equation (3.10),

$$\begin{cases} w(c_1) &= \frac{1-a_1p_1-a_2p_2}{a_{-2}+a_{-1}}, \\ w(c_2) &= \frac{-a_1p_{-2}-a_2p_{-1}}{a_{-2}+a_{-1}}, \end{cases} \qquad (3.12)$$

which result from using half-sample symmetric extension at the left boundary F for a balanced decomposition. On the other hand, in equation (3.11),

$$\begin{cases} w(c_1) &= \frac{1-a_{-2}p_1-a_1p_1-a_2p_2}{a_{-1}}, \\ w(c_2) &= \frac{-a_{-2}p_2-a_1p_2-a_2p_{-1}}{a_{-1}}, \end{cases} \qquad (3.13)$$

which result from using whole-sample symmetric extension instead. Now, according to Fig. 3.5, f_1 is reconstructed as follows:

$$f_1 = p_2(\alpha c_i) + p_{-1}c_1 + q_2(\alpha d_k) - q_{-1}d_1. \qquad (3.14)$$

If we consider $\alpha c_i = -c_1$ in equation (3.14) for example, then $w(c_1) = -p_2 + p_{-1}$ and $w(c_2) = 0$. If $-c_1$ is substituted in Fig. 3.5 in place of αc_i, it would then reveal the need for half-sample

antisymmetric extension for the left boundary of C to be used during reconstruction. In this manner, Table 3.1 lists the sufficient conditions for all possible values of αc_i. Note that each possible value of αc_i yields a particular type of extension (listed in Table 3.1) for the left boundary of C.

Table 3.1: Sufficient conditions for symmetric and antisymmetric extensions.

Case	**Sufficient Conditions**	αc_i	**Type of Extension**
I	$\begin{cases} w(c_1) = p_2 + p_{-1} \\ w(c_2) = 0 \end{cases}$	c_1	Half-sample symmetry
II	$\begin{cases} w(c_1) = -p_2 + p_{-1} \\ w(c_2) = 0 \end{cases}$	$-c_1$	Half-sample antisymmetry
III	$\begin{cases} w(c_1) = p_{-1} \\ w(c_2) = p_2 \end{cases}$	c_2	Whole-sample symmetry
IV	$\begin{cases} w(c_1) = p_{-1} \\ w(c_2) = -p_2 \end{cases}$	$-c_2$	Whole-sample antisymmetry

Now, if we substitute the actual values of the corresponding regular filters of quadratic B-spline from equation (3.1) in equations (3.12) and (3.13), we find that equation (3.12) only satisfies the sufficient conditions under case I (i.e. $\alpha c_i = c_1$) in Table 3.1 and equation (3.13) does not satisfy the sufficient conditions under any of the cases. Recall that equation (3.12) was obtained by the use of half-sample symmetric extension on the left boundary of F for a balanced decomposition. This implies that the use of half-sample symmetric extension at the left boundary of F for a balanced decomposition will ensure the perfect reconstruction of that boundary only using regular reconstruction filters. Similarly, for the regular filters of quadratic B-spline from equation (3.1), we can show that $\beta c_j = c_4$, $\gamma d_k = -d_1$, and $\delta d_l = -d_4$; and they all require the use of half-sample symmetric extension at the boundaries of F for a balanced decomposition.

In the above manner, we can show that for any set of symmetric/antisymmetric filter vectors $\mathbf{a}$, $\mathbf{b}$, $\mathbf{p}$, and $\mathbf{q}$, where w_{a} and w_{b} are even, half-sample symmetric extension can be used at the boundaries of a column vector of fine samples for a balanced decomposition

to ensure a perfect reconstruction only using the regular reconstruction filters from **p** and **q**. A similar proof can be outlined to show that odd values of w_{a} and w_{b} imply the use of whole-sample symmetric extension instead.

3.2.4 Further Demonstration by Example

The example in this subsection illustrates the use of decomposition filter vectors of odd width for a balanced decomposition as opposed to the even width of decomposition filter vectors in the previous example (sections 3.2.1 and 3.2.2). Further examples are provided in appendix A.

Balanced decomposition. Here we demonstrate our general approach described in subsection 3.2.1 using the decomposition filter vectors **a** and **b** from following set of local regular multiresolution filters [BS00, SBO07]:

$$\begin{cases} \mathbf{a} &= \begin{bmatrix} \frac{1}{8} & -\frac{1}{2} & \frac{3}{8} & 1 & \frac{3}{8} & -\frac{1}{2} & \frac{1}{8} \end{bmatrix}, \\ \mathbf{b} &= \begin{bmatrix} -\frac{1}{8} & \frac{1}{2} & -\frac{3}{4} & \frac{1}{2} & -\frac{1}{8} \end{bmatrix}, \\ \mathbf{p} &= \begin{bmatrix} \frac{1}{8} & \frac{1}{2} & \frac{3}{4} & \frac{1}{2} & \frac{1}{8} \end{bmatrix}, \\ \mathbf{q} &= \begin{bmatrix} \frac{1}{8} & \frac{1}{2} & \frac{3}{8} & -1 & \frac{3}{8} & \frac{1}{2} & \frac{1}{8} \end{bmatrix}. \end{cases} \tag{3.15}$$

The filter vectors in equation (3.15) are known as the *inverse powers of two* filters of cubic (fourth order) B-spline [SBO07]. We explain the balanced decomposition process using the decomposition filter vectors in equation (3.15) through the example shown in Fig. 3.6. Similar to the previous example shown in Fig. 3.1, here we have a column vector of 8 fine samples $F = \begin{bmatrix} f_1 & f_2 & \dots & f_8 \end{bmatrix}^T$ that we want to decompose into the column vectors of coarse samples $C = \begin{bmatrix} c_1 & c_2 & c_3 & c_4 \end{bmatrix}^T$ and detail samples $D = \begin{bmatrix} d_1 & d_2 & d_3 & d_4 \end{bmatrix}^T$.

Fig. 3.6 shows one possible balanced decomposition using our general approach presented in section 3.2.1. Step 1 of our *general construction* given in section 3.2.1 reveals that 5 extra samples are required to ensure a balanced decomposition. As noted earlier, w_{a} and

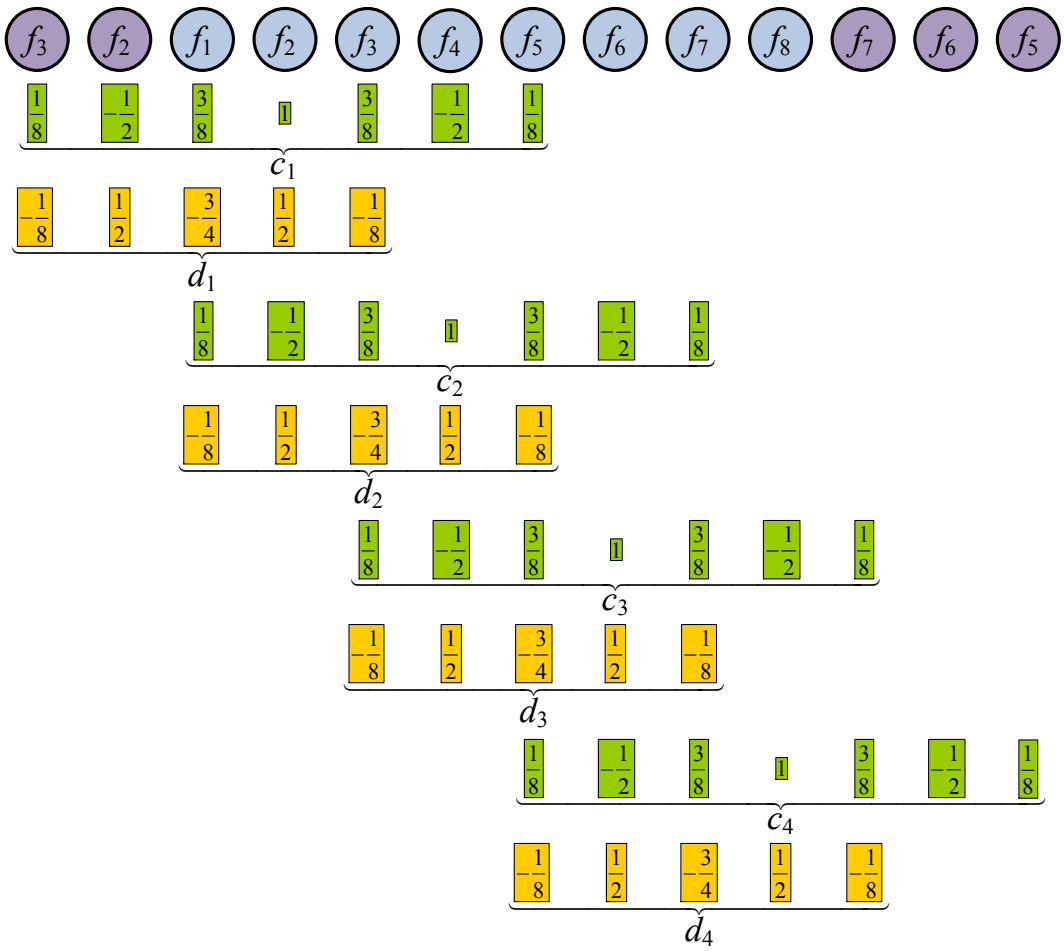

Figure 3.6: Balanced decomposition of 8 fine samples using the decomposition filter vectors **a** and **b** from equation (3.15).

w_{b} for the filter vectors in equation (3.15) are odd. For this reason, according to step 2, whole-sample symmetric extension is used to introduce 2 extra samples at one end and 3 extra samples at the other end of F to obtain the extended column vector of fine samples $F' = \begin{bmatrix} f_3 & f_2 & f_1 & f_2 & \dots & f_8 & f_7 & f_6 & f_5 \end{bmatrix}^T$. Finally, according to step 3, the filter vectors **a** and **b** from equation (3.15) are applied to F' to obtain C and D by means of the equations $C = \mathbf{A}F'$ and $D = \mathbf{B}F'$, analogous to equations (2.6) and (2.7).

Therefore, for $n \in \mathbb{Z}^+$, a balanced multiresolution scheme based on the *inverse powers of*

two filters of cubic B-spline given in equation (3.15) can make use of the matrix equations

$$\begin{bmatrix} c_1 \\ c_2 \\ \vdots \\ c_n \end{bmatrix} = \begin{bmatrix} \frac{1}{8} & -\frac{1}{2} & \frac{3}{8} & 1 & \frac{3}{8} & -\frac{1}{2} & \frac{1}{8} & 0 & 0 & 0 & \cdots \\ 0 & 0 & \frac{1}{8} & -\frac{1}{2} & \frac{3}{8} & 1 & \frac{3}{8} & -\frac{1}{2} & \frac{1}{8} & 0 & \cdots \\ \vdots & \vdots & \vdots & \vdots & \vdots & \vdots & \vdots & \vdots & \vdots & \vdots & \ddots \end{bmatrix} \begin{bmatrix} f_3 \\ f_2 \\ f_1 \\ f_2 \\ \vdots \\ f_{2n-1} \\ f_{2n} \\ f_{2n-1} \\ f_{2n-2} \\ f_{2n-3} \end{bmatrix}$$

and

$$\begin{bmatrix} d_1 \\ d_2 \\ \vdots \\ d_n \end{bmatrix} = \begin{bmatrix} -\frac{1}{8} & \frac{1}{2} & -\frac{3}{4} & \frac{1}{2} & -\frac{1}{8} & 0 & 0 & 0 & \cdots \\ 0 & 0 & -\frac{1}{8} & \frac{1}{2} & -\frac{3}{4} & \frac{1}{2} & -\frac{1}{8} & 0 & \cdots \\ \vdots & \vdots & \vdots & \vdots & \vdots & \vdots & \vdots & \vdots & \ddots \end{bmatrix} \begin{bmatrix} f_3 \\ f_2 \\ f_1 \\ f_2 \\ \vdots \\ f_{2n-1} \\ f_{2n} \\ f_{2n-1} \end{bmatrix}$$

for the decomposition process, analogous to equations (2.6) and (2.7).

Perfect reconstruction. Here we demonstrate our general approach described in subsection 3.2.2 using the reconstruction filter vectors **p** and **q** given in equation (3.15). They can reverse the application of the decomposition filters vectors **a** and **b** from equation (3.15). Given the column vectors of coarse samples $C = \begin{bmatrix} c_1 & c_2 & c_3 & c_4 \end{bmatrix}^T$ and detail samples $D = \begin{bmatrix} d_1 & d_2 & d_3 & d_4 \end{bmatrix}^T$ (obtained as shown in Fig. 3.6), we now want to perfectly

reconstruct the column vector fine samples $F = \begin{bmatrix} f_1 & f_2 & \dots & f_8 \end{bmatrix}^T$.

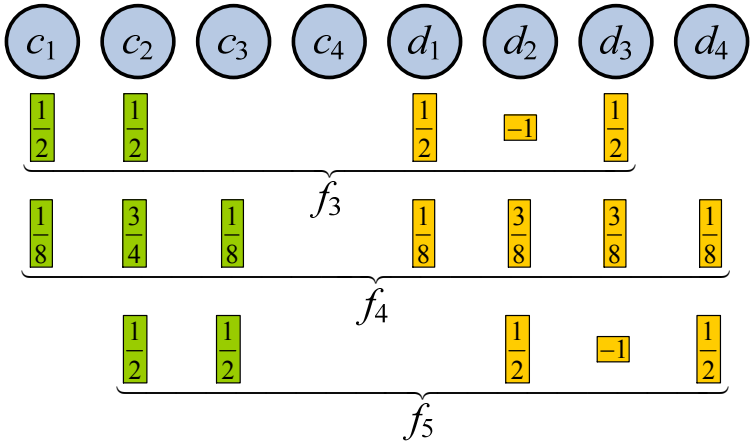

Figure 3.7: Perfect reconstruction of 3 of the 8 fine samples using the reconstruction filter vectors **p** and **q** from equation (3.15).

Fig. 3.7 shows the reconstruction of $F_m = \begin{bmatrix} f_3 & f_4 & f_5 \end{bmatrix}^T$ according to step 1 of our *general construction* given in section 3.2.2. $F_l = \begin{bmatrix} f_1 & f_2 \end{bmatrix}^T$ and $F_r = \begin{bmatrix} f_6 & f_7 & f_8 \end{bmatrix}^T$ are yet to be reconstructed.

Next, following step 2(a) of our given *general construction*, we form the following system of 2 linear equations in 2 unknowns (f_1 and f_2 in F_l):

$$\begin{cases} c_1 &= \frac{1}{8}f_3 - \frac{1}{2}f_2 + \frac{3}{8}f_1 + f_2 + \frac{3}{8}f_3 - \frac{1}{2}f_4 + \frac{1}{8}f_5, \\ d_1 &= -\frac{1}{8}f_3 + \frac{1}{2}f_2 - \frac{3}{4}f_1 + \frac{1}{2}f_2 - \frac{1}{8}f_3. \end{cases} \tag{3.16}$$

The equations in (3.16) were obtained from Fig. 3.6, which shows how c_1 and d_1 were computed during decomposition. Note that in (3.16), we can replace f_3, f_4, and f_5 with the corresponding linear combinations of coarse and detail samples from Fig. 3.7. Then following step 2(b), solving the 2×2 system formed by the equations in (3.16) gives

$$\begin{cases} f_1 &= c_1 - d_1 + d_2, \\ f_2 &= \frac{7}{8}c_1 + \frac{1}{8}c_2 + \frac{3}{8}d_1 + \frac{1}{2}d_2 + \frac{1}{8}d_3. \end{cases} \tag{3.17}$$

Now, according to step 2(c), the equations in (3.17) can be rewritten as follows such that the coefficients of the coarse and detail samples are all regular filters from equation (3.15):

$$\begin{cases} f_1 &= \frac{1}{2}c_1 + \frac{1}{2}c_1 + \frac{1}{2}d_2 + (-1)d_1 + \frac{1}{2}d_2, \\ f_2 &= \frac{1}{8}c_1 + \frac{3}{4}c_1 + \frac{1}{8}c_2 + \frac{1}{8}d_2 + \frac{3}{8}d_1 + \frac{3}{8}d_2 + \frac{1}{8}d_3. \end{cases} \tag{3.18}$$

This rewriting required two implicit sample split operations on the right-hand side of each equation in (3.18).

Finally, following step 3 of our *general construction* to reconstruct F_r, we form the following system of 3 linear equations in 3 unknowns (f_6, f_7, and f_8 in F_r):

$$\begin{cases} c_3 &= \frac{1}{8}f_3 - \frac{1}{2}f_4 + \frac{3}{8}f_5 + f_6 + \frac{3}{8}f_7 - \frac{1}{2}f_8 + \frac{1}{8}f_7, \\ c_4 &= \frac{1}{8}f_5 - \frac{1}{2}f_6 + \frac{3}{8}f_7 + f_8 + \frac{3}{8}f_7 - \frac{1}{2}f_6 + \frac{1}{8}f_5, \\ d_4 &= -\frac{1}{8}f_5 + \frac{1}{2}f_6 - \frac{3}{4}f_7 + \frac{1}{2}f_8 - \frac{1}{8}f_7. \end{cases} \tag{3.19}$$

The equations in (3.19) were obtained from Fig. 3.6, which shows how c_3, c_4, and d_4 were evaluated during decomposition. Observe that in (3.19), we can replace f_3, f_4, and f_5 with the corresponding linear combinations of coarse and detail samples from Fig. 3.7. Then solving the 3×3 system formed by the equations in (3.19) gives

$$\begin{cases} f_6 &= \frac{1}{8}c_2 + \frac{3}{4}c_3 + \frac{1}{8}c_4 + \frac{1}{8}d_2 + \frac{3}{8}d_3 + \frac{1}{2}d_4, \\ f_7 &= \frac{1}{2}c_3 + \frac{1}{2}c_4 + \frac{1}{2}d_3 - \frac{1}{2}d_4, \\ f_8 &= \frac{1}{4}c_3 + \frac{3}{4}c_4 + \frac{1}{4}d_3 + \frac{3}{4}d_4. \end{cases} \tag{3.20}$$

Now, the equations in (3.20) can be rewritten as follows such that the coefficients of the

coarse and detail samples are all regular filters from equation (3.15):

$$\begin{cases} f_6 &= \frac{1}{8}c_2 + \frac{3}{4}c_3 + \frac{1}{8}c_4 + \frac{1}{8}d_2 + \frac{3}{8}d_3 + \frac{3}{8}d_4 + \frac{1}{8}d_4, \\ f_7 &= \frac{1}{2}c_3 + \frac{1}{2}c_4 + \frac{1}{2}d_3 + (-1)d_4 + \frac{1}{2}d_4, \\ f_8 &= \frac{1}{8}c_3 + \frac{3}{4}c_4 + \frac{1}{8}c_3 + \frac{1}{8}d_3 + \frac{3}{8}d_4 + \frac{3}{8}d_4 + \frac{1}{8}d_3. \end{cases} \tag{3.21}$$

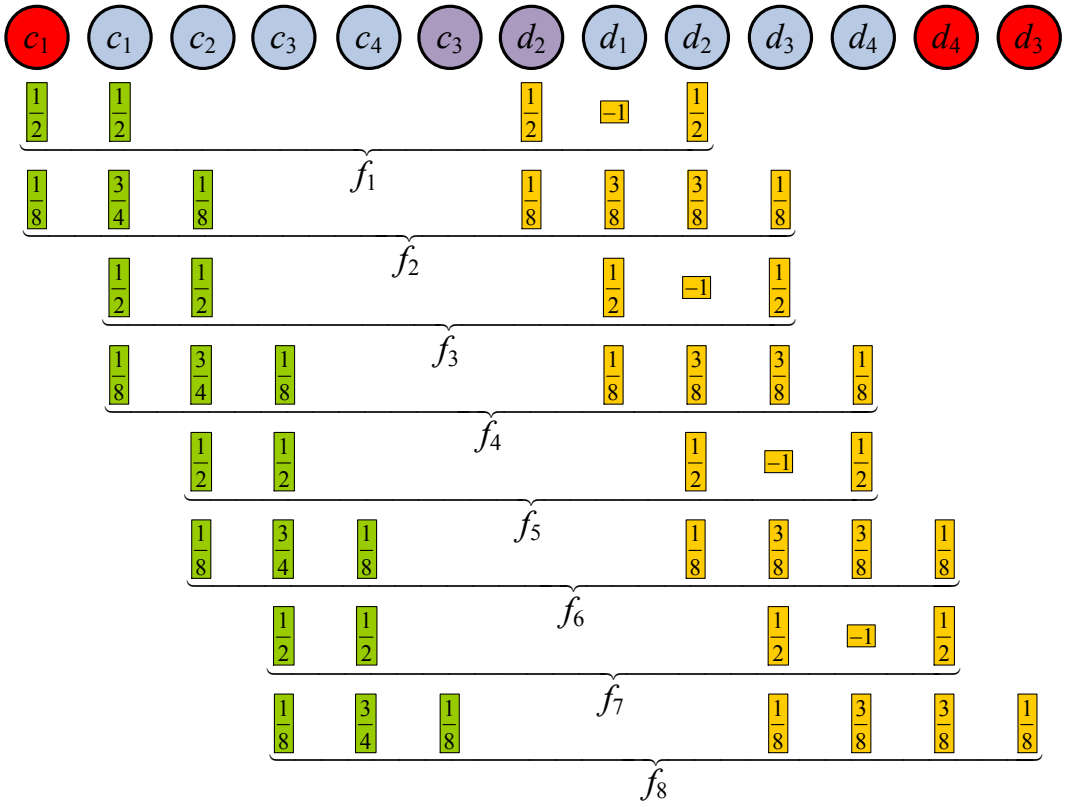

Figure 3.8: Perfect reconstruction of 8 fine samples using the decomposition filter vectors **a** and **b** from equation (3.15).

As we mentioned in the *general construction* given in section 3.2.2, note that the equations in (3.18) and (3.21) yield a specific type of symmetric extension for each boundary of C and D as shown in Fig. 3.8. Therefore, based on (3.18) and (3.21), for a given column vector of

$2n$ fine samples ($n \in \mathbb{Z}^+$), we get

$$\begin{cases} f_1 &= \frac{1}{2}c_1 + \frac{1}{2}c_1 + \frac{1}{2}d_2 + (-1)d_1 + \frac{1}{2}d_2, \\ f_2 &= \frac{1}{8}c_1 + \frac{3}{4}c_1 + \frac{1}{8}c_2 + \frac{1}{8}d_2 + \frac{3}{8}d_1 + \frac{3}{8}d_2 + \frac{1}{8}d_3, \\ f_{2n-2} &= \frac{1}{8}c_{n-2} + \frac{3}{4}c_{n-1} + \frac{1}{8}c_n + \frac{1}{8}d_{n-2} + \frac{3}{8}d_{n-1} + \frac{3}{8}d_n + \frac{1}{8}d_n, \\ f_{2n-1} &= \frac{1}{2}c_{n-1} + \frac{1}{2}c_n + \frac{1}{2}d_{n-1} + (-1)d_n + \frac{1}{2}d_n, \\ f_{2n} &= \frac{1}{8}c_{n-1} + \frac{3}{4}c_n + \frac{1}{8}c_{n-1} + \frac{1}{8}d_{n-1} + \frac{3}{8}d_n + \frac{3}{8}d_n + \frac{1}{8}d_{n-1}. \end{cases}$$

As a result, a balanced multiresolution scheme based on the *inverse powers of two* filters of cubic B-spline given in equation (3.15) can make use of the matrix equation

$$\begin{bmatrix} f_1 \\ f_2 \\ \vdots \\ f_{2n} \end{bmatrix} = \begin{bmatrix} \frac{1}{2} & \frac{1}{2} & 0 & \cdots & 0 & 0 & 0 & 0 & 0 \\ \frac{1}{8} & \frac{3}{4} & \frac{1}{8} & \cdots & 0 & 0 & 0 & 0 & 0 \\ \vdots & \vdots & \vdots & \ddots & \vdots & \vdots & \vdots & \vdots & \vdots \\ 0 & 0 & 0 & \cdots & 0 & \frac{1}{8} & \frac{3}{4} & \frac{1}{8} & 0 \\ 0 & 0 & 0 & \cdots & 0 & 0 & \frac{1}{2} & \frac{1}{2} & 0 \\ 0 & 0 & 0 & \cdots & 0 & 0 & \frac{1}{8} & \frac{3}{4} & \frac{1}{8} \end{bmatrix} \begin{bmatrix} c_1 \\ c_1 \\ c_2 \\ \vdots \\ c_{n-1} \\ c_n \\ c_{n-1} \end{bmatrix} + \begin{bmatrix} \frac{1}{2} & -1 & \frac{1}{2} & 0 & \cdots & 0 & 0 & 0 & 0 & 0 \\ \frac{1}{8} & \frac{3}{8} & \frac{3}{8} & \frac{1}{8} & \cdots & 0 & 0 & 0 & 0 & 0 \\ \vdots & \vdots & \vdots & \vdots & \ddots & \vdots & \vdots & \vdots & \vdots & \vdots \\ 0 & 0 & 0 & 0 & \cdots & \frac{1}{8} & \frac{3}{8} & \frac{3}{8} & \frac{1}{8} & 0 \\ 0 & 0 & 0 & 0 & \cdots & 0 & \frac{1}{2} & -1 & \frac{1}{2} & 0 \\ 0 & 0 & 0 & 0 & \cdots & 0 & \frac{1}{8} & \frac{3}{8} & \frac{3}{8} & \frac{1}{8} \end{bmatrix} \begin{bmatrix} d_2 \\ d_1 \\ d_2 \\ \vdots \\ d_{n-1} \\ d_n \\ d_n \\ d_{n-1} \end{bmatrix} \tag{3.22}$$

for the reconstruction process, analogous to equation (2.8).

3.3 Discussion

Not using the type of symmetric extension suggested by our *general construction* in subsection 3.2.1 to obtain the extra fine samples required for a balanced decomposition may lead to the use of extraordinary boundary filters. For the sake of comparison, we used half-sample symmetric extension in place of the suggested whole-sample symmetric extension to obtain the five extra fine samples required for a balanced decomposition using the decomposition

filter vectors in equation (A.3), which contains the *wide* and *optimal* filters of cubic B-spline. This led to the following matrix equation for a perfect reconstruction, both $\mathbf{P}$ and $\mathbf{Q}$ matrices containing unwanted extraordinary boundary filters:

$$
\begin{bmatrix} f_1 \\ f_2 \\ \vdots \\ f_{2n} \end{bmatrix} = \left[\begin{array}{cccccccc}
\frac{11}{10} & -\frac{1}{10} & 0 & \cdots & 0 & 0 & 0 & 0 \\
\frac{9}{10} & \frac{1}{10} & 0 & \cdots & 0 & 0 & 0 & 0 \\
\hline
\frac{1}{2} & \frac{1}{2} & 0 & \cdots & 0 & 0 & 0 & 0 \\
\frac{1}{8} & \frac{3}{4} & \frac{1}{8} & \cdots & 0 & 0 & 0 & 0 \\
\vdots & \vdots & \vdots & \ddots & \vdots & \vdots & \vdots & \vdots \\
0 & 0 & 0 & \cdots & \frac{1}{8} & \frac{3}{4} & \frac{1}{8} & 0 \\
0 & 0 & 0 & \cdots & 0 & \frac{1}{2} & \frac{1}{2} & 0 \\
\hline
0 & 0 & 0 & \cdots & 0 & \frac{1199}{9730} & \frac{1472}{1946} & \frac{84}{695} \\
0 & 0 & 0 & \cdots & 0 & -\frac{69}{9730} & \frac{1019}{1946} & \frac{336}{695} \\
0 & 0 & 0 & \cdots & 0 & -\frac{23}{1946} & \frac{401}{1946} & \frac{112}{139}
\end{array}\right] \begin{bmatrix} c_1 \\ c_2 \\ \vdots \\ c_n \end{bmatrix}
$$

$$
+ \left[\begin{array}{cccccccccc}
\frac{263}{52} & -\frac{82}{65} & \frac{23}{260} & 0 & \cdots & 0 & 0 & 0 & 0 \\
\frac{37}{52} & -\frac{33}{65} & -\frac{23}{260} & 0 & \cdots & 0 & 0 & 0 & 0 \\
\hline
-\frac{23}{52} & 1 & -\frac{23}{52} & 0 & \cdots & 0 & 0 & 0 & 0 \\
-\frac{23}{208} & -\frac{63}{208} & -\frac{63}{208} & -\frac{23}{208} & \cdots & 0 & 0 & 0 & 0 \\
\vdots & \vdots & \vdots & \vdots & \ddots & \vdots & \vdots & \vdots & \vdots \\
0 & 0 & 0 & 0 & \cdots & -\frac{23}{208} & -\frac{63}{208} & -\frac{63}{208} & -\frac{23}{208} \\
0 & 0 & 0 & 0 & \cdots & 0 & -\frac{23}{52} & 1 & -\frac{23}{52} \\
\hline
0 & 0 & 0 & 0 & \cdots & 0 & -\frac{27577}{252980} & -\frac{566}{1807} & -\frac{4841}{19460} \\
0 & 0 & 0 & 0 & \cdots & 0 & \frac{1587}{252980} & -\frac{874}{1807} & \frac{307743}{252980} \\
0 & 0 & 0 & 0 & \cdots & 0 & \frac{529}{50596} & -\frac{391}{1807} & \frac{5281}{50596}
\end{array}\right] \begin{bmatrix} d_1 \\ d_2 \\ \vdots \\ d_n \end{bmatrix}
$$

in place of equation (A.4). Note that such extraordinary boundary filters in $\mathbf{P}$ and $\mathbf{Q}$ matrices do not allow the anticipated sample split operations that yield suitable symmetric/antisymmetric extensions to use for C and D for a perfect reconstruction only by the use of regular filters.

Our method can be used to devise a balanced multiresolution scheme for any set of given regular multiresolution filter vectors. However, if the scheme would only make use of regular reconstruction filters is determined by the properties of the given multiresolution filter vectors. If the given filter vectors are symmetric/antisymmetric, then our method can devise a balanced multiresolution scheme that only uses regular filters. Otherwise, some extraordinary boundary reconstruction filters are introduced (see appendix B, for instance).

The balanced multiresolution schemes devised by our approach can also be applied to open curves and tensor product meshes (surfaces and volumes) in applications where boundary interpolation is not important but a balanced decomposition is preferred, for reasons such as partitioning the curve or the mesh into *even* and *odd* vertices. Such a partitioning allows the storage of coarse vertices and details in even and odd vertices, respectively, as proposed in [OSB07]. However, some of the devised balanced multiresolution schemes may support boundary interpolation only in the context of subdivision i.e. when we only consider the result of $\mathbf{P}C'$ in order to increase the resolution of C. For example, the filters of second order B-spline in equation (A.1) and the *short* filters of third order B-spline in equation (3.1) lead to such boundary interpolating subdivisions.

3.4 Summary

In this chapter, we presented our general construction for devising a BMR scheme from a given set of symmetric/antisymmetric regular multiresolution filters. Our presented methodology uses a compatible combination of symmetric/antisymmetric extensions near fine image, coarse image, and detail boundaries, which correlate to performing sample split operations. We

also provided a proof outline justifying our choice of symmetric extension for a balanced decomposition leading to a perfect reconstruction without the use of extraordinary boundary filters. Furthermore, we included two example BMR schemes devised by our method — one for odd-width and another for even-width decomposition filter vectors.

Chapter 4

Reversible Integer-to-Integer Balanced Wavelet Transform

The balanced multiresolution (BMR) framework we presented in chapter 3 provides a mathematically clean and computationally efficient way for on-demand reconstruction of regions of interest (ROIs) in a low-resolution image from a previously constructed balanced wavelet transform (BWT) of the high-resolution version of that image. However, the BWT of an image consists of floating-point values (i.e. real values) as opposed to the original image that is composed of integer intensity values. This happens because typically, the decomposition filters used in the construction of BWTs are floating-point values. Therefore, BWTs map real values (including integers) to real values in general. In this chapter, we extend our BMR framework to construct reversible *balanced integer wavelet transforms* (BIWTs) from a given symmetric/antisymmetric decomposition filter vector of width less or equal to four.

4.1 Problem Definition

Given a symmetric/antisymmetric decomposition filter vector $\mathbf{a}$ with $w_{\mathrm{a}} \leq 4$, devise a balanced multiresolution scheme applicable to a column vector of fine (high-resolution) integer samples F that satisfies:

(i) the decomposition of F produces a column vector of coarse (low-resolution) integer samples C and a column vector of detail integer samples D, where $C \approx \mathbf{A}F'$ (i.e. C is approximately equal to $\mathbf{A}F'$), $F \rightarrow F'$ by the use of symmetric extensions at its boundaries, and the nonzero entries in each row of $\mathbf{A}$ correspond to the regular filters

in the given decomposition filter vector **a**;

(*ii*) $sizeof(C) = sizeof(D)$ i.e. a balanced decomposition;

(*iii*) $sizeof(C) + sizeof(D) = sizeof(F)$ i.e. a compact representation of the resulting balanced integer wavelet transform (BIWT);

(*iv*) the resulting BIWT is reversible i.e. F can be perfectly reconstructed from C' and D', where $C \rightarrow C'$ and $D \rightarrow D'$ by the use of symmetric/antisymmetric extensions at their boundaries; and

(*v*) no extraordinary boundary filters are used for the balanced decomposition and perfect reconstruction of F.

4.2 Methodology

In this section, we explain and demonstrate by examples how our method achieves balanced decomposition and subsequent perfect reconstruction while mapping integers to integers.

4.2.1 Balanced Decomposition

Method overview. Given a symmetric/antisymmetric decomposition filter vector **a** with $w_{\mathrm{a}} \leq 4$, to achieve a balanced decomposition of a column vector F containing an even number of fine integer samples, first an extended column vector F' is obtained from F through symmetric extension at its boundaries, based on the value and parity of w_{a}, which represents the width of **a**. Next, to obtain each coarse integer sample, we perturb the coarse real sample suggested by **a** such that it becomes an integer. To accomplish this, we rewrite the linear combination of the contributing fine integer samples suggested by **a** using optimal sample split operations, with an added application of a rounding operator. This rewriting step translates an intermediate integer sample, represented by an affine integer combination of some of the contributing fine samples, to obtain the final coarse integer sample closely approximating the

coarse real sample suggested by **a**. The translation vectors moving the intermediate integer samples to the locations of the final coarse integer samples give us the detail integer samples. Minimizing the length of such translation vectors dictates the optimality of the sample split operations in the prior rewriting step. To guarantee local perfect reconstruction, we construct every other detail sample differently, resulting in alternating rewriting steps for every other coarse sample.

Demonstration by example. Before we outline the general construction for the balanced decomposition process, here we demonstrate by means of an example how it works for a given decomposition filter vector **a**. In this example, we consider the decomposition filter vector **a** from the first equation in (3.1), which is a part of the *short*, local, regular multiresolution filters of quadratic (third order) B-spline [SBO07, SB04]:

$$\mathbf{a} = \begin{bmatrix} -\frac{1}{4} & \frac{3}{4} & \frac{3}{4} & -\frac{1}{4} \end{bmatrix}. \tag{4.1}$$

Recall from section 2.5 that filter vector **a** contain the nonzero entries in a representative row of analysis filter matrix **A**.

For the sake of demonstration, assume that we are given a fine column vector of $2n$ integer samples $F = \begin{bmatrix} f_1 & f_2 & \dots & f_{2n} \end{bmatrix}^T$ for a suitably large $n \in \mathbb{Z}^+$, on which we have to perform a balanced decomposition. Provided $sizeof(F) = 2n$, a balanced decomposition should result in column vectors of coarse integer samples $C = \begin{bmatrix} c_1 & c_2 & \dots & c_n \end{bmatrix}^T$ and detail integer samples $D = \begin{bmatrix} d_1 & d_2 & \dots & d_n \end{bmatrix}^T$.

First, we determine the number of extra samples required to obtain F' from F based on value and parity of w_{a}, for which we make use of equation 3.3. However, equation 3.3 also requires the value of w_{b}, which represents the width of filter vector **b**. Recall from section 2.5 that filter vector **b** contains the nonzero entries in a representative row of analysis filter matrix **B**. Based on our proposed construction, the filter values in our intended **b** filter vector operate on either some or all of the same fine integer samples that the filter values

from **a** from equation (4.1) will operate on; therefore,

$$w_{\mathrm{b}} \leq w_{\mathrm{a}}. \tag{4.2}$$

Now, because $w_{\mathrm{a}} = 4$ for the given filter vector **a**, the inequality in (4.2) implies,

$$max(w_{\mathrm{a}}, w_{\mathrm{b}}) = 4. \tag{4.3}$$

Furthermore, as stated in section 3.2.1, for the families of multiresolution filters we consider in this thesis, w_{a} and w_{b} are either both even or both odd (see [SBO07, CDF92, Dau92, Mey90], for example), which makes both w_{a} and w_{b} even in this example. Now, provided their even parity and equation 4.3,

$$F' = \begin{bmatrix} f_1 & f_1 & f_2 & \dots & f_{2n} & f_{2n} \end{bmatrix}^T \tag{4.4}$$

is obtained based on equation (3.3) to determine that two extra samples required for a balanced decomposition and section 3.2.3 to use of half-sample symmetric extensions for introducing the extra samples.

Next, based on the given decomposition filter vector **a** in equation (4.1), a real coarse sample c_i^r can be written as a linear combination of fine integer samples, f_j, f_{j+1}, f_{j+2}, and f_{j+3} as follows:

$$c_i^r = -\frac{1}{4}f_j + \frac{3}{4}f_{j+1} + \frac{3}{4}f_{j+2} - \frac{1}{4}f_{j+3}. \tag{4.5}$$

Now, as suggested in the *method overview* above, we rewrite the right-hand side of equation 4.5 such that coarse real sample c_i^r represents the translation an intermediate integer sample, represented by an affine integer combination of some of the contributing fine samples, implying

$$c_i^r = c_i' + d_i', \tag{4.6}$$

where c_i' and d_i' represent the intermediate integer sample and the translation vector, respectively. Note that now applying a rounding operator on the translation vector d_i' will produce our intended coarse integer sample c_i closely approximating the coarse real sample c_i^r. This

justifies the rewriting step of our methodology. Next, we want to obtain the corresponding detail integer sample d_i. For this, we rewrite d'_i in equation 4.6 as λd_i, implying

$$c_i^r = c'_i + \lambda d_i, \tag{4.7}$$

when substituted in equation 4.6, where $\lambda \in \mathbb{R}$ and the coefficients of the fine samples contributing to d_i are all integers, making d_i an integer. The requirement that the coefficients in d_i are all integers in equation (4.7), however, restricts the family of given symmetric/antisymmetric decomposition filter vectors that our method can process – if the filter values in $\mathbf{a}$ are not rational numbers, formation of d_i with all integer coefficients in equation (4.7) is not guaranteed.

With c'_i and d_i both being integers in equation (4.7), the only term that contributes to c_i^r not always being an integer is the scalar value λ. Therefore, we adjust the length of the translation vector λd_i with a rounding operator (here, the *floor* operator) to obtain an integer coarse sample c_i as follows:

$$c_i = c'_i + \lfloor \lambda d_i \rfloor . \tag{4.8}$$

While forming the intermediate integer sample c'_i in equation (4.7), we try to minimize the value of detail integer sample d_i because smaller detail values contribute toward better compression efficiency. Furthermore, because c_i in equation (4.8) is obtained by rewriting the linear combination of fine integer samples for c_i^r from equation (4.5), with only an added application of a rounding operator, we argue that c_i is a good approximation of c_i^r.

As indicated above, we want to find a c'_i that optimally minimizes d_i. In other words, the intended c'_i should minimize $\|d_i\|_2$. From equation (4.7), we get,

$$d_i = \frac{1}{\lambda}\,(c_i^r - c'_i). \tag{4.9}$$

Therefore,

$$\min \|d_i\|_2 = \min \left\| \frac{1}{\lambda}\,(c_i^r - c'_i) \right\|_2 \Rightarrow \min \|c_i^r - c'_i\|_2. \tag{4.10}$$

We can write c_i' from equation (4.7) as an affine integer combination of the involved fine samples as follows:

$$c_i' = \alpha_1 f_j + \alpha_2 f_{j+1} + \alpha_3 f_{j+2} + \alpha_4 f_{j+3}, \tag{4.11}$$

where $\alpha_1 + \alpha_2 + \alpha_3 + \alpha_4 = 1$. Then by substituting the values of c_i^r from equation (4.5) and c_i' from equation (4.11) in the function from (4.10), we get,

$$\begin{aligned}
&\min \|c_i^r - c_i'\|_2 \\
=\ &\min \left\| \left(-\frac{1}{4} f_j + \frac{3}{4} f_{j+1} + \frac{3}{4} f_{j+2} - \frac{1}{4} f_{j+3} \right) - (\alpha_1 f_j + \alpha_2 f_{j+1} + \alpha_3 f_{j+2} + \alpha_4 f_{j+3}) \right\|_2 \\
=\ &\min \left\| \left(-\frac{1}{4} - \alpha_1 \right) f_j + \left(\frac{3}{4} - \alpha_2 \right) f_{j+1} + \left(\frac{3}{4} - \alpha_3 \right) f_{j+2} + \left(-\frac{1}{4} - \alpha_4 \right) f_{j+3} \right\|_2 \\
=\ &\min \left\{ \left(-\tfrac{1}{4} - \alpha_1\right)^2 f_j^2 + \left(\tfrac{3}{4} - \alpha_2\right)^2 f_{j+1}^2 + \left(\tfrac{3}{4} - \alpha_3\right)^2 f_{j+2}^2 + \left(-\tfrac{1}{4} - \alpha_4\right)^2 f_{j+3}^2 \right\}.
\end{aligned} \tag{4.12}$$

The assumption that the given fine integer samples are uniformly distributed allows treating them as constants and makes the function in (4.12) imply

$$\min \left\{ \left(-\frac{1}{4} - \alpha_1 \right)^2 + \left(\frac{3}{4} - \alpha_2 \right)^2 + \left(\frac{3}{4} - \alpha_3 \right)^2 + \left(-\frac{1}{4} - \alpha_4 \right)^2 \right\}. \tag{4.13}$$

Because $w_{\mathrm{a}} = 4$ and the dilation factor is 2, the last $w_{\mathrm{a}} - 2 = 2$ fine samples that contribute to the construction of c_i, namely f_{j+2} and f_{j+3}, will also contribute as the first two fine samples in the construction of c_{i+1}. For this reason, in function (4.13), for c_i', we set α_1 and α_2 to 0 because they do not correspond to the last two fine samples contributing in the construction of c_i. For c_i, that makes $\alpha_3 + \alpha_4 = 1$ in function (4.13), where $\alpha_3, \alpha_4 \in \mathbb{Z}_{\neq 0}$. We require α_3 and α_4 to be nonzero because we want the corresponding fine integer samples to contribute in the construction of c_i'. Alternatively, in function (4.13), for c_{i+1}', we set α_3 and α_4 to 0 because they do not correspond to the first two fine samples contributing in the construction of c_{i+1}. For c_{i+1}, that makes $\alpha_1 + \alpha_2 = 1$, where $\alpha_1, \alpha_2 \in \mathbb{Z}_{\neq 0}$. The steps described in this paragraph cause alternating definitions detail samples and makes local perfect reconstruction possible. However, it affects the achievable minimum value of d_i in equation (4.8).

As mentioned above, setting α_1 and α_2 to 0 in function (4.13), we obtain,

$$\begin{aligned} & \min\left\{\frac{1}{16}+\frac{9}{16}+\left(\frac{3}{4}-\alpha_3\right)^2+\left(-\frac{1}{4}-\alpha_4\right)^2\right\} \\ \Rightarrow\ & \min\left\{\left(\frac{3}{4}-\alpha_3\right)^2+\left(-\frac{1}{4}-\alpha_4\right)^2\right\}. \end{aligned} \tag{4.14}$$

Provided $\alpha_3 = 1 - \alpha_4$, by substituting the value of α_3 in function (4.14), we get,

$$\begin{aligned} & \min\left\{\left(\frac{3}{4}-1+\alpha_4\right)^2+\left(-\frac{1}{4}-\alpha_4\right)^2\right\} \\ =\ & \min\left\{\left(-\frac{1}{4}+\alpha_4\right)^2+\left(-\frac{1}{4}-\alpha_4\right)^2\right\} \\ =\ & \min\left(\frac{1}{16}-\frac{1}{2}\alpha_4+\alpha_4^2+\frac{1}{16}+\frac{1}{2}\alpha_4+\alpha_4^2\right) \\ =\ & \min\left(2\alpha_4^2+\frac{1}{8}\right) \end{aligned} \tag{4.15}$$

Through a simple exhaustive search along the integer number line on both sides of 0, we find that

$$\min\left(2\alpha_4^2+\frac{1}{8}\right)=\frac{17}{8}, \tag{4.16}$$

where $\alpha_4 = -1$, making $\alpha_3 = 1 - \alpha_4 = 2$. Substituting the values of α_1, α_2, α_3, and α_4 in equation (4.11), we get,

$$c_i' = 2f_{j+2} - f_{j+3}. \tag{4.17}$$

If we rewrite the right-hand side of equation (4.5) in the form of that of equation (4.7) and then substitute the value of c_i' from equation (4.17), we get,

$$c_i^r = (2f_{j+2} - f_{j+3}) + \frac{1}{4}\left(-f_j + 3f_{j+1} - 5f_{j+2} + 3f_{j+3}\right), \tag{4.18}$$

revealing

$$\lambda = \frac{1}{4} \tag{4.19}$$

and

$$d_i = -f_j + 3f_{j+1} - 5f_{j+2} + 3f_{j+3}. \tag{4.20}$$

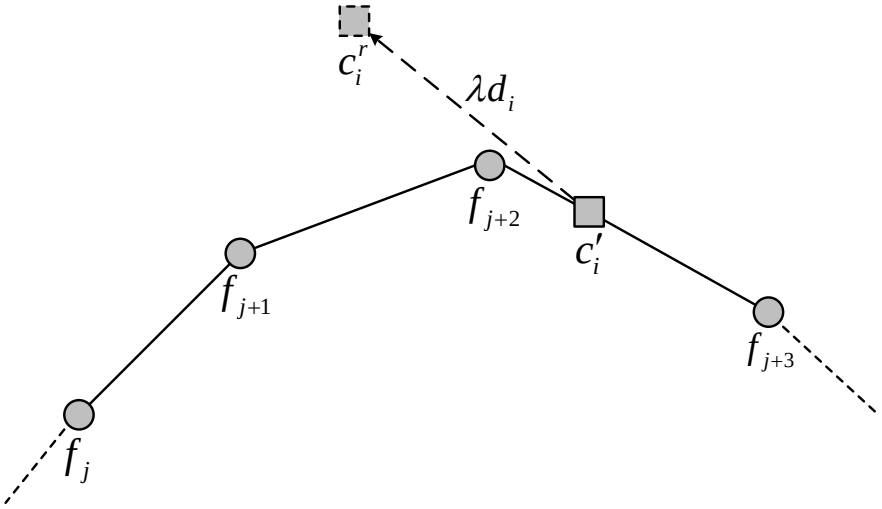

(a) The coarse real sample c_i^r is suggested by the given **a** as a linear combination of fine integer samples $f_j \ldots f_{j+3}$. Here, c_i^r is shown as a translation of an intermediate integer sample c_i', which is an affine integer combination of f_{j+2} and f_{j+3}. λd_i is the associated translation vector, where d_i is our desired detail integer sample.

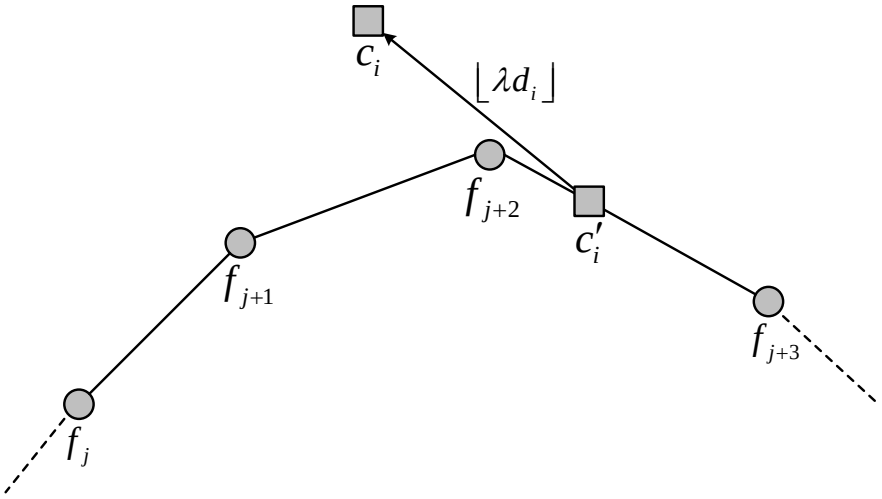

(b) The length of the translation vector is adjusted using a floor operator to obtain a coarse integer sample c_i in place of the coarse real sample c_i^r.

Figure 4.1: Construction of a coarse and a detail integer sample.

Obtaining equation (4.18) from equation (4.5) is equivalent to employing two sample split operations on fine integer samples f_{j+2} and f_{j+3}. Finally, substituting the values of λ from equation (4.19), c'_i from equation (4.17), and d_i from equation (4.20) in equation (4.8), we obtain the coarse integer sample,

$$c_i = (2f_{j+2} - f_{j+3}) + \left\lfloor \frac{1}{4}(-f_j + 3f_{j+1} - 5f_{j+2} + 3f_{j+3}) \right\rfloor. \tag{4.21}$$

Fig. 4.1 shows pictorial representations of c^r_i, λd_i, c'_i, and c_i from equations (4.18), (4.19), (4.20), (4.17), and (4.21), respectively, in an attempt to demonstrate how c_i and d_i are constructed.

Now, in a similar manner, based on the next coarse real sample,

$$c^r_{i+1} = -\frac{1}{4}f_{j+2} + \frac{3}{4}f_{j+3} + \frac{3}{4}f_{j+4} - \frac{1}{4}f_{j+5}, \tag{4.22}$$

we can show that the next coarse integer sample,

$$c_{i+1} = (-f_{j+2} + 2f_{j+3}) + \left\lfloor \frac{1}{4}(3f_{j+2} - 5f_{j+3} + 3f_{j+4} - f_{j+5}) \right\rfloor, \tag{4.23}$$

where

$$c'_{i+1} = \alpha_1 f_{j+2} + \alpha_2 f_{j+3} + \alpha_3 f_{j+4} + \alpha_4 f_{j+5} = -f_{j+2} + 2f_{j+3} \tag{4.24}$$

with $\alpha_1 = -1$, $\alpha_2 = 2$, $\alpha_3 = 0$, and $\alpha_4 = 0$, and

$$d_{i+1} = 3f_{j+2} - 5f_{j+3} + 3f_{j+4} - f_{j+5}. \tag{4.25}$$

It is important to note that while finding the values of α_1 and α_2 for c_{i+1}, we enforce that vector $[\ \alpha_1\ \ \alpha_2\ ]$ for c'_{i+1} is linearly independent of the vector $[\ \alpha_3\ \ \alpha_4\ ]$ for c'_i. This allows us to form linear systems of independent equations for the perfect reconstruction of fine integer samples, f_{j+2} and f_{j+3}, as demonstrated later in section 4.2.2.

For demonstration purposes, based on the the definitions of F', c_i, and c_{i+1} in equations (4.4), (4.21) and (4.23), respectively, we show a balanced decomposition of 16 fine integer samples i.e. for $n = 16$ in (D.3). The relationship between the indices of the coarse and detail

integer samples and the corresponding fine integer samples in (D.3) allows us to generalize the recipe for the devised balanced decomposition method for the given decomposition filter vector $\mathbf{a}$ as follows:

$$
\begin{cases}
c_1 = (-f_1 + 2f_1) + \left\lfloor \frac{1}{4} \underbrace{(3f_1 - 5f_1 + 3f_2 - f_3)}_{d_1} \right\rfloor, \\
c_2 = (2f_4 - f_5) + \left\lfloor \frac{1}{4} \underbrace{(-f_2 + 3f_3 - 5f_4 + 3f_5)}_{d_2} \right\rfloor, \\
\vdots \\
c_i = (2f_{2i} - f_{2i+1}) + \left\lfloor \frac{1}{4} \underbrace{(-f_{2i-2} + 3f_{2i-1} - 5f_{2i} + 3f_{2i+1})}_{d_i} \right\rfloor, \\
c_{i+1} = (-f_{2i} + 2f_{2i+1}) + \left\lfloor \frac{1}{4} \underbrace{(3f_{2i} - 5f_{2i+1} + 3f_{2i+2} - f_{2i+3})}_{d_{i+1}} \right\rfloor, \\
\vdots \\
c_{n-1} = (-f_{2n-4} + 2f_{2n-3}) + \left\lfloor \frac{1}{4} \underbrace{(3f_{2n-4} - 5f_{2n-3} + 3f_{2n-2} - f_{2n-1})}_{d_{n-1}} \right\rfloor, \\
c_n = (2f_{2n} - f_{2n}) + \left\lfloor \frac{1}{4} \underbrace{(-f_{2n-2} + 3f_{2n-1} - 5f_{2n} + 3f_{2n})}_{d_n} \right\rfloor.
\end{cases}
\tag{4.26}
$$

Because the indices of coarse, detail, and fine integer samples in (4.26) are all written in terms of i, where i is an even index in $\{2, \ldots, n\}$, it facilitates straightforward, on-demand, random-access to the coarse and detail integer samples corresponding to fine integer samples of interest. From application point of view, it makes locating detail integer samples of interest within the hierarchy of details in a BIWT simple and efficient.

For another example of balanced decomposition using given Haar decomposition filters [Haa10, SDS96], see the second and third columns of table C.1.

General construction. Now we present our general approach for achieving a balanced decomposition. Given the symmetric/antisymmetric decomposition filter vector,

$$
\mathbf{a} = \begin{bmatrix} a_1 & a_2 & \ldots & a_k \end{bmatrix} \tag{4.27}
$$

with $k \leq 4$, containing only regular filters, carry out the following steps to achieve a balanced decomposition of a fine column vector of integer samples,

$$F = \begin{bmatrix} f_1 & f_2 & \dots & f_{2n} \end{bmatrix}^T, \tag{4.28}$$

where $sizeof(F) = 2n$ for a suitably large $n \in \mathbb{Z}^+$.

1. Assuming $w_{\mathrm{b}} \leq w_{\mathrm{a}}$, determine x, the number of extra samples required for a balanced decomposition using equation (3.3).

2. Assuming w_{b} will have the same parity as w_{a}, if w_{a} is even, extend F with x extra samples using half-sample symmetric extension to obtain F'. Use whole-sample symmetric extension instead if w_{a} is odd. Justification for our choice of symmetric extension can be found in section 3.2.3. To avoid giving inconsistent importance to any end (boundary) of F:

   (a) If x is even, introduce $x/2$ samples at each end of F.

   (b) If x is odd, introduce $\lfloor x/2 \rfloor$ samples at one end and $\lfloor x/2 \rfloor + 1$ samples at the other end of F. Let us refer to the end at which $\lfloor x/2 \rfloor + 1$ samples are introduced as the *odd end*. Alternate between the ends of F as the choice of the odd end during multiple levels of decomposition.

3. Find

$$m = \max(1, m') \tag{4.29}$$

   where m' consecutive fine integer samples contribute in the construction of m' consecutive coarse real samples for $w_{\mathrm{a}} = k$ and dilation factor of 2. Here, $m \in \mathbb{Z}^+$ and $m < k$.

   (In the example above for the given decomposition filter vector in equation (4.1), $m = 2$.)

4. Rewrite each linear combination of fine integer samples suggested by the given decomposi-

tion filter vector $\mathbf{a}$ for a local neighbourhood of m coarse real samples,

$$\begin{bmatrix} c_i^r \\ \vdots \\ c_{i+m-1}^r \end{bmatrix} = \begin{bmatrix} a_1 f_j + a_2 f_{j+1} + \ldots + a_k f_{j+k-1} \\ \vdots \\ a_1 f_{j+2m-2} + a_2 f_{j+2m-1} + \ldots + a_k f_{j+2m+k-3} \end{bmatrix} \tag{4.30}$$

as a translation of an intermediate integer sample by a vector, implying

$$\begin{bmatrix} c_i^r \\ \vdots \\ c_{i+m-1}^r \end{bmatrix} = \underbrace{\begin{bmatrix} c'_i \\ \vdots \\ c'_{i+m-1} \end{bmatrix}}_{\substack{\text{Intermediate} \\ \text{integer samples}}} + \lambda \underbrace{\begin{bmatrix} d_i \\ \vdots \\ d_{i+m-1} \end{bmatrix}}_{\substack{\text{Translation} \\ \text{vectors}}}, \tag{4.31}$$

where the corresponding m intermediate integer samples,

$$\begin{bmatrix} c'_i \\ \vdots \\ c'_{i+m-1} \end{bmatrix} = \begin{bmatrix} \alpha_{11} f_{j+k-m} + \ldots + \alpha_{1m} f_{j+k-1} \\ \vdots \\ \alpha_{m1} f_{j+k-m} + \ldots + \alpha_{mm} f_{j+k-1} \end{bmatrix} \tag{4.32}$$

and the corresponding m detail integer samples,

$$\begin{bmatrix} d_i \\ \vdots \\ d_{i+m-1} \end{bmatrix} = \begin{bmatrix} \beta_{11} f_j + \beta_{12} f_{j+1} + \ldots + \beta_{1k} f_{j+k-1} \\ \vdots \\ \beta_{m1} f_{j+2m-2} + \beta_{m2} f_{j+2m-1} + \ldots + \beta_{mk} f_{j+2m+k-3} \end{bmatrix}, \tag{4.33}$$

such that:

(a) each element of $\begin{bmatrix} c'_i & c'_{i+1} & \ldots & c'_{i+m-1} \end{bmatrix}^T$ in equation (4.32) is an integer affine combination of the same m consecutive fine integer samples $f_{j+k-m}, \ldots, f_{j+k-1}$, implying

$$\begin{cases} \alpha_{11} + \ldots + \alpha_{1m} = 1, \\ \vdots \\ \alpha_{m1} + \ldots + \alpha_{mm} = 1, \end{cases} \tag{4.34}$$

where $\alpha_{xy} \in \mathbb{Z}_{\neq 0}$ for $x, y \in \{1, \ldots, m\}$;

(b) the m vectors formed by the coefficients of the fine integer samples $f_{j+k-m}, \ldots, f_{j+k-1}$ in equation (4.32) are linearly independent i.e. the following vectors are linearly independent:

$$\begin{cases} [\alpha_{11} \ldots \alpha_{1m}], \\ \qquad \vdots \\ [\alpha_{m1} \ldots \alpha_{mm}]; \end{cases} \tag{4.35}$$

(c) for each of the m detail samples in $\begin{bmatrix} d_i & d_{i+1} & \ldots & d_{i+m-1} \end{bmatrix}^T$ from equation (4.33), the coefficients of all contributing fine integer samples are integers i.e. in equation (4.33), $\beta_{xy} \in \mathbb{Z}$ for $x, y \in \{1, \ldots, k\}$, making each detail sample an integer; here, (4.34) implies that

$$\begin{cases} \beta_{11} + \beta_{12} + \ldots + \beta_{1k} = 0, \\ \qquad \vdots \\ \beta_{m1} + \beta_{m2} + \ldots + \beta_{mk} = 0, \end{cases} \tag{4.36}$$

because in equation (4.27), $a_1 + a_2 + \ldots + a_k = 1$; and

(d) each element of $\begin{bmatrix} d_i & d_{i+1} & \ldots & d_{i+m-1} \end{bmatrix}^T$ is minimized by evaluating the function,

$$\min \left\{ \begin{bmatrix} c_i^r \\ \vdots \\ c_{i+m-1}^r \end{bmatrix} - \begin{bmatrix} c_i' \\ \vdots \\ c_{i+m-1}' \end{bmatrix} \right\}. \tag{4.37}$$

(In the example above for the given decomposition filter vector in equation (4.1), equations (4.5) and (4.22) for fine real samples correspond to equation (4.30), equations (4.17) and (4.24) for obtaining intermediate integer samples correspond to equation (4.32), and equations (4.20) and (4.25) for obtaining detail integer samples correspond to equation (4.33) at this step.)

5. By applying a rounding operator (here, the *floor* operator) on the second term in right-hand side of equation (4.31), obtain the corresponding local neighbourhood of m coarse

integer samples as

$$\begin{bmatrix} c_i \\ \vdots \\ c_{i+m-1} \end{bmatrix} = \begin{bmatrix} c'_i \\ \vdots \\ c'_{i+m-1} \end{bmatrix} + \left\lfloor \lambda \begin{bmatrix} d_i \\ \vdots \\ d_{i+m-1} \end{bmatrix} \right\rfloor$$

$$\Rightarrow \begin{bmatrix} c_i \\ \vdots \\ c_{i+m-1} \end{bmatrix} = \begin{bmatrix} \alpha_{11} f_{j+k-m} + \ldots + \alpha_{1m} f_{j+k-1} \\ \vdots \\ \alpha_{m1} f_{j+k-m} + \ldots + \alpha_{mm} f_{j+k-1} \end{bmatrix} + \left\lfloor \lambda \begin{bmatrix} d_i \\ \vdots \\ d_{i+m-1} \end{bmatrix} \right\rfloor, \quad (4.38)$$

after substituting the value of $\begin{bmatrix} c'_i & c'_{i+1} & \ldots & c'_{i+m-1} \end{bmatrix}^T$ from equation (4.32). In equation (4.38), the floor operator on $\lambda \begin{bmatrix} d_i & d_{i+1} & \ldots & d_{i+m-1} \end{bmatrix}^T$ works elementwise i.e. it results in $\begin{bmatrix} \lfloor \lambda d_i \rfloor & \lfloor \lambda d_{i+1} \rfloor & \ldots & \lfloor \lambda d_{i+m-1} \rfloor \end{bmatrix}^T$.

(In the example above for the given decomposition filter vector in equation (4.1), equations (4.21) and (4.23) for obtaining coarse integer samples correspond to equation (4.38) at this step.)

6. Keeping the values of $\alpha_{xy} \in \mathbb{Z}_{\neq 0}$ for $x, y \in \{1, \ldots, m\}$ and $\beta_{xy} \in \mathbb{Z}$ for $x, y \in \{1, \ldots, k\}$ constant, use equations (4.33) and (4.38) to respectively obtain m detail integer samples and m coarse integer samples for each of the n/m representative m-sample neighbourhood of coarse real samples suggested by the application of $\mathbf{a}$ on F'. This will result in n coarse integer samples and n detail integer samples to respectively form the column vectors C and D referred to in section 4.1 as

$$C = \begin{bmatrix} c_1 & c_2 & \ldots & c_n \end{bmatrix}^T \quad (4.39)$$

and

$$D = \begin{bmatrix} d_1 & d_2 & \ldots & d_n \end{bmatrix}^T, \quad (4.40)$$

yielding a balanced decomposition of the column vection of $2n$ fine integer samples F.

4.2.2 Perfect Reconstruction

Method overview. Given the column vectors of coarse and detail integer samples C and D from a prior balanced decomposition of a column vector of fine integer samples F, to achieve a perfect reconstruction of F, we first reconstruct as many interior samples of F as possible taking each k-sample neighbourhood of F into consideration, where $k = w_a$. During the prior balanced decomposition, if m fine integer samples, where $m < k$, contributed to the construction of each intermediate integer sample like c_i in equation (4.17), we form and symbolically solve an $m \times m$ system of linear equations based on the construction of those intermediate integer samples to reconstruct the m contributing fine integer samples in a representative k-sample neighbourhood of F. Next, to reconstruct the other $k - m$ fine integer samples in the k-sample neighbourhood, we form and symbolically solve another $(k - m) \times (k - m)$ system of linear equations based on the prior construction of $k - m$ detail samples from $k - m$ consecutive, overlapping k-sample neighbourhood of F. At this point, we will have a general recipe to perfectly reconstruct an interior k-sample neighbourhood of F.

Finally, if applicable, to perfectly reconstruct the fine integer samples at each boundary of F, we symbolically solve one or more square systems of linear equations that are formed based on the prior construction of some coarse and detail boundary integer samples, to which the unknown fine boundary samples made contributions. By means of sample split operations, we then rewrite the obtained symbolic solutions for the fine boundary samples to match the corresponding parts of the previously obtained general recipe for the reconstruction of an interior k-sample neighbourhood of F. This rewriting step reveals how many extra samples must be introduced via what types of symmetric/antisymmetric extensions to obtain C' and D' from C and D, respectively, to avoid the use of extraordinary boundary reconstruction filters and rounding operators.

Demonstration by example. Here we demonstrate how we perform a perfect reconstruction of F following its balanced decomposition into C and D by means of an example, before

giving the general construction for our perfect reconstruction process. This example to demonstrate our perfect reconstruction process is an extension of the example shown in section 4.2.1. Therefore, from the resulting column vectors of coarse integer samples C from equation (4.39) and detail integer samples D from equation (4.40), we now want to reconstruct the corresponding column vector of fine integer samples F as in equation (4.28).

Based on the definitions of c_i and c_{i+1} from the general recipe for balanced decomposition in (4.26) for the given decomposition filter vector $\mathbf{a}$ in equation (4.1), we can form the following linear system of two equations with two unknowns, f_{2i} and f_{2i+1}, where i is an even index in $\{2, \ldots, n\}$:

$$\begin{cases} 2f_{2i} - f_{2i+1} = c_i - \left\lfloor \frac{d_i}{4} \right\rfloor, \\ -f_{2i} + 2f_{2i+1} = c_{i+1} - \left\lfloor \frac{d_{i+1}}{4} \right\rfloor. \end{cases} \tag{4.41}$$

Symbolically solving the 2×2 system in (4.41) provides us with the following general recipe for perfectly reconstructing the fine integer samples, f_{2i} and f_{2i+1}:

$$\begin{cases} f_{2i} = \frac{2}{3}c_i + \frac{1}{3}c_{i+1} - \frac{2}{3}\left\lfloor \frac{d_i}{4} \right\rfloor - \frac{1}{3}\left\lfloor \frac{d_{i+1}}{4} \right\rfloor, \\ f_{2i+1} = \frac{1}{3}c_i + \frac{2}{3}c_{i+1} - \frac{1}{3}\left\lfloor \frac{d_i}{4} \right\rfloor - \frac{2}{3}\left\lfloor \frac{d_{i+1}}{4} \right\rfloor. \end{cases} \tag{4.42}$$

Based on the general recipe in (4.42), we can obtain the fine integer samples, f_{2i-4} and f_{2i-3} as follows:

$$\begin{cases} f_{2i-4} = \frac{2}{3}c_{i-2} + \frac{1}{3}c_{i-1} - \frac{2}{3}\left\lfloor \frac{d_{i-2}}{4} \right\rfloor - \frac{1}{3}\left\lfloor \frac{d_{i-1}}{4} \right\rfloor, \\ f_{2i-3} = \frac{1}{3}c_{i-2} + \frac{2}{3}c_{i-1} - \frac{1}{3}\left\lfloor \frac{d_{i-2}}{4} \right\rfloor - \frac{2}{3}\left\lfloor \frac{d_{i-1}}{4} \right\rfloor. \end{cases} \tag{4.43}$$

Now that f_{2i-4}, f_{2i-3}, f_{2i}, and f_{2i+1} are all known, based on the definitions of d_{i-1} and d_i from the general recipe in (4.26), we can form the following linear system of two equations with two unknowns, f_{2i-2} and f_{2i-1}:

$$\begin{cases} 3f_{2i-2} - f_{2i-1} = d_{i-1} - 3f_{2i-4} - 5f_{2i-3}, \\ -f_{2i-2} + 3f_{2i-1} = d_i + 5f_{2i} - 3f_{2i+1}. \end{cases} \tag{4.44}$$

Symbolically solving the 2×2 system in (4.44) provides the following general recipe for the

perfect reconstruction of interior fine integer samples, f_{2i-2} and f_{2i-1}:

$$\begin{cases} f_{2i-2} = -\frac{1}{8}c_{i-2} + \frac{7}{8}c_{i-1} + \frac{7}{24}c_i - \frac{1}{24}c_{i+1} + \frac{3}{8}d_{i-1} + \frac{1}{8}d_i + \frac{1}{8}\left\lfloor \frac{d_{i-2}}{4} \right\rfloor - \frac{7}{8}\left\lfloor \frac{d_{i-1}}{4} \right\rfloor - \frac{7}{24}\left\lfloor \frac{d_i}{4} \right\rfloor + \frac{1}{24}\left\lfloor \frac{d_{i+1}}{4} \right\rfloor, \\ f_{2i-1} = -\frac{1}{24}c_{i-2} + \frac{7}{24}c_{i-1} + \frac{7}{8}c_i - \frac{1}{8}c_{i+1} + \frac{1}{8}d_{i-1} + \frac{3}{8}d_i + \frac{1}{24}\left\lfloor \frac{d_{i-2}}{4} \right\rfloor - \frac{7}{24}\left\lfloor \frac{d_{i-1}}{4} \right\rfloor - \frac{7}{8}\left\lfloor \frac{d_i}{4} \right\rfloor + \frac{1}{8}\left\lfloor \frac{d_{i+1}}{4} \right\rfloor. \end{cases} \tag{4.45}$$

Putting together the general recipes from (4.43) and (4.45), we get the following general recipe for perfectly reconstructing a representative 4-sample interior neighbourhood of F:

$$\begin{cases} f_{2i-2} = -\frac{1}{8}c_{i-2} + \frac{7}{8}c_{i-1} + \frac{7}{24}c_i - \frac{1}{24}c_{i+1} + \frac{3}{8}d_{i-1} + \frac{1}{8}d_i + \frac{1}{8}\left\lfloor \frac{d_{i-2}}{4} \right\rfloor - \frac{7}{8}\left\lfloor \frac{d_{i-1}}{4} \right\rfloor - \frac{7}{24}\left\lfloor \frac{d_i}{4} \right\rfloor + \frac{1}{24}\left\lfloor \frac{d_{i+1}}{4} \right\rfloor, \\ f_{2i-1} = -\frac{1}{24}c_{i-2} + \frac{7}{24}c_{i-1} + \frac{7}{8}c_i - \frac{1}{8}c_{i+1} + \frac{1}{8}d_{i-1} + \frac{3}{8}d_i + \frac{1}{24}\left\lfloor \frac{d_{i-2}}{4} \right\rfloor - \frac{7}{24}\left\lfloor \frac{d_{i-1}}{4} \right\rfloor - \frac{7}{8}\left\lfloor \frac{d_i}{4} \right\rfloor + \frac{1}{8}\left\lfloor \frac{d_{i+1}}{4} \right\rfloor, \\ f_{2i} = \frac{2}{3}c_i + \frac{1}{3}c_{i+1} - \frac{2}{3}\left\lfloor \frac{d_i}{4} \right\rfloor - \frac{1}{3}\left\lfloor \frac{d_{i+1}}{4} \right\rfloor, \\ f_{2i+1} = \frac{1}{3}c_i + \frac{2}{3}c_{i+1} - \frac{1}{3}\left\lfloor \frac{d_i}{4} \right\rfloor - \frac{2}{3}\left\lfloor \frac{d_{i+1}}{4} \right\rfloor. \end{cases} \tag{4.46}$$

Here we care about a 4-sample neighbourhood because for the given decomposition filter vector $\mathbf{a}$, $w_a = 4$.

Next, we reconstruct the first fine integer boundary sample f_1 based on the construction of c_1 in (4.26) as follows:

$$\begin{aligned} -f_1 + 2f_1 &= c_1 - \left\lfloor \frac{d_1}{4} \right\rfloor \\ \Rightarrow f_1 &= c_1 - \left\lfloor \frac{d_1}{4} \right\rfloor. \end{aligned} \tag{4.47}$$

Finding c_1 this way is equivalent to solving a 1×1 system of linear equation. The right-hand side of equation (4.47) can be rewritten via two sample split operations as follows:

$$f_1 = \frac{1}{3}c_1 + \frac{2}{3}c_1 - \frac{1}{3}\left\lfloor \frac{d_1}{4} \right\rfloor - \frac{2}{3}\left\lfloor \frac{d_1}{4} \right\rfloor, \tag{4.48}$$

yielding the use of half-sample symmetric extensions for the corresponding boundaries of C and D to be able to only use regular reconstruction filters used in (4.46) for reconstruction purposes (more specifically, compare the definition of f_1 from equation (4.48) with the definition of f_{2i+1} in (4.46)). Furthermore, the reconstruction of the next two fine integer boundary samples, f_2 and f_3 requires symbolically solving the following 2×2 system of linear equations like that in (4.44), formed based on the construction of d_1 and d_2 in (4.26):

$$\begin{cases} 3f_2 - f_3 &= d_1 - 3f_1 + 5f_1, \\ -f_2 + 3f_3 &= d_2 - 5f_4 + 3f_5. \end{cases} \tag{4.49}$$

In (4.49), f_1 is known from equation (4.48), and f_4 and f_5 are known as follows, based on the general recipe for the perfect reconstruction of interior fine integer samples in (4.46):

$$\begin{cases} f_4 = \frac{2}{3}c_2 + \frac{1}{3}c_3 - \frac{2}{3}\left\lfloor \frac{d_2}{4} \right\rfloor - \frac{1}{3}\left\lfloor \frac{d_3}{4} \right\rfloor, \\ f_5 = \frac{1}{3}c_2 + \frac{2}{3}c_3 - \frac{1}{3}\left\lfloor \frac{d_2}{4} \right\rfloor - \frac{2}{3}\left\lfloor \frac{d_3}{4} \right\rfloor. \end{cases}$$

Then by symbolically solving the 2×2 system in (4.49), we obtain

$$\begin{cases} f_2 = \frac{3}{4}c_1 + \frac{7}{24}c_2 - \frac{1}{24}c_3 + \frac{3}{8}d_1 + \frac{1}{8}d_2 - \frac{3}{4}\left\lfloor \frac{d_1}{4} \right\rfloor - \frac{7}{24}\left\lfloor \frac{d_2}{4} \right\rfloor + \frac{1}{24}\left\lfloor \frac{d_3}{4} \right\rfloor, \\ f_3 = \frac{1}{4}c_1 + \frac{7}{8}c_2 - \frac{1}{8}c_3 + \frac{1}{8}d_1 + \frac{3}{8}d_2 - \frac{1}{4}\left\lfloor \frac{d_1}{4} \right\rfloor - \frac{7}{8}\left\lfloor \frac{d_2}{4} \right\rfloor + \frac{1}{8}\left\lfloor \frac{d_3}{4} \right\rfloor, \end{cases} \tag{4.50}$$

and rewrite them via sample split operations as

$$\begin{cases} f_2 = -\frac{1}{8}c_1 + \frac{7}{8}c_1 + \frac{7}{24}c_2 - \frac{1}{24}c_3 + \frac{3}{8}d_1 + \frac{1}{8}d_2 + \frac{1}{8}\left\lfloor \frac{d_1}{4} \right\rfloor - \frac{7}{8}\left\lfloor \frac{d_1}{4} \right\rfloor - \frac{7}{24}\left\lfloor \frac{d_2}{4} \right\rfloor + \frac{1}{24}\left\lfloor \frac{d_3}{4} \right\rfloor, \\ f_3 = -\frac{1}{24}c_1 + \frac{7}{24}c_1 + \frac{7}{8}c_2 - \frac{1}{8}c_3 + \frac{1}{8}d_1 + \frac{3}{8}d_2 + \frac{1}{24}\left\lfloor \frac{d_1}{4} \right\rfloor - \frac{7}{24}\left\lfloor \frac{d_1}{4} \right\rfloor - \frac{7}{8}\left\lfloor \frac{d_2}{4} \right\rfloor + \frac{1}{8}\left\lfloor \frac{d_3}{4} \right\rfloor, \end{cases} \tag{4.51}$$

to only use regular reconstruction filters used in (4.46).

In a similar manner, we can determine last three fine integer boundary samples, namely, f_{2n-2}, f_{2n-1}, and f_{2n} at the other boundary of F. Putting them all together with the findings from (4.46), (4.48), and (4.51), provides the following general recipe for the perfect reconstruction of F from $C' = \begin{bmatrix} c_1 & c_1 & c_2 & \dots & c_n & c_n \end{bmatrix}^T$ and detail integer samples $D' =$

$$\begin{bmatrix} d_1 & d_1 & d_2 & \dots & d_n & d_n \end{bmatrix}^T :$$

$$\begin{cases}
f_1 = \frac{1}{3}c_1 + \frac{2}{3}c_1 - \frac{1}{3}\left\lfloor \frac{d_1}{4} \right\rfloor - \frac{2}{3}\left\lfloor \frac{d_1}{4} \right\rfloor, \\
f_2 = -\frac{1}{8}c_1 + \frac{7}{8}c_1 + \frac{7}{24}c_2 - \frac{1}{24}c_3 + \frac{3}{8}d_1 + \frac{1}{8}d_2 + \frac{1}{8}\left\lfloor \frac{d_1}{4} \right\rfloor - \frac{7}{8}\left\lfloor \frac{d_1}{4} \right\rfloor - \frac{7}{24}\left\lfloor \frac{d_2}{4} \right\rfloor + \frac{1}{24}\left\lfloor \frac{d_3}{4} \right\rfloor, \\
f_3 = -\frac{1}{24}c_1 + \frac{7}{24}c_1 + \frac{7}{8}c_2 - \frac{1}{8}c_3 + \frac{1}{8}d_1 + \frac{3}{8}d_2 + \frac{1}{24}\left\lfloor \frac{d_1}{4} \right\rfloor - \frac{7}{24}\left\lfloor \frac{d_1}{4} \right\rfloor - \frac{7}{8}\left\lfloor \frac{d_2}{4} \right\rfloor + \frac{1}{8}\left\lfloor \frac{d_3}{4} \right\rfloor, \\
\vdots \\
f_{2i-2} = -\frac{1}{8}c_{i-2} + \frac{7}{8}c_{i-1} + \frac{7}{24}c_i - \frac{1}{24}c_{i+1} + \frac{3}{8}d_{i-1} + \frac{1}{8}d_i + \frac{1}{8}\left\lfloor \frac{d_{i-2}}{4} \right\rfloor - \frac{7}{8}\left\lfloor \frac{d_{i-1}}{4} \right\rfloor - \frac{7}{24}\left\lfloor \frac{d_i}{4} \right\rfloor + \frac{1}{24}\left\lfloor \frac{d_{i+1}}{4} \right\rfloor, \\
f_{2i-1} = -\frac{1}{24}c_{i-2} + \frac{7}{24}c_{i-1} + \frac{7}{8}c_i - \frac{1}{8}c_{i+1} + \frac{1}{8}d_{i-1} + \frac{3}{8}d_i + \frac{1}{24}\left\lfloor \frac{d_{i-2}}{4} \right\rfloor - \frac{7}{24}\left\lfloor \frac{d_{i-1}}{4} \right\rfloor - \frac{7}{8}\left\lfloor \frac{d_i}{4} \right\rfloor + \frac{1}{8}\left\lfloor \frac{d_{i+1}}{4} \right\rfloor, \\
f_{2i} = \frac{2}{3}c_i + \frac{1}{3}c_{i+1} - \frac{2}{3}\left\lfloor \frac{d_i}{4} \right\rfloor - \frac{1}{3}\left\lfloor \frac{d_{i+1}}{4} \right\rfloor, \\
f_{2i+1} = \frac{1}{3}c_i + \frac{2}{3}c_{i+1} - \frac{1}{3}\left\lfloor \frac{d_i}{4} \right\rfloor - \frac{2}{3}\left\lfloor \frac{d_{i+1}}{4} \right\rfloor, \\
\vdots \\
f_{2n-2} = -\frac{1}{8}c_{n-2} + \frac{7}{8}c_{n-1} + \frac{7}{24}c_n - \frac{1}{24}c_n + \frac{3}{8}d_{n-1} + \frac{1}{8}d_n + \frac{1}{8}\left\lfloor \frac{d_{n-2}}{4} \right\rfloor - \frac{7}{8}\left\lfloor \frac{d_{n-1}}{4} \right\rfloor - \frac{7}{24}\left\lfloor \frac{d_n}{4} \right\rfloor + \frac{1}{24}\left\lfloor \frac{d_n}{4} \right\rfloor, \\
f_{2n-1} = -\frac{1}{24}c_{n-2} + \frac{7}{24}c_{n-1} + \frac{7}{8}c_n - \frac{1}{8}c_n + \frac{1}{8}d_{n-1} + \frac{3}{8}d_n + \frac{1}{24}\left\lfloor \frac{d_{n-2}}{4} \right\rfloor - \frac{7}{24}\left\lfloor \frac{d_{n-1}}{4} \right\rfloor - \frac{7}{8}\left\lfloor \frac{d_n}{4} \right\rfloor + \frac{1}{8}\left\lfloor \frac{d_n}{4} \right\rfloor, \\
f_{2n} = \frac{2}{3}c_n + \frac{1}{3}c_n - \frac{2}{3}\left\lfloor \frac{d_n}{4} \right\rfloor - \frac{1}{3}\left\lfloor \frac{d_n}{4} \right\rfloor.
\end{cases} \tag{4.52}$$

For another example of perfect reconstruction following a balanced decomposition using given Haar decomposition filters [Haa10, SDS96], see the second and third columns of table C.1.

General construction. Now we describe our general approach to achieve perfect reconstruction. Carry out the following steps to perfectly reconstruct the column vector of $2n$ fine samples F as in equation (4.28) from its prior balanced decomposition into column vectors of n coarse integer samples C as in equation (4.39) and n detail integer samples D as in equation (4.40).

1. Assume that $F = \begin{bmatrix} {F_l}^T & {F_m}^T & {F_r}^T \end{bmatrix}^T$, where ${F_l}^T$ and ${F_r}^T$ respectively contain zero or more samples at the left and right boundaries of F^T, and F_m contains the remaining interior samples of F. Provided $w_a = k$, to devise a general recipe for the perfect reconstruction of a k-sample neighbourhood of F_m:

(a) Form the following $m \times m$ system of linear equations based on how a local neighbourhood of m coarse integer samples was constructed in equation (4.38) during the balanced decomposition process:

$$\begin{bmatrix} \alpha_{11} f_{j+k-m} + \ldots + \alpha_{1m} f_{j+k-1} \\ \vdots \\ \alpha_{m1} f_{j+k-m} + \ldots + \alpha_{mm} f_{j+k-1} \end{bmatrix} = \begin{bmatrix} c_i \\ \vdots \\ c_{i+m-1} \end{bmatrix} - \left\lfloor \lambda \begin{bmatrix} d_i \\ \vdots \\ d_{i+m-1} \end{bmatrix} \right\rfloor . \tag{4.53}$$

Solving the $m \times m$ system in equation (4.53) will provide a general recipe for perfectly reconstructing the m fine samples, $f_{j+k-m}, \ldots, f_{j+k-1}$ from a representative k-sample neighbourhood of F_m.

(b) To devise a general recipe for perfectly reconstructing the remaining $k - m$ fine samples, $f_j, \ldots, f_{j+k-m-1}$ in a representative k-sample neighbourhood of F_m, form and symbolically another $(k - m) \times (k - m)$ system of linear equations based on the prior construction of $k - m$ detail samples from $k - m$ consecutive, overlapping k-sample neighbourhood of F:

$$\begin{bmatrix} \beta_{11} f_j + \beta_{12} f_{j+1} + \ldots + \beta_{1k} f_{j+k-1} \\ \vdots \\ \beta_{m1} f_{j+2m-2} + \beta_{m2} f_{j+2m-1} + \ldots + \beta_{mk} f_{j+2m+k-3} \end{bmatrix} = \begin{bmatrix} d_i \\ \vdots \\ d_{i+m-1} \end{bmatrix} . \tag{4.54}$$

While forming the $(k - m) \times (k - m)$ system of linear equations, substitute the symbolic solution for each fine sample for which the general recipe is already known from either step 1(a).

(In the example above, we had $F_l = \begin{bmatrix} f_1 & f_2 & f_3 \end{bmatrix}^T$, $F_m = \begin{bmatrix} f_4 & f_5 & \ldots & f_{2n-3} \end{bmatrix}^T$, and $F_r = \begin{bmatrix} f_{2n-2} & f_{2n-1} & f_{2n} \end{bmatrix}^T$. The 2×2 systems in (4.41) and (4.44) were formed and symbolically solved as per steps 1(a) and 1(b), respectively.)

2. Provided F_l is not empty, to reconstruct the samples in F_l:

(a) Form and symbolically solve one or more square systems of linear equations based on the prior construction of some coarse and detail boundary integer samples, to which the fine samples in F_l made some contributions during the decomposition process. While forming these square systems of linear equations, substitute the symbolic solution for each fine sample for which the general recipe is already known from either step 1 or the already completed part of this current step.

(For example, see the 1×1 system in equation (4.47) and the 2×2 system in (4.49).)

(b) Solving the systems formed in step 2(a) symbolically will evaluate each sample in F_l as a symbolic solution in terms of some boundary samples from C and D.

(For example, see equation (4.47) and the two equations in (4.50).)

(c) Rewrite the symbolic solution(s) referred to in step 2(b) using the regular reconstruction filters used in the general recipe obtained for a representative k-sample neighbourhood of F_m in step 1. Such rewriting here correlates to performing sample split operations. This will reveal the following two pieces of information applicable to the left boundaries of C and D for a perfect reconstruction: (i) the type of symmetric/antisymmetric extension that must be used and (ii) the number of extra samples that must be to introduced to avoid the use of extraordinary boundary reconstruction filters and operators.

(For example, see equation (4.48) and the equations in (4.51).)

3. Use an approach similar to that in step 2 to reconstruct the samples in F_r if F_r is not empty.

Note that steps 2-3 above allow the generation of C' and D' respectively from C and D, such that condition (iv) of the problem definition given in section 4.1 is satisfied.

4.2.3 Error Metric

The error caused by the use rounding operator in our proposed balanced decomposition process can be characterized by the column vector of scalars

$$E = \begin{bmatrix} e_1 & e_2 & \dots & e_n \end{bmatrix}^T = \mathbf{A}F' - C,$$

where $|e_i| < 1$ with $i \in \{1 \dots n\}$ for a suitably large $n \in \mathbb{Z}^+$. Here, $e_i = c_i^r - c_i$, is a vector representing the difference between the coarse real sample c_i^r (an element of $\mathbf{A}F'$) and the obtained coarse integer sample c_i.

4.3 Discussion

In this section, we explain how our presented decomposition and reconstruction processes differ from those in a conventional multiresolution framework governed by equations (2.6), (2.7), and (2.8). If we disregard the effect of rounding operator in our presented balanced decomposition and perfect reconstruction processes applicable to BIWTs, we end up with a multiresolution framework represented by the following three equations, like those for our balanced multiresolution framework in section 3.1, analogous to equations (2.6), (2.7), and (2.8), respectively:

$$C = \mathbf{A}F', \tag{4.55}$$

$$D = \mathbf{B}^*F', \tag{4.56}$$

$$F = \mathbf{P}^*C' + \mathbf{Q}^*D'. \tag{4.57}$$

Note that in equations (4.55) and (4.56), C and D are columns vectors of coarse and detail real samples, respectively, due to disregarding the effect of rounding operator.

The nonzero entries in a representative row of the analysis filter matrix $\mathbf{A}$ in equation (4.55) is represented by the given symmetric/antisymmetric filter vector $\mathbf{a}$. However, our presented framework forms and uses a new analysis filter matrix $\mathbf{B}^*$ in equation (4.56) and new synthesis

filter matrices $\mathbf{P}^*$ and $\mathbf{Q}^*$ in equation (4.57). The $\mathbf{B}^*$, $\mathbf{P}^*$, and $\mathbf{Q}^*$ filter matrices are still of banded, repetitive, and slanted structure but each of them will require two filter vectors to represent the nonzero entries in their alternating representative columns. Let us demonstrate that by example. For the balanced decomposition example in section 4.2.1, equations (4.55) and (4.56) with the corresponding values of each filter matrix and column vector of samples substituted will look like

$$\begin{bmatrix} c_1 \\ c_2 \\ \vdots \\ c_n \end{bmatrix} = \begin{bmatrix} -\frac{1}{4} & \frac{3}{4} & \frac{3}{4} & -\frac{1}{4} & 0 & 0 & 0 & \cdots \\ 0 & 0 & -\frac{1}{4} & \frac{3}{4} & \frac{3}{4} & -\frac{1}{4} & 0 & \cdots \\ \vdots & \vdots & \vdots & \vdots & \vdots & \vdots & \vdots & \ddots \end{bmatrix} \begin{bmatrix} f_1 \\ f_1 \\ f_2 \\ \vdots \\ f_{2n-1} \\ f_{2n} \\ f_{2n} \end{bmatrix}$$

and

$$\begin{bmatrix} d_1 \\ d_2 \\ \vdots \\ d_n \end{bmatrix} = \begin{bmatrix} 3 & -5 & 3 & -1 & 0 & 0 & 0 & \cdots \\ 0 & 0 & -1 & 3 & -5 & 3 & 0 & \cdots \\ \vdots & \vdots & \vdots & \vdots & \vdots & \vdots & \vdots & \ddots \end{bmatrix} \begin{bmatrix} f_1 \\ f_1 \\ f_2 \\ \vdots \\ f_{2n-1} \\ f_{2n} \\ f_{2n} \end{bmatrix}, \tag{4.58}$$

respectively, where the decomposition filter vectors are as follows:

$$\begin{cases} \mathbf{a} = \begin{bmatrix} -\frac{1}{4} & \frac{3}{4} & \frac{3}{4} & -\frac{1}{4} \end{bmatrix}, \\ \mathbf{b}_{\text{odd}} = \mathbf{b} = \begin{bmatrix} 3 & -5 & 3 & -1 \end{bmatrix}, \\ \mathbf{b}_{\text{even}} = \mathbf{b}^R = \begin{bmatrix} -1 & 3 & -5 & 3 \end{bmatrix}. \end{cases} \tag{4.59}$$

Here, the nonzero entries in alternating representative rows of $\mathbf{B}^*$ are represented by decomposition filter vectors $\mathbf{b}_{\text{odd}} = \mathbf{b}$ and $\mathbf{b}_{\text{even}} = \mathbf{b}^R$, meaning that $\mathbf{b}$ and $\mathbf{b}^R$ represent the nonzero entries in the odd and even numbered rows of $\mathbf{B}^*$, respectively. On the other hand, for the perfect reconstruction example in section 4.2.2, if we disregard the rounding operations in (4.52), we obtain

$$
\begin{cases}
f_1 = \frac{1}{3}c_1 + \frac{2}{3}c_1 - \frac{1}{12}d_1 - \frac{1}{6}d_1, \\
f_2 = -\frac{1}{8}c_1 + \frac{7}{8}c_1 + \frac{7}{24}c_2 - \frac{1}{24}c_3 + \frac{1}{32}d_1 + \frac{5}{32}d_1 + \frac{5}{96}d_2 + \frac{1}{96}d_3, \\
f_3 = -\frac{1}{24}c_1 + \frac{7}{24}c_1 + \frac{7}{8}c_2 - \frac{1}{8}c_3 + \frac{1}{96}d_1 + \frac{5}{96}d_1 + \frac{5}{32}d_2 + \frac{1}{32}d_3, \\
\vdots \\
f_{2i-2} = -\frac{1}{8}c_{i-2} + \frac{7}{8}c_{i-1} + \frac{7}{24}c_i - \frac{1}{24}c_{i+1} + \frac{1}{32}d_{i-2} + \frac{5}{32}d_{i-1} + \frac{5}{96}d_i + \frac{1}{96}d_{i+1}, \\
f_{2i-1} = -\frac{1}{24}c_{i-2} + \frac{7}{24}c_{i-1} + \frac{7}{8}c_i - \frac{1}{8}c_{i+1} + \frac{1}{96}d_{i-2} + \frac{5}{96}d_{i-1} + \frac{5}{32}d_i + \frac{1}{32}d_{i+1}, \\
f_{2i} = \frac{2}{3}c_i + \frac{1}{3}c_{i+1} - \frac{1}{6}d_i - \frac{1}{12}d_{i+1}, \\
f_{2i+1} = \frac{1}{3}c_i + \frac{2}{3}c_{i+1} - \frac{1}{12}d_i - \frac{1}{6}d_{i+1}, \\
\vdots \\
f_{2n-2} = -\frac{1}{8}c_{n-2} + \frac{7}{8}c_{n-1} + \frac{7}{24}c_n - \frac{1}{24}c_n + \frac{1}{32}d_{n-2} + \frac{5}{32}d_{n-1} + \frac{5}{96}d_n + \frac{1}{96}d_n, \\
f_{2n-1} = -\frac{1}{24}c_{n-2} + \frac{7}{24}c_{n-1} + \frac{7}{8}c_n - \frac{1}{8}c_n + \frac{1}{96}d_{n-2} + \frac{5}{96}d_{n-1} + \frac{5}{32}d_n + \frac{1}{32}d_n, \\
f_{2n} = \frac{2}{3}c_n + \frac{1}{3}c_n - \frac{1}{6}d_n - \frac{1}{12}d_n,
\end{cases}
\tag{4.60}
$$

leading to

$$\begin{bmatrix} f_1 \\ f_2 \\ \vdots \\ f_{2n} \end{bmatrix} = \begin{bmatrix} \frac{1}{3} & \frac{2}{3} & 0 & 0 & 0 & 0 & \cdots & 0 & 0 & 0 & 0 \\ -\frac{1}{8} & \frac{7}{8} & \frac{7}{24} & -\frac{1}{24} & 0 & 0 & \cdots & 0 & 0 & 0 & 0 \\ -\frac{1}{24} & \frac{7}{24} & \frac{7}{8} & -\frac{1}{8} & 0 & 0 & \cdots & 0 & 0 & 0 & 0 \\ 0 & 0 & \frac{2}{3} & \frac{1}{3} & 0 & 0 & \cdots & 0 & 0 & 0 & 0 \\ 0 & 0 & \frac{1}{3} & \frac{2}{3} & 0 & 0 & \cdots & 0 & 0 & 0 & 0 \\ 0 & 0 & -\frac{1}{8} & \frac{7}{8} & \frac{7}{24} & -\frac{1}{24} & \cdots & 0 & 0 & 0 & 0 \\ 0 & 0 & -\frac{1}{24} & \frac{7}{24} & \frac{7}{8} & -\frac{1}{8} & \cdots & 0 & 0 & 0 & 0 \\ \vdots & \vdots & \vdots & \vdots & \vdots & \vdots & \ddots & \vdots & \vdots & \vdots & \vdots \\ 0 & 0 & 0 & 0 & 0 & 0 & \cdots & \frac{1}{3} & \frac{2}{3} & 0 & 0 \\ 0 & 0 & 0 & 0 & 0 & 0 & \cdots & -\frac{1}{8} & \frac{7}{8} & \frac{7}{24} & -\frac{1}{24} \\ 0 & 0 & 0 & 0 & 0 & 0 & \cdots & -\frac{1}{24} & \frac{7}{24} & \frac{7}{8} & -\frac{1}{8} \\ 0 & 0 & 0 & 0 & 0 & 0 & \cdots & 0 & 0 & \frac{2}{3} & \frac{1}{3} \end{bmatrix} \begin{bmatrix} c_1 \\ c_1 \\ c_2 \\ \vdots \\ c_n \\ c_n \end{bmatrix}$$

$$+ \begin{bmatrix} -\frac{1}{12} & -\frac{1}{6} & 0 & 0 & 0 & 0 & \cdots & 0 & 0 & 0 & 0 \\ \frac{1}{32} & \frac{5}{32} & \frac{5}{96} & \frac{1}{96} & 0 & 0 & \cdots & 0 & 0 & 0 & 0 \\ \frac{1}{96} & \frac{5}{96} & \frac{5}{32} & \frac{1}{32} & 0 & 0 & \cdots & 0 & 0 & 0 & 0 \\ 0 & 0 & -\frac{1}{6} & -\frac{1}{12} & 0 & 0 & \cdots & 0 & 0 & 0 & 0 \\ 0 & 0 & -\frac{1}{12} & -\frac{1}{6} & 0 & 0 & \cdots & 0 & 0 & 0 & 0 \\ 0 & 0 & \frac{1}{32} & \frac{5}{32} & \frac{5}{96} & \frac{1}{96} & \cdots & 0 & 0 & 0 & 0 \\ 0 & 0 & \frac{1}{96} & \frac{5}{96} & \frac{5}{32} & \frac{1}{32} & \cdots & 0 & 0 & 0 & 0 \\ \vdots & \vdots & \vdots & \vdots & \vdots & \vdots & \ddots & \vdots & \vdots & \vdots & \vdots \\ 0 & 0 & 0 & 0 & 0 & 0 & \cdots & -\frac{1}{12} & -\frac{1}{6} & 0 & 0 \\ 0 & 0 & 0 & 0 & 0 & 0 & \cdots & \frac{1}{32} & \frac{5}{32} & \frac{5}{96} & \frac{1}{96} \\ 0 & 0 & 0 & 0 & 0 & 0 & \cdots & \frac{1}{96} & \frac{5}{96} & \frac{5}{32} & \frac{1}{32} \\ 0 & 0 & 0 & 0 & 0 & 0 & \cdots & 0 & 0 & -\frac{1}{6} & -\frac{1}{12} \end{bmatrix} \begin{bmatrix} d_1 \\ d_1 \\ d_2 \\ \vdots \\ d_n \\ d_n \end{bmatrix}, \tag{4.61}$$

for equation (4.57) with the corresponding values of each filter matrix and column vector of

samples substituted. For $\mathbf{P}^*$ and $\mathbf{Q}^*$ in equation (4.61), the reconstruction filter vectors are

$$\begin{cases} \mathbf{p}_{\text{odd}} = \mathbf{p} = \begin{bmatrix} \frac{7}{24} & \frac{7}{8} & \frac{2}{3} & \frac{1}{3} & -\frac{1}{8} & -\frac{1}{24} \end{bmatrix}, \\ \mathbf{p}_{\text{even}} = \mathbf{p}^R = \begin{bmatrix} -\frac{1}{24} & -\frac{1}{8} & \frac{1}{3} & \frac{2}{3} & \frac{7}{8} & \frac{7}{24} \end{bmatrix}, \\ \mathbf{q}_{\text{odd}} = \mathbf{q} = \begin{bmatrix} \frac{5}{96} & \frac{5}{32} & -\frac{1}{6} & -\frac{1}{12} & \frac{1}{32} & \frac{1}{96} \end{bmatrix}, \\ \mathbf{q}_{\text{even}} = \mathbf{q}^R = \begin{bmatrix} \frac{1}{96} & \frac{1}{32} & -\frac{1}{12} & -\frac{1}{6} & \frac{5}{32} & \frac{5}{96} \end{bmatrix}. \end{cases} \tag{4.62}$$

Therefore, the nonzero entries in alternating representative columns of $\mathbf{P}^*$ are represented by reconstruction filter vectors $\mathbf{p}_{\text{odd}} = \mathbf{p}$ and $\mathbf{p}_{\text{even}} = \mathbf{p}^R$, meaning that $\mathbf{p}$ and $\mathbf{p}^R$ represent the nonzero entries in the odd and even numbered columns of $\mathbf{P}^*$, respectively. Likewise, $\mathbf{q}$ and $\mathbf{q}^R$ represent the nonzero entries in the odd and even numbered columns of $\mathbf{Q}^*$, respectively.

Note that only $\mathbf{a}$ in (4.59) is symmetric; $\mathbf{b}$ in (4.59) and $\mathbf{p}$ and $\mathbf{q}$ in (4.62) are neither symmetric nor antisymmetric. However, still the alternating representative row setup for $\mathbf{B}^*$ in equation (4.58) and the alternating representative columns setup for $\mathbf{P}^*$ and $\mathbf{Q}^*$ in equation (4.61) managed to use symmetric extensions for extending C, D, and F to offer a balanced decomposition and subsequent perfect reconstruction without the use of any extraordinary boundary filters. This constitutes an important finding with regards to extending the family of multiresolution filter vectors for which we can consider devising balanced multiresolution schemes without introducing extraordinary boundary filters.

On a separate note, in our presented general construction for a balanced decomposition, it is possible to set the m consecutive, intermediate integer samples in equation (4.32) to m consecutive fine integer samples i.e.

$$\begin{bmatrix} c'_i \\ \vdots \\ c'_{i+m-1} \end{bmatrix} = \begin{bmatrix} f_{j+k-m} \\ \vdots \\ f_{j+k-1} \end{bmatrix}. \tag{4.63}$$

Such a setup requires symbolically solving m 1×1 systems instead of one $m \times m$ system in step 1(a) of the general construction for devising the recipe for perfect reconstruction we

presented in section 4.2.2. The general recipe for a balanced decomposition under such a setup for the give decomposition filter vector in equation (4.1) will look like

$$
\begin{cases}
c_1 = f_1 + \left\lfloor \frac{1}{4} \underbrace{(-f_1 - f_1 + 3f_2 - f_3)}_{d_1} \right\rfloor, \\
c_2 = f_4 + \left\lfloor \frac{1}{4} \underbrace{(-f_2 + 3f_3 - f_4 - f_5)}_{d_2} \right\rfloor, \\
\vdots \\
c_i = f_{2i} + \left\lfloor \frac{1}{4} \underbrace{(-f_{2i-2} + 3f_{2i-1} - f_{2i} - f_{2i+1})}_{d_i} \right\rfloor, \\
c_{i+1} = f_{2i+1} + \left\lfloor \frac{1}{4} \underbrace{(-f_{2i} - f_{2i+1} + 3f_{2i+2} - f_{2i+3})}_{d_{i+1}} \right\rfloor, \\
\vdots \\
c_{n-1} = f_{2n-3} + \left\lfloor \frac{1}{4} \underbrace{(-f_{2n-4} - f_{2n-3} + 3f_{2n-2} - f_{2n-1})}_{d_{n-1}} \right\rfloor, \\
c_n = f_{2n} + \left\lfloor \frac{1}{4} \underbrace{(-f_{2n-2} + 3f_{2n-1} - f_{2n} - f_{2n})}_{d_n} \right\rfloor,
\end{cases}
\tag{4.64}
$$

with the corresponding general recipe for a perfect reconstruction as follows:

$$\begin{cases} f_1 = c_1 - \left\lfloor \frac{d_1}{4} \right\rfloor, \\ f_2 = \frac{3}{8}c_1 + \frac{3}{8}c_1 + \frac{1}{8}c_2 + \frac{1}{8}c_3 + \frac{3}{8}d_1 + \frac{1}{8}d_2 - \frac{3}{8}\left\lfloor \frac{d_1}{4} \right\rfloor - \frac{3}{8}\left\lfloor \frac{d_1}{4} \right\rfloor - \frac{1}{8}\left\lfloor \frac{d_2}{4} \right\rfloor - \frac{1}{8}\left\lfloor \frac{d_3}{4} \right\rfloor, \\ f_3 = \frac{1}{8}c_1 + \frac{1}{8}c_1 + \frac{3}{8}c_2 + \frac{3}{8}c_3 + \frac{1}{8}d_1 + \frac{3}{8}d_2 - \frac{1}{8}\left\lfloor \frac{d_1}{4} \right\rfloor - \frac{1}{8}\left\lfloor \frac{d_1}{4} \right\rfloor - \frac{3}{8}\left\lfloor \frac{d_2}{4} \right\rfloor - \frac{3}{8}\left\lfloor \frac{d_3}{4} \right\rfloor, \\ \vdots \\ f_{2i-2} = \frac{3}{8}c_{i-2} + \frac{3}{8}c_{i-1} + \frac{1}{8}c_i + \frac{1}{8}c_{i+1} + \frac{3}{8}d_{i-1} + \frac{1}{8}d_i - \frac{3}{8}\left\lfloor \frac{d_{i-2}}{4} \right\rfloor - \frac{3}{8}\left\lfloor \frac{d_{i-1}}{4} \right\rfloor - \frac{1}{8}\left\lfloor \frac{d_i}{4} \right\rfloor - \frac{1}{8}\left\lfloor \frac{d_{i+1}}{4} \right\rfloor, \\ f_{2i-1} = \frac{1}{8}c_{i-2} + \frac{1}{8}c_{i-1} + \frac{3}{8}c_i - \frac{3}{8}c_{i+1} + \frac{1}{8}d_{i-1} + \frac{3}{8}d_i - \frac{1}{8}\left\lfloor \frac{d_{i-2}}{4} \right\rfloor - \frac{1}{8}\left\lfloor \frac{d_{i-1}}{4} \right\rfloor - \frac{3}{8}\left\lfloor \frac{d_i}{4} \right\rfloor - \frac{3}{8}\left\lfloor \frac{d_{i+1}}{4} \right\rfloor, \\ f_{2i} = c_i - \left\lfloor \frac{d_i}{4} \right\rfloor, \\ f_{2i+1} = c_{i+1} - \left\lfloor \frac{d_{i+1}}{4} \right\rfloor, \\ \vdots \\ f_{2n-2} = \frac{3}{8}c_{n-2} + \frac{3}{8}c_{n-1} + \frac{1}{8}c_n + \frac{1}{8}c_n + \frac{3}{8}d_{n-1} + \frac{1}{8}d_n - \frac{3}{8}\left\lfloor \frac{d_{n-2}}{4} \right\rfloor - \frac{3}{8}\left\lfloor \frac{d_{n-1}}{4} \right\rfloor - \frac{1}{8}\left\lfloor \frac{d_n}{4} \right\rfloor - \frac{1}{8}\left\lfloor \frac{d_n}{4} \right\rfloor, \\ f_{2n-1} = \frac{1}{8}c_{n-2} + \frac{1}{8}c_{n-1} + \frac{3}{8}c_n + \frac{3}{8}c_n + \frac{1}{8}d_{n-1} + \frac{3}{8}d_n - \frac{1}{8}\left\lfloor \frac{d_{n-2}}{4} \right\rfloor - \frac{1}{8}\left\lfloor \frac{d_{n-1}}{4} \right\rfloor - \frac{3}{8}\left\lfloor \frac{d_n}{4} \right\rfloor - \frac{3}{8}\left\lfloor \frac{d_n}{4} \right\rfloor, \\ f_{2n} = c_n - \left\lfloor \frac{d_n}{4} \right\rfloor. \end{cases} \tag{4.65}$$

In (4.64) and (4.65), i is an even index in $\{2, \ldots, n\}$ for a suitably large $n \in \mathbb{Z}^+$.

4.4 Summary

In this chapter, we presented our general construction for devising an integer-to-integer BMR scheme for a given symmetric/antisymmetric decomposition filter vector of width less or equal to four. Our proposed methodology for achieving a balanced decomposition involves rewriting the linear combination of fine samples suggested by the given decomposition filter vector as the translation of an intermediate integer sample, which is represented by an affine integer combination of some of the involved fine samples. This allows us to obtain an intended coarse integer sample by applying a rounding operator on the associated translation vector. Next, to obtain the corresponding detail integer sample, the un-rounded translation vector is rewritten as the product of a scalar and the intended detail integer sample. Our presented methodology algebraically devises the recipe for a subsequent perfect reconstruction

by solving some square systems of linear equations formed based on the prior construction of coarse and detail integer samples. Like our original BMR framework presented in chapter 3, here also we used a compatible combination of symmetric/antisymmetric extensions near fine image, coarse image, and detail boundaries, which correlate to performing sample split operations. Furthermore, we included the general recipes for two example BMR schemes devised by our method and discussed how our presented framework for devising BIWTs differ from a conventional multiresolution framework.

Chapter 5

Application in Multilevel Focus+Context Visualization

In this chapter, we present the construction of an interactive multilevel focus+context visualization framework for the navigation and exploration of large-scale 2D and 3D images. The presented framework utilizes a *balanced multiresolution* (BMR) technique supported by an underlying *balanced wavelet transform* (BWT). It extends the mode of focus+context visualization, where spatially separate magnification of *regions of interest* (ROIs) is performed, as opposed to in-place magnification. Each resulting visualization scenario resembles a tree structure, where the root constitutes the main context, each non-root internal node plays the dual roles of both focus and context, and each leaf solely represents a focus. Our developed prototype supports interactive manipulation of the visualization hierarchy, such as addition and deletion of ROIs and desired changes in their resolutions at any level of the hierarchy on the fly. We describe the underlying data structure that efficiently supports such operations. Changes in the spatial locations of query windows defining the ROIs trigger on-demand reconstruction queries. We explain in detail how to efficiently process such reconstruction queries within the hierarchy of *details* (wavelet coefficients) contained in the BWT in order to ensure real-time feedback. As the BWT needs only be constructed once in a preprocessing phase on the server-side and robust on-demand reconstruction queries cause minimal data communication overhead, our presented framework is a suitable candidate for efficient web-based visualization of complex large-scale imagery. We also discuss the implications of using a *balanced integer wavelet transform* (BIWT) in place of an underlying BWT and the performance characteristics of our proposed framework from various aspects, such as time and space complexities and achieved frame rates.

We support our multilevel focus+context visualization framework using an underlying

BWT constructed by a BMR scheme for two reasons. Firstly, a BWT provides straightforward access to details corresponding to a ROI in a multilevel hierarchy. Secondly, a BMR scheme does not require any extraordinary boundary filters, the use of which leads to irregular reconstruction of ROI sub-regions near image boundaries. Additionally, we present an efficient technique for processing reconstruction queries to ensure real-time feedback and a sample normalization and quantization method we adopted for rendering purposes. Most of our work presented in this chapter have been published in [HSJ14, HSJ15].

5.1 Balanced Multiresolution

We utilize a BMR scheme devised according to the construction procedure presented in chapter 3. Using a given set of regular multiresolution filter vectors **a**, **b**, **p**, and **q** that are symmetric/asymmetric in structure, a BMR scheme allows for a balanced decomposition and a subsequent perfect reconstruction of a dataset. Here, balanced decomposition is defined such that $sizeof(C) = sizeof(D) = sizeof(F)/2$, where $sizeof(\ldots)$ returns the number of elements in the argument vector.

A BMR scheme avoids the use of extraordinary boundary filters using an extended version of the column vector of fine samples F for decomposition and, similarly, extended versions of the column vectors of coarse samples C and detail samples D for reconstruction. Let F' denote the extended version of F, obtained through symmetric extensions at the boundaries. Also, let C' and D' denote the extended versions of C and D, respectively, obtained through symmetric/antisymmetric extensions at their boundaries. Then the decomposition and reconstruction processes of a BMR scheme are governed by the equations

$$C = \mathbf{A}F', \tag{5.1}$$

$$D = \mathbf{B}F', \tag{5.2}$$

$$F = \mathbf{P}C' + \mathbf{Q}D', \tag{5.3}$$

analogous to equations (2.6), (2.7), and (2.8), respectively.

5.1.1 Multiresolution Filters

The BMR scheme we use is devised using the *short* local filters of quadratic (third order) B-spline:

$$\begin{cases} \mathbf{a} = \begin{bmatrix} a_{-2} & a_{-1} & a_1 & a_2 \end{bmatrix} = \begin{bmatrix} -\frac{1}{4} & \frac{3}{4} & \frac{3}{4} & -\frac{1}{4} \end{bmatrix}, \\ \mathbf{b} = \begin{bmatrix} b_{-2} & b_{-1} & b_1 & b_2 \end{bmatrix} = \begin{bmatrix} \frac{1}{4} & -\frac{3}{4} & \frac{3}{4} & -\frac{1}{4} \end{bmatrix}, \\ \mathbf{p} = \begin{bmatrix} p_{-2} & p_{-1} & p_1 & p_2 \end{bmatrix} = \begin{bmatrix} \frac{1}{4} & \frac{3}{4} & \frac{3}{4} & \frac{1}{4} \end{bmatrix}, \\ \mathbf{q} = \begin{bmatrix} q_{-2} & q_{-1} & q_1 & q_2 \end{bmatrix} = \begin{bmatrix} -\frac{1}{4} & -\frac{3}{4} & \frac{3}{4} & \frac{1}{4} \end{bmatrix}. \end{cases} \tag{5.4}$$

The filter vectors in (5.4) were constructed by reversing Chaikin subdivision [Cha74] in [SBO07]. Note that they are symmetric/antisymmetric about their centers, as required for setting up a BMR scheme.

5.1.2 Balanced Decomposition

Following the general construction for a balanced decomposition presented in chapter 3, for a column vector of fine samples $F = [f_1 \ f_2 \ \dots \ f_{2n}]^T$ where $n \in \mathbb{Z}^+$, we obtain

$$F' = [f_1 \ f_1 \ \dots \ f_{2n} \ f_{2n}]^T$$

through half-sample symmetric extensions at the two boundaries of F. Then the column vectors of coarse samples $C = [c_1 \ c_2 \ \dots \ c_n]^T$ and detail samples $D = [d_1 \ d_2 \ \dots \ d_n]^T$ are

obtained as follows:

$$\begin{cases} c_1 &= a_{-2}f_1 + a_{-1}f_1 + a_1 f_2 + a_2 f_3, \\ d_1 &= b_{-2}f_1 + b_{-1}f_1 + b_1 f_2 + b_2 f_3, \\ \vdots & \\ c_i &= a_{-2}f_{2i-2} + a_{-1}f_{2i-1} + a_1 f_{2i} + a_2 f_{2i+1}, \\ d_i &= b_{-2}f_{2i-2} + b_{-1}f_{2i-1} + b_1 f_{2i} + b_2 f_{2i+1}, \\ \vdots & \\ c_n &= a_{-2}f_{2n-2} + a_{-1}f_{2n-1} + a_1 f_{2n} + a_2 f_{2n}, \\ d_n &= b_{-2}f_{2n-2} + b_{-1}f_{2n-1} + b_1 f_{2n} + b_2 f_{2n}, \end{cases} \tag{5.5}$$

for $i = 2 \ldots (n-1)$. Note that (5.5) shows a linear evaluation of C and D using matrix equations (5.1) and (5.2), respectively.

Balanced decomposition along one or more dimensions of an image for a desired number of levels creates the corresponding BWT. For the purpose of demonstration, Fig. 5.1 shows the BWT resulting after two levels of heightwise and widthwise balanced decompositions of a 1024×512 Blue Marble image (data source: Visible Earth, NASA). Note that in practice, images that require multilevel focus+context visualization are larger in size.

5.1.3 Perfect Reconstruction

According to the general construction for a perfect reconstruction presented in chapter 3, we obtain

$$C' = [c_1 \; c_1 \; \ldots \; c_n \; c_n]^T$$

using half-sample symmetric extensions at the two boundaries of C and

$$D' = [-d_1 \; d_1 \; \ldots \; d_n \; -d_n]^T$$

using half-sample antisymmetric extensions at the two boundaries of D. Then the column vector of fine samples F is reconstructed from C' and D' as follows:

$$\begin{cases} f_1 &= p_2 c_1 + p_{-1} c_1 + q_2(-d_1) + q_{-1} d_1, \\ \vdots & \\ f_{2i} &= p_1 c_i + p_{-2} c_{i+1} + q_1 d_i + q_{-2} d_{i+1}, \\ f_{2i+1} &= p_2 c_i + p_{-1} c_{i+1} + q_2 d_i + q_{-1} d_{i+1}, \\ \vdots & \\ f_{2n} &= p_1 c_n + p_{-2} c_n + q_1 d_n + q_{-2}(-d_n), \end{cases} \tag{5.6}$$

for $i = 1 \ldots (n-1)$. Observe that (5.6) shows a linear evaluation of F using the matrix equation (5.3).

5.2 Reconstruction Queries

In this section, we focus on various aspects of efficiently processing on-demand reconstruction queries in a multilevel focus+context visualization framework.

5.2.1 On-demand Access to Details

For processing reconstruction queries in our multilevel focus+context visualization framework, we need to perform on-demand reconstruction of context sub-regions that define the ROIs from an underlying BWT. To do this, we need to locate the details corresponding to each ROI. Fig. 5.1 shows a ROI in the coarse approximation of an image and corresponding details contained within the BWT of a Blue Marble image. Regardless of what level of the visualization hierarchy a ROI is from, the balanced structure of the BWT makes locating the corresponding details straightforward. For instance, observe the reconstruction of interior samples in (5.6) — if the first coarse sample in the reconstruction of a fine sample is c_i, then

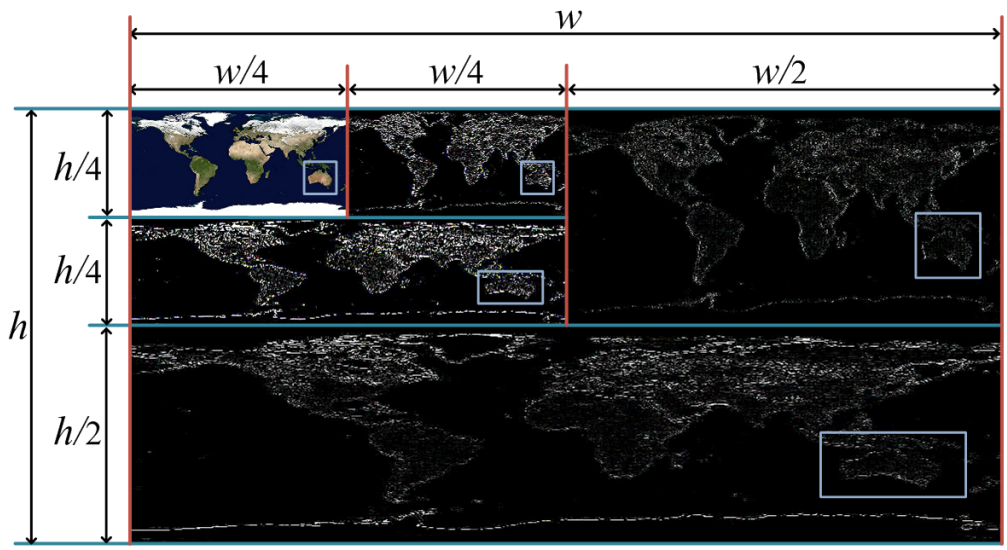

Figure 5.1: BWT of a $w \times h$ Blue Marble image after two levels of balanced decomposition, with rectangles enclosing all levels of details corresponding to a ROI in the coarse approximation of the image (in the top-left corner). Source image dimensions: 1024×512.

d_i is the first detail sample to use in the reconstruction of that fine sample. Furthermore, that fine sample is either f_{2i} or f_{2i+1} depending on which reconstruction filters are used.

5.2.2 L-updating: Avoiding Redundant Reconstructions

Depending on the depth of the multilevel visualization hierarchy where a moving query window (defining changing ROIs) is located, the triggered reconstruction queries can become computationally expensive. This negatively affects the ability to provide real-time feedback. To address this issue, here we describe an *L-updating* technique we employed to avoid redundant reconstruction operations. It works in a manner similar to clipmap-update for terrain rendering performed by Losasso and Hoppe, where they utilized L-like clip regions [LH04].

We explain the concept of L-updating for 2D images, which is extendable to work with 3D images in a straightforward manner. The ROI in a coarse approximation of a 2D image is identified by a movable rectangular query window. Fig. 5.2(a) shows four configurations of how such a query window can move. In each configuration, the rectangles with black and

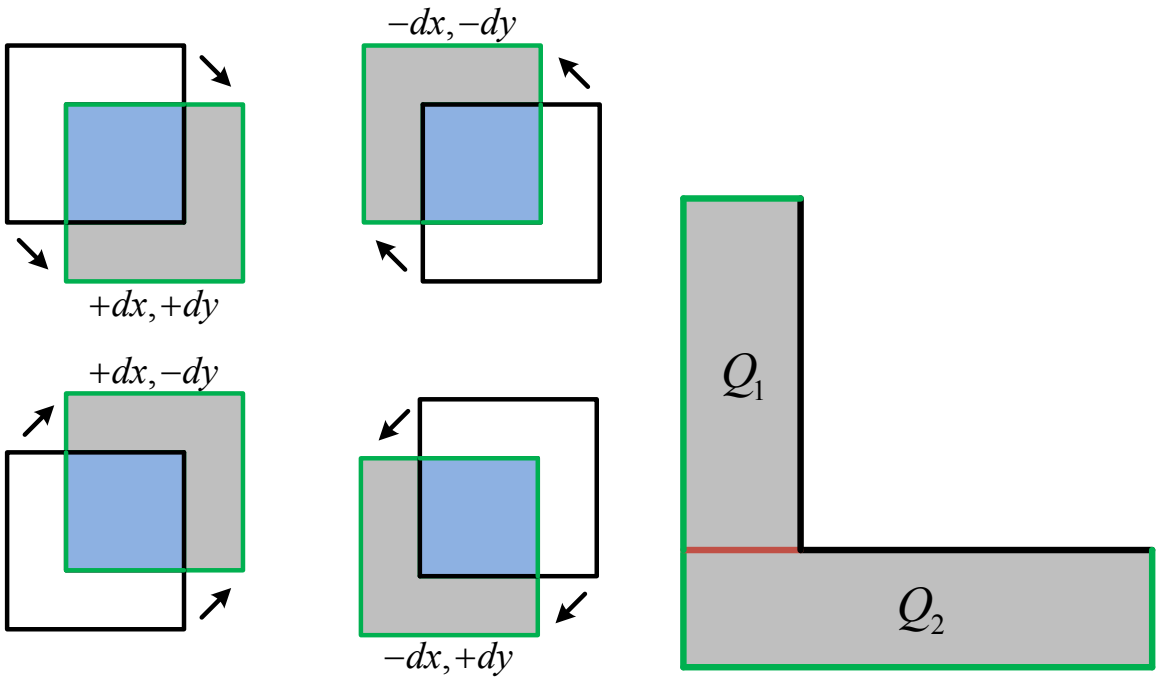

(a) L-updating scenarios. (b) L-updating queries.

Figure 5.2: The L-updating technique.

green edges represent the old and new locations of the query window before and after a move, respectively. The rectangular area shaded in light-blue represents the intersection between the old and new ROIs for each configuration. The signed dx and dy values represent the direction and magnitude of the move made by the query window.

In most scenarios, the old and new ROIs intersect. Provided that the high-resolution approximation of the old ROI has already been reconstructed, that for the intersection region (shown in light-blue for the each scenario in Fig. 5.2(a)) can be reused directly from the old enlarged ROI while obtaining the new enlarged ROI. Therefore, for each scenario, we only need to reconstruct the high-resolution approximation for the L-like polygonal area of the new ROI shaded in grey.

In order to reconstruct the high-resolution approximation for the L-like polygonal area of the new ROI, we break it down into two rectangular reconstruction queries, Q_1 and Q_2, as shown in Fig. 5.2(b). Note that if either dx or dy is zero, then there will be only one

reconstruction query instead. From the standpoint of implementation, the same memory area can be used to update the high-resolution approximation of the old ROI into the high-resolution approximation of the new ROI. This process involves shifting the reusable high-resolution approximation of the old ROI to the opposite corner (observe in Fig. 5.2(a)) and copying the results of Q_1 and Q_2 to the appropriate locations.

The L-updating technique significantly reduces the computational overhead by eliminating redundant reconstruction operations. While exploiting a 3D query probe for interactive visualization and exploration of 3D images, utilizing the L-updating technique can result in a substantial gain in performance. It can also greatly minimize the data communication overheads in applications of our presented framework to web-based visualization and exploration of large-scale imagery.

5.3 Data Structure

Supporting interactive manipulation of the multilevel focus+context visualization hierarchy mandates efficient hierarchy traversal capabilities of the underlying implementation. For example, addition and deletion of ROIs at any level of the hierarchy on the fly, changing the resolution of an enlarged ROI at some level in the hierarchy, and adjusting the visualization layout changing the locations of enlarged ROIs on the screen – they all require real-time traversal of the hierarchy. Therefore, we need to keep track of the tree-like structure of visualization scenarios supported by our presented framework.

Because a context window may contain any number of ROIs, each resulting visualization scenario resembles an N-ary tree structure (where each node has no more than N children). In order to allow for efficient traversal of the multilevel hierarchy on-demand and storage of pertinent information in a 1D array T, Hasan *et al.* made use of a *left-child right-sibling* (LC-RS) binary tree [HSJ14], corresponding to the N-ary tree that represents the layout of a visualization scenario. However, because t_{2i} and t_{2i+1} store the two children of the parent

stored in t_i, the array T required $O(2^x)$ storage, where x is the maximum number of ROIs allowed in a visualization scenario. At any instance of time, only a maximum of x of the $O(2^x)$ array locations were useful.

In order to eliminate the waste of storage noted above, we exploit a linked list representation of the N-ary tree corresponding to a visualization scenario. Each node of the linked list contains a pointer to an object containing relevant ROI information and four additional pointers to the tree-nodes containing its parent, first-child, left-sibling, and right-sibling. The object containing ROI information stores the enlarged ROI for rendering and further reconstruction purposes, in addition to some pertaining information, such as its location in the main context, screen coordinates, etc. The main context, which is a part of the BWT, is not stored separately in such an object for reducing storage requirement.

5.4 Rendering: Sample Normalization and Quantization

When a decomposition filter value is applied to a sample, it is applied independently to each of its components (such as red, green, and blue). The resulting sample will usually have each of its components as floating-point values, which must be stored to ensure a perfect (lossless) reconstruction. These floating-point values may also fall outside the interval of $[0, iMax]$, where $iMax$ is the maximum integer intensity value. However, for rendering purposes, these floating-point values must be mapped to the integer range of 0 to $iMax$. A simple strategy for normalization is to replace the floating-point values less than the minimum intensity of 0 with 0 and greater than the maximum intensity $iMax$ with $iMax$. Rounding up or down according to a preset criterion can quantize the floating-point values between 0 and $iMax$. For the purpose of rendering, we obtain an integer intensity value i from a floating-point

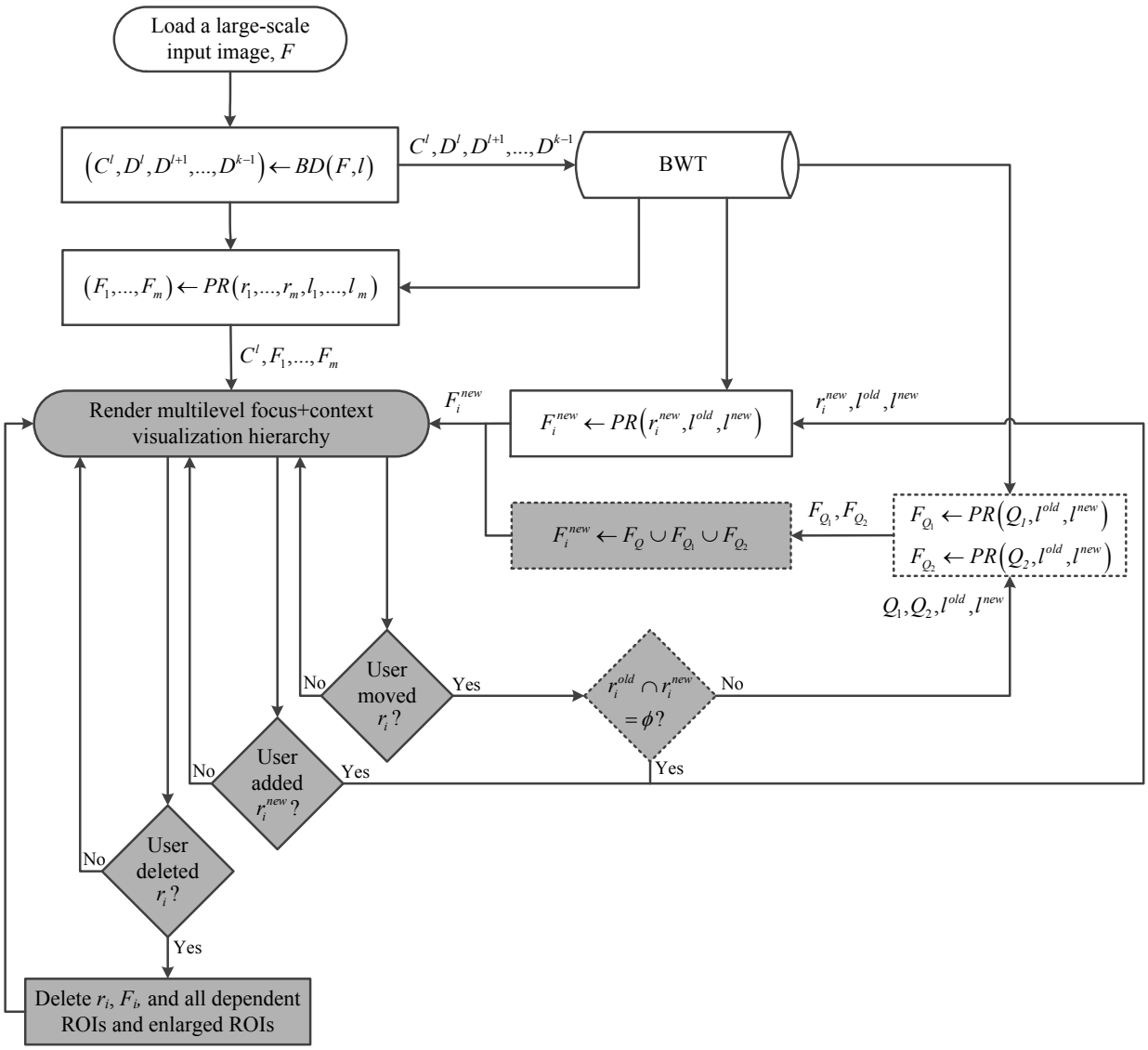

Figure 5.3: Flowchart for the proposed multilevel focus+context visualization framework.

value f as follows:

$$i = \begin{cases} 0 & \text{if } f \leq 0, \\ \lfloor f \rfloor & \text{if } 0 < f < iMax \wedge (f - \lfloor f \rfloor) \leq 0.5, \\ \lceil f \rceil & \text{if } 0 < f < iMax \wedge (f - \lfloor f \rfloor) > 0.5, \\ iMax & \text{if } f \geq iMax. \end{cases} \tag{5.7}$$

The experimental results provided in section 5.6 are rendered using the conditions in (5.7). Other commonly used approaches involve uniformly mapping either the pre-calculated possible

interval or the actual interval of the resulting floating-point values to the integer range of 0 to $iMax$. These approaches have varying impacts on the contrast of the resulting images.

One can avoid the sample quantization step by using BMR schemes that map integer samples to integer samples, such as those presented in chapter 4.

5.5 Multilevel Focus+Context Visualization Framework

The high-level flowchart in Fig. 5.3 illustrates the pipeline and the important components of our proposed visualization framework. For simplification purposes, changes in existing ROIs' levels of resolution, modification of visualization hierarchy layout (relocating the enlarged ROIs on the screen), etc. supported by our developed prototype were not taken into consideration in this flowchart. In case of a web-based implementation, the grey components of this flowchart should to be performed on the client-side and the rest on the server-side. The three components with dashed borders constitute the L-updating technique described in section 5.2.2. Several of the processes in this flowchart use the $BD(\ldots)$ and $PR(\ldots)$ methods to perform balance decomposition(s) and perfect reconstruction(s), respectively.

The first process loads a large-scale image F. In the second process, F undergoes l levels of balanced decomposition to construct the corresponding BWT (as defined in sections 2.5.3 and 5.1.2). The following process relies on the constructed BWT to perfectly reconstruct the initial set of enlarged ROIs $F_1, ..., F_m$ with levels of resolution $l_1, ..., l_m$ based on the regions enclosed by the corresponding ROIs $r_1, ..., r_m$ in C^l, respectively. Then $C^l, F_1, ..., F_m$ are passed to the following process for rendering a multilevel focus+context visualization hierarchy. The visualization task may terminate at the end of this process.

Next, if the user moves a ROI r_i, and the old and new regions enclosed by r_i intersect, i.e. $r_i^{old} \cap r_i^{new} \neq \phi$, then Q_1 and Q_2 (as defined in section 5.2.2) are passed to the following process with their current and expected levels of resolutions, l^{old} and l^{new}. Taking these, the following process perfectly reconstructs F_{Q_1} and F_{Q_2} relying on the BWT of image F.

Provided F_{Q_1} and F_{Q_2}, the next process combines these to the reusable part of F_i (shaded in ligh-blue in Fig. 5.2), denoted by F_Q in the flowchart, to obtain F_i^{new}. F_i^{new} is then passed to the rendering process to update the previously rendered visualization hierarchy.

On the other hand, if the user moves a ROI r_i, and the old and new regions enclosed by r_i do not intersect, i.e. $r_i^{old} \cap r_i^{new} = \phi$, then F_i^{new} is perfectly reconstructed from r_i^{new}, l^{old}, l^{new} and the BWT by a different process as shown in the flowchart. The process also perfectly reconstructs an enlarged ROI F_i^{new} if the user adds a new ROI r_i^{new} at some level in the hierarchy. Conversely, if the user deletes a ROI r_i from some level in the hierarchy, then a process deletes r_i, it enlarged version F_i, and all dependent ROIs and enlarged ROIs.

5.6 Results

We have developed a visualization tool prototype to validate our presented multilevel focus+context visualization framework for images. In Figs. 5.4 and 5.5, the associated levels of decomposition and reconstruction are shown at the bottom-right corner of each main context and at the top-right corner of each enlarged ROI, respectively.

Fig. 5.4 shows several focus+context visualization and exploration scenarios for 2D images facilitated by our developed tool. Fig. 5.4(a) and 5.4(b) present multilevel focus+context visualization of a diseased leaf (data source: S. Fraser-Smith, Wikipedia; used under the Creative Commons Attribution 2.0 Generic license) and the topography of Long Island (data source: G. Hanson, Stony Brook University, USA), respectively. Fig. 5.4(c) draws a comparison between the ice near the coasts of the Prince of Wales Island and the Alexander Island using a Blue Marble image showing Earth's topography and bathymetry (data source: Visible Earth, NASA). Our developed prototype also allows fractional changes in the resolution of an enlarged ROI through trilinear interpolation between two consecutive integer resolutions of the ROI; Fig. 5.4(d) shows such a ROI at floating-point resolution 4.15, magnifying a thin section cut through a bone marrow area in the kneecap of a mouse (data source: Dartmouth

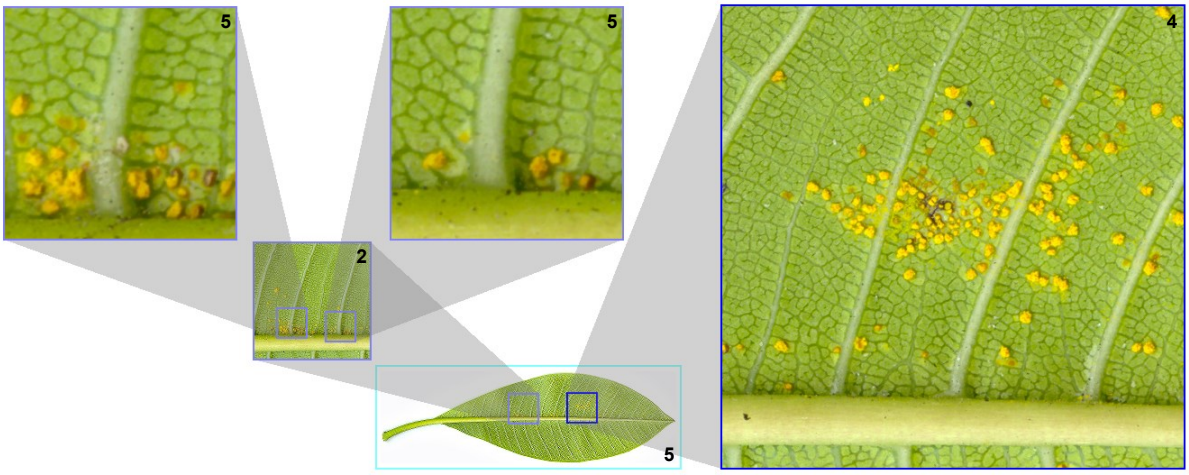

(a) Plumeria rubra leaf with frangipani rust. Source image dimensions: 10496×3328.

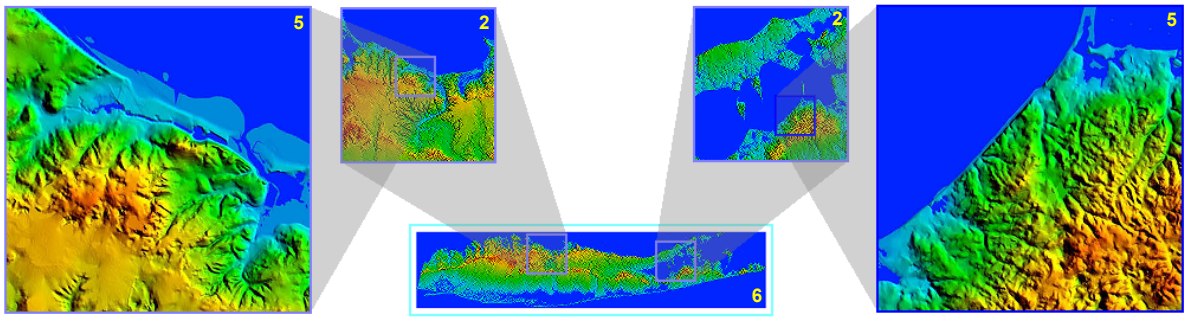

(b) Topographic shading of Long Island. Source image dimensions: 18944×4224.

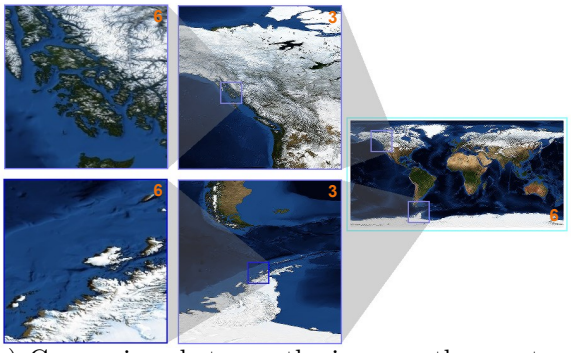

(c) Comparison between the ice near the coasts of the Prince of Wales Island (top) and the Alexander Island (bottom). Source image dimensions: 21632×10816.

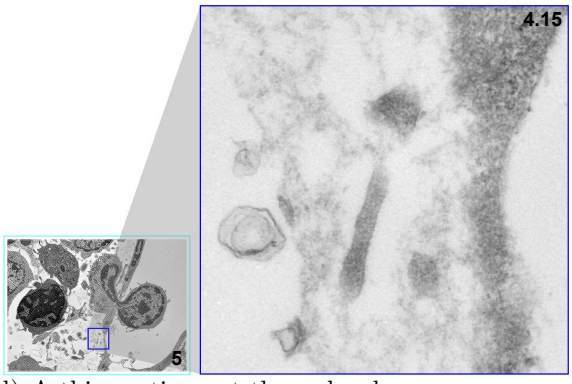

(d) A thin section cut through a bone marrow area near the cartilage/bone interface in a mouse kneecap. Source image dimensions: 9216×6784.

Figure 5.4: Various multilevel focus+context visualization hierarchies for 2D images.

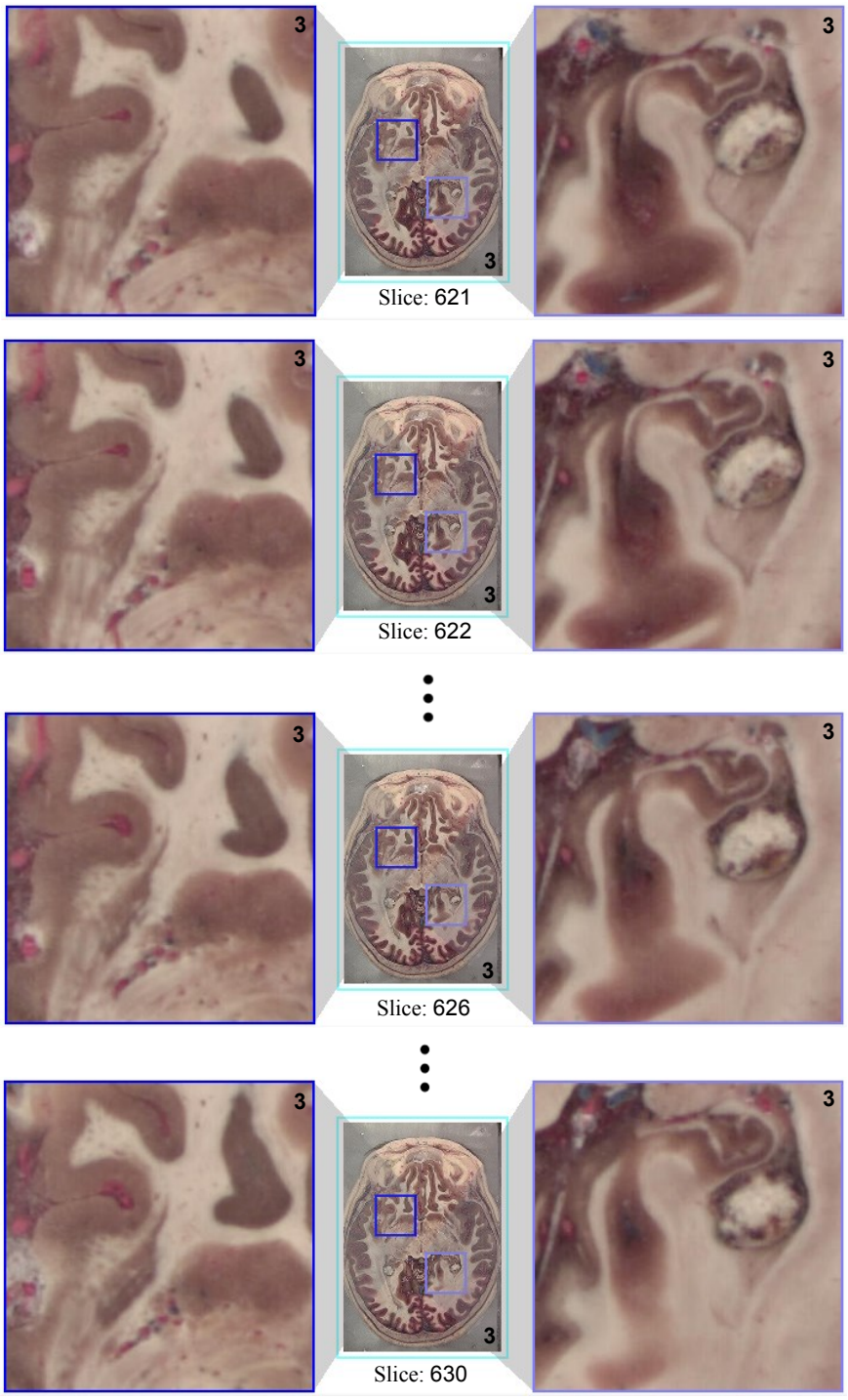

Figure 5.5: A fly-through focus+context visualization for a 3D image – part of a male's head. Source image dimensions: $1056 \times 1528 \times 150$.

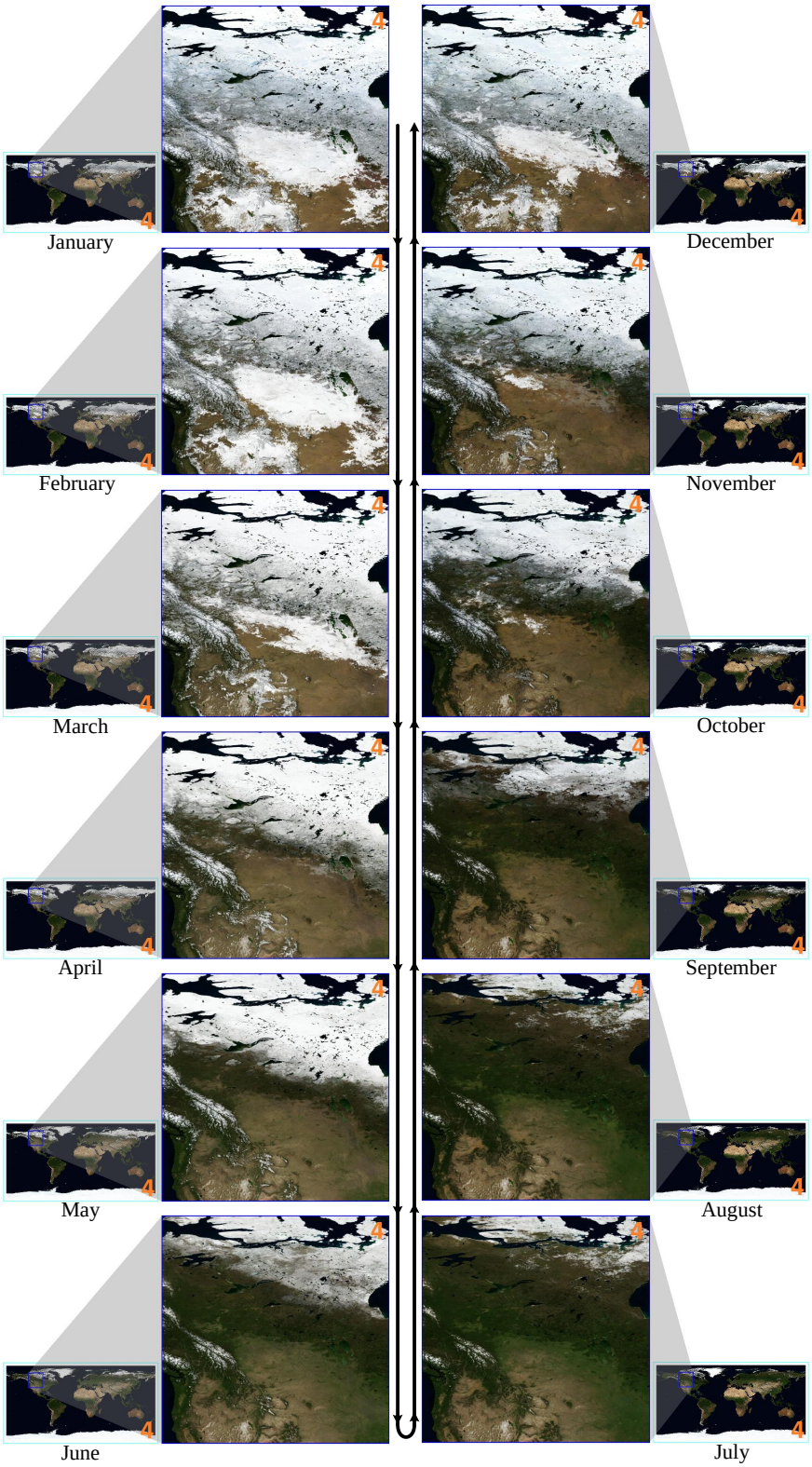

Figure 5.6: Focus+context visualization of time-lapse imagery - monthly global images. Source image dimensions: $5440 \times 2752 \times 12$.

College Electron Microscope Facility, USA).

Our prototype allows focus+context visualization and exploration of a 3D image by means of interactive depthwise transitions of query windows defining the ROIs. Such transitions are controlled by the user either through the use of the attached mouse scroll wheel or the up and down arrow keys on the attached keyboard. Currently, our prototype only performs widthwise and heightwise decompositions of 3D images, keeping the number of 2D slices along the depth constant for depthwise volume exploration. Fig. 5.5 presents such a visualization scenario created in our prototype. For the sake of demonstration, it only shows the fly-through transition of two query windows through ten of the 150 sequential slices loaded into our prototype for this visualization task. The dimensions of the original dataset are $1056 \times 1528 \times 1477$ (data source: Male head, The Visible Human Project, U.S. National Library of Medicine).

In a similar manner, our developed prototype is also suitable for the visualization and exploration of large-scale time-lapse imagery, constraining the query windows to move back and forth along the time dimension. For instance, Fig. 5.6 shows 12 unique frames from the interactive transition through the 12 slices of monthly global images (data source: R. Stöckli, Monthly Global Images, NASA). The order of frames is shown by directions marked on the curved-arrow in the middle. The ROI covers most of northwestern North America and shows the transition from one winter to the following winter.

5.7 BWT versus BIWT

We could alternatively use a *balanced integer wavelet transform* (BIWT) in place of a *balanced wavelet transform* to support the multilevel focus+context visualization framework presented in this chapter. For comparison purposes, in Fig. 5.7, we present the context image from Fig. 5.4(a) after 4 levels of balanced decomposition from its BWT and BIWT representations and their difference, respectively. Similarly, Fig. 5.8 shows the context image from Fig. 5.4(b)

(a) Coarse image from BWT.

(b) Coarse image from BIWT.

(c) Difference between the coarse samples from BWT and BIWT.

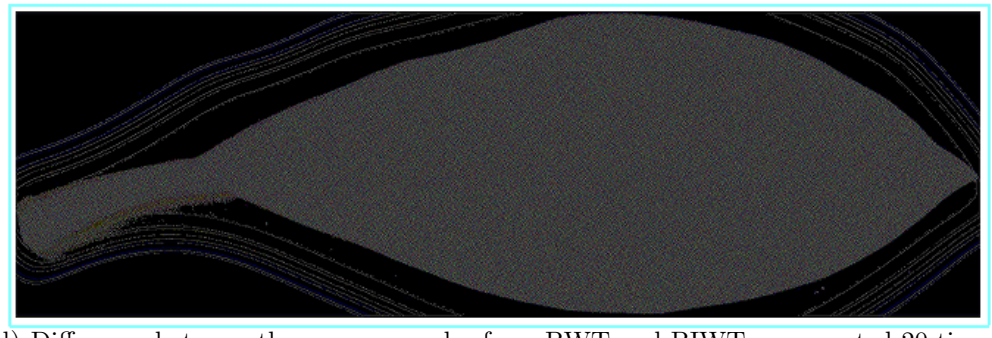

(d) Difference between the coarse samples from BWT and BIWT exaggerated 20 times.

Figure 5.7: Coarse images of Plumeria rubra leaf with frangipani rust from BWT and BIWT after 4 levels of balanced decomposition and their difference. Source image dimensions: 3328×10496.

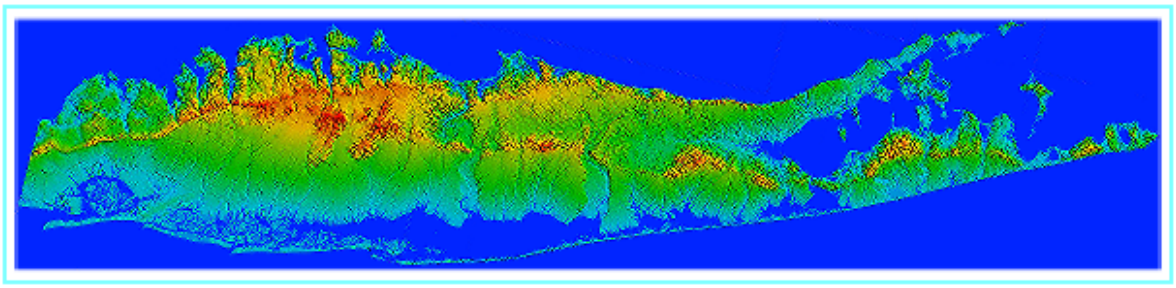

(a) Coarse image from BWT.

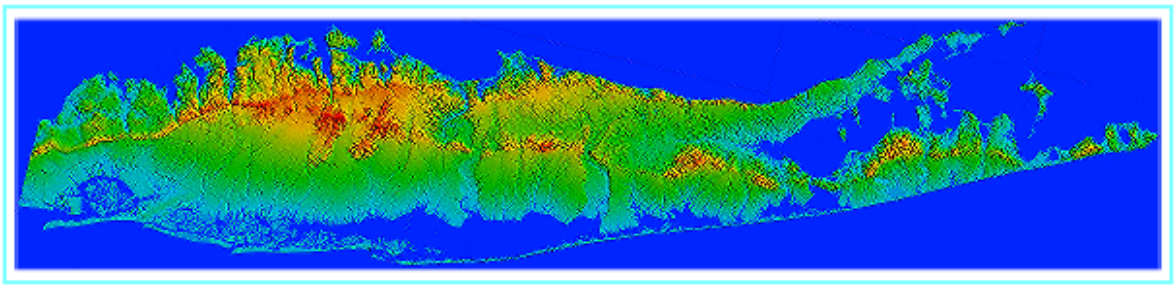

(b) Coarse image from BIWT.

(c) Difference between the coarse samples from BWT and BIWT.

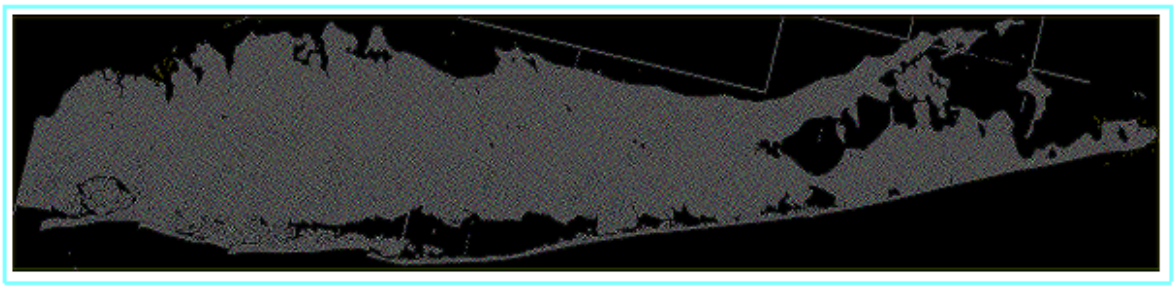

(d) Difference between the coarse samples from BWT and BIWT exaggerated 20 times.

Figure 5.8: Coarse images of topographic shading of Long Island from BWT and BIWT after 5 levels of balanced decomposition and their difference. Source image dimensions: 18944×4224.

after 5 levels of balanced decomposition from its BWT and BIWT representations and their difference, respectively. The BIWTs for the images in Fig. 5.7 and 5.8 were constructed using the general recipe from 4.26 that correspond to the same given decomposition filter vector **a** for the BMR scheme utilized in this chapter.

Because coarse integer samples in BIWT are close approximations of the coarse real samples from the corresponding BWT, in Fig. 5.7 and 5.8, a visual comparison of the coarse images resulting from BWTs and BIWTs does not reveal any noticeable difference. The difference images included in Fig. 5.7 and 5.8 show samples with near-zero values as expected. The ripples around the leaf in Fig. 5.7(d) are due to illumination (lighting) effects that exist in the original source image. Note that no such ripples are observed in Fig. 5.8(d) because the original source image was computer-generated with more consistent lighting conditions across the image.

The noteworthy advantages of using a BIWT in place of a BWT for supporting a multilevel focus+context visualization framework lie in reduced memory requirements for storing the BIWT compared to that for the equivalent BWT, as well as in saving the computation time required for sample quantization for coarse images resulting from BWTs as described in section 5.4. However, the choice and application of rounding operators in BIWTs may add some computation overhead as discussed in the relevant literature [Ada02].

5.8 Performance Characteristics

The runtimes for the performed decomposition and reconstruction operations are linear on the number of processed samples. For our implementation, the memory usage is linear on the total number of samples in the source image and the enlarged ROIs.

On a Dell Precision T7500 desktop computer with two Intel® Xeon® E5506 2.13 GHz processors, NVIDIA Quadro FX 1800 graphics card, and 12 GB of RAM, our experiments revealed the average frame rates shown in Table 5.1. They were obtained during ROI

movement for different levels of enlarged ROI resolution. We used the diseased leaf image shown in Fig. 5.4(a) in these experiments. Each frame rate value in the table is the average of frame rates from three different sets of user interactions (involving only ROI movement), keeping the level of enlarged ROI resolution constant. The second and third columns of the table show the average frames per second (FPS) values achieved with and without the use of L-updating technique during ROI movement, respectively. The last column shows how many times higher the average frame rates are while using our proposed L-updating technique.

Table 5.1: Average frame rates during ROI movement at different levels of enlarged ROI resolution

Level	FPS_1 (L-updating)	FPS_2 (No L-updating)	FPS_1/FPS_2
2	44.84	40.38	1.11
3	43.24	17.56	2.46
4	20.52	4.62	4.45
5	8.11	1.50	5.41

The functionalities of our presented multilevel focus+context visualization framework is not dependent on the choice of multiresolution filters (see section 5.1.1). One may choose to use a different set of symmetric/anti-symmetric multiresolution filters, which will only affect the balanced decomposition (see section 5.1.2) and perfect reconstruction (see section 5.1.3) parts of our presented framework. However, the choice of multiresolution filters will affect the performance. Use of filter vectors with shorter widths will imply faster reconstruction (due to reduced number of multiplications) and consequently, higher frame rate.

5.9 Summary

In this chapter, we presented the construction of a multilevel focus+context visualization framework supported by a BMR scheme devised by our proposed BMR framework. In addition to presenting a set of experimental results, we described the *L-updating* technique to avoid redundant reconstruction operations during user-interactions, the underlying data structure to efficiently support the manipulation of such a multilevel visualization hierarchy,

and sample normalization and quantization techniques for rendering purposes. We also explained how our framework can efficiently support web-based multilevel focus+context visualization of large-scale imagery via progressive transmission with minimal communication overhead. We concluded the chapter by discussing the implications of using a BIWT in place of an underlying BWT and the performance characteristics of our multilevel focus+context visualization framework.

Chapter 6

Conclusion and Future Work

6.1 Balanced Multiresolution

In this thesis, we first presented a novel method for devising a *balanced multiresolution* (BMR) scheme, primarily applicable to images, using a given set of symmetric/antisymmetric filter vectors containing regular multiresolution filters. A balanced multiresolution scheme resulting from our method allows balanced decomposition and subsequent perfect reconstruction of images without using any extraordinary boundary filters. This is achieved by the use of an appropriate combination of symmetric and antisymmetric extensions at the image and detail boundaries, correlating to implicit sample split operations. Balanced wavelet transform of an image constructed through balanced decompositions provides straightforward and efficient access to details corresponding to a ROI on demand.

In order to support smooth multiresolution representations of images beyond Haar wavelets and the associated scaling functions, and still exploit the advantages of a balanced decomposition, we used our method to devise balanced multiresolution schemes for some commonly used sets of local multiresolution filters obtained from higher order scaling functions and their wavelets. Any such balanced multiresolution scheme can be used to generate a *balanced wavelet transform* (BWT) representation of a multidimensional image in a preprocessing phase, which can then be utilized to support its multilevel focus+context visualization in an efficient manner.

There is a number of directions for future research. In this thesis, we covered the commonly used types of symmetric and antisymmetric extensions. It would be useful to investigate and develop extension types that can be utilized to devise balanced multiresolution schemes for near-symmetric and asymmetric filter vectors in order to ensure a perfect reconstruction

solely by the use of regular filters. To start with, the devised balanced multiresolution scheme given in appendix A for Daubechies' asymmetric D4 filters may provide some insights.

In addition, further investigations are needed for an in-depth understanding of the relations between the symmetry/antisymmetry exhibited by the filter vectors, parity of their widths, and the determined types of symmetric/antisymmetric extensions required at coarse image and detail boundaries for a perfect reconstruction using only regular filters. For instance, compare the multiresolution filter vectors containing the *inverse powers of two* filters of fourth order B-spline in equation (3.15) and the *wide* and *optimal* filters of fourth order B-spline in equation (A.3). In these two sets, the corresponding filter vectors have the same widths and they are all symmetric. Now, observe that the two balanced multiresolution schemes we devised using these two sets of filter vectors suggest exactly the same type of symmetric extensions for the column vectors of fine, coarse, and detail samples. Therefore, the determined types of symmetric/antisymmetric extensions are not dependant on actual filter values. Several other such scenarios are shown in Table A.1.

6.2 Reversible Integer-to-Integer Balanced Wavelet Transform

Next in this thesis, we extended our original BMR framework to construct reversible *balanced integer wavelet transforms* (BIWTs) from a given symmetric/antisymmetric decomposition filter vector of width less or equal to four. In our proposed methodology, we perturb the coarse real sample suggested by the given decomposition filter vector to obtain a coarse integer sample. The desired perturbation is achieved by adjusting the linear combination of contributing fine integer samples via optimal sample split operations and by the application of a rounding operator. Such adjustments obtain integer coarse samples closely approximating the coarse real samples suggested by the given decomposition filter vector by translating an affine integer combination of some of the contributing fine samples. The detail samples are constructed from the associated translation vectors that may be different for every other coarse integer sample

in order to support local perfect reconstruction. Devising the associated perfect reconstruction scheme involves symbolically solving some square systems of linear equations that are formed based on how coarse and detail integer samples were constructed during the prior balanced decomposition. If applicable, we make use of symmetric/antisymmetric extensions at fine image, coarse image, and detail boundaries to avoid the use of extraordinary boundary filters and rounding operators during balanced decomposition and perfect reconstruction.

In comparison to their integer-to-real counterparts, the resulting reversible BIWTs are less memory-intensive, highly compressible, and do not require sample quantization for rendering purposes. Integer-to-integer BMR schemes devised by our framework facilitate straightforward, on-demand, random-access to the coarse and detail integer samples corresponding to fine integer samples of interest, which makes them notably suitable for use in applications supporting interactive multilevel focus+context visualization for the navigation and exploration of large-scale 2D and 3D images.

Similar to that with our BMR framework presented in chapter 3, directions for future work include developing reversible BIWTs for given decomposition filter vectors that are either near-symmetric or asymmetric, while gaining a deeper understanding of the relationship between the symmetry/antisymmetry exhibited by filter vectors, the parity of their widths, and types of extensions utilized at fine image, coarse image, and detail boundaries to avoid the use of extraordinary boundary filters during balanced decomposition and perfect reconstruction. In that regard, the detail construction and perfect reconstruction only by the use of regular filters in equations(4.58) and (4.61), respectively, provide some important insights because the associated $\mathbf{b}$ filter vector in (4.59) and the $\mathbf{p}$ and $\mathbf{q}$ filter vectors in (4.62) are neither symmetric nor antisymmetric. Another important venue for future work is extending our presented framework for devising reversible BIWTs to support wider symmetric/antisymmetric decomposition filter vectors to facilitate further generalization of our presented approach.

6.3 Application in Multilevel Focus+Context Visualization

Further in this thesis, we presented a multilevel focus+context visualization framework for effective and manageable navigation and exploration of large-scale 2D and 3D images. Our presented framework extends the discontinuous and undistorted mode of focus+context visualization based on an underlying BWT, utilized by means of a BMR scheme. The BMR scheme we used is devised based on the local multiresolution filters of quadratic B-spline. Unlike preexisting multiresolution approaches to focus+context visualization, our use of a BMR scheme facilitates straightforward access to details required for on-demand reconstruction of enlarged ROIs and allows us to avoid the use of extraordinary boundary filters.

We also described an *L-updating* technique that ensures real-time feedback by avoiding redundant reconstruction operations in processing reconstruction queries, triggered by a moving query window defining changing ROIs. Our developed prototype allows real-time exploration of large-scale images through interactive manipulation of the visualization hierarchy. We described the data structure that efficiently supports such user interactions. Finally, we discussed the implications of using a BIWT instead of an underlying BWT as well as various performance characteristics of our presented multilevel focus+context visualization framework.

With the growth of data size, the increasing depth of a multilevel visualization hierarchy supported by a multilevel focus+context framework may cause user disorientation. To address this issue, an important direction for future work involves augmenting enlarged ROIs with supplementary textual and visual information in order to reduce user disorientation. This direction for future work is also aligned with the *scalability and multilevel hierarchy* challenge identified in [WSJ*12], that highlights the navigation of deep multilevel hierarchies and identifying optimal resolutions (for ROIs, in our context) as major challenges.

Last but not the least, a more flexible multilevel focus+context visualization framework

for large-scale 3D images is achievable through an extension of our developed prototype to support their depthwise balanced decompositions and exploration using 3D ROIs that do not need to be axis-aligned.

Appendix A

Balanced Wavelet Transform Recipes for Various Symmetric/Antisymmetric Filter Vectors

Further to the examples in chapter 3, this appendix demonstrates our general approach for devising a balanced multiresolution scheme described in section 3.2 by means of three more examples.

Our first example here involves the multiresolution filter vectors containing the local regular filters of second order B-spline,

$$\begin{cases} \mathbf{a} = \begin{bmatrix} -\frac{1}{6} & \frac{1}{3} & \frac{2}{3} & \frac{1}{3} & -\frac{1}{6} \end{bmatrix}, \\ \mathbf{b} = \begin{bmatrix} -\frac{1}{2} & 1 & -\frac{1}{2} \end{bmatrix}, \\ \mathbf{p} = \begin{bmatrix} \frac{1}{2} & 1 & \frac{1}{2} \end{bmatrix}, \\ \mathbf{q} = \begin{bmatrix} -\frac{1}{6} & -\frac{1}{3} & \frac{2}{3} & -\frac{1}{3} & -\frac{1}{6} \end{bmatrix}, \end{cases} \tag{A.1}$$

derived by Sadeghi [Sad11] by reversing Faber subdivision [Fab09] based on the construction procedure presented by Samavati and Bartels in [SB99, BS00]. For the filter vectors in equation (A.1), the matrix equations for a balanced multiresolution scheme we devised using

our method for $n \in \mathbb{Z}^+$ are

$$\begin{bmatrix} c_1 \\ c_2 \\ \vdots \\ c_n \end{bmatrix} = \begin{bmatrix} -\frac{1}{6} & \frac{1}{3} & \frac{2}{3} & \frac{1}{3} & -\frac{1}{6} & 0 & 0 & 0 & \cdots \\ 0 & 0 & -\frac{1}{6} & \frac{1}{3} & \frac{2}{3} & \frac{1}{3} & -\frac{1}{6} & 0 & \cdots \\ \vdots & \vdots & \vdots & \vdots & \vdots & \vdots & \vdots & \vdots & \ddots \end{bmatrix} \begin{bmatrix} f_2 \\ f_1 \\ f_2 \\ \vdots \\ f_{2n-1} \\ f_{2n} \\ f_{2n-1} \\ f_{2n-2} \end{bmatrix},$$

$$\begin{bmatrix} d_1 \\ d_2 \\ \vdots \\ d_n \end{bmatrix} = \begin{bmatrix} -\frac{1}{2} & 1 & -\frac{1}{2} & 0 & 0 & 0 & \cdots \\ 0 & 0 & -\frac{1}{2} & 1 & -\frac{1}{2} & 0 & \cdots \\ \vdots & \vdots & \vdots & \vdots & \vdots & \vdots & \ddots \end{bmatrix} \begin{bmatrix} f_2 \\ f_1 \\ f_2 \\ \vdots \\ f_{2n} \end{bmatrix},$$

and

$$\begin{bmatrix} f_1 \\ f_2 \\ \vdots \\ f_{2n} \end{bmatrix} = \begin{bmatrix} \frac{1}{2} & \frac{1}{2} & 0 & \cdots & 0 & 0 \\ 0 & 1 & 0 & \cdots & 0 & 0 \\ 0 & \frac{1}{2} & \frac{1}{2} & \cdots & 0 & 0 \\ \vdots & \vdots & \vdots & \ddots & \vdots & \vdots \\ 0 & 0 & 0 & \cdots & \frac{1}{2} & \frac{1}{2} \\ 0 & 0 & 0 & \vdots & 0 & 1 \end{bmatrix} \begin{bmatrix} c_1 \\ c_1 \\ c_2 \\ \vdots \\ c_n \end{bmatrix} + \begin{bmatrix} -\frac{1}{6} & \frac{2}{3} & -\frac{1}{6} & 0 & \cdots & 0 & 0 & 0 \\ 0 & -\frac{1}{3} & -\frac{1}{3} & 0 & \cdots & 0 & 0 & 0 \\ 0 & -\frac{1}{6} & \frac{2}{3} & -\frac{1}{6} & \cdots & 0 & 0 & 0 \\ \vdots & \vdots & \vdots & \vdots & \ddots & \vdots & \vdots & \vdots \\ 0 & 0 & 0 & 0 & \cdots & -\frac{1}{6} & \frac{2}{3} & -\frac{1}{6} \\ 0 & 0 & 0 & 0 & \cdots & 0 & -\frac{1}{3} & -\frac{1}{3} \end{bmatrix} \begin{bmatrix} d_2 \\ d_1 \\ d_2 \\ \vdots \\ d_n \\ d_n \end{bmatrix},$$

analogous to equations (2.6), (2.7), and (2.8), respectively.

The next example involves the following multiresolution filter vectors containing the local

regular filters of cubic (fourth order) B-spline from [SBO07]:

$$\begin{cases} \mathbf{a} = \begin{bmatrix} -\frac{1}{2} & 2 & -\frac{1}{2} \end{bmatrix}, \\ \mathbf{b} = \begin{bmatrix} \frac{1}{4} & -1 & \frac{3}{2} & -1 & \frac{1}{4} \end{bmatrix}, \\ \mathbf{p} = \begin{bmatrix} \frac{1}{8} & \frac{1}{2} & \frac{3}{4} & \frac{1}{2} & \frac{1}{8} \end{bmatrix}, \\ \mathbf{q} = \begin{bmatrix} \frac{1}{4} & 1 & \frac{1}{4} \end{bmatrix}. \end{cases} \tag{A.2}$$

The filter vectors in equation (A.2) are called the *short* filters of cubic B-spline. For these filter vectors, the matrix equations for a balanced multiresolution scheme we devised using our method for $n \in \mathbb{Z}^+$ are

$$\begin{bmatrix} c_1 \\ c_2 \\ \vdots \\ c_n \end{bmatrix} = \begin{bmatrix} -\frac{1}{2} & 2 & -\frac{1}{2} & 0 & 0 & 0 & \cdots \\ 0 & 0 & -\frac{1}{2} & 2 & -\frac{1}{2} & 0 & \cdots \\ \vdots & \vdots & \vdots & \vdots & \vdots & \vdots & \ddots \end{bmatrix} \begin{bmatrix} f_2 \\ f_1 \\ f_2 \\ \vdots \\ f_{2n} \end{bmatrix},$$

$$\begin{bmatrix} d_1 \\ d_2 \\ \vdots \\ d_n \end{bmatrix} = \begin{bmatrix} \frac{1}{4} & -1 & \frac{3}{2} & -1 & \frac{1}{4} & 0 & 0 & 0 & \cdots \\ 0 & 0 & \frac{1}{4} & -1 & \frac{3}{2} & -1 & \frac{1}{4} & 0 & \cdots \\ \vdots & \vdots & \vdots & \vdots & \vdots & \vdots & \vdots & \vdots & \ddots \end{bmatrix} \begin{bmatrix} f_2 \\ f_1 \\ f_2 \\ \vdots \\ f_{2n-1} \\ f_{2n} \\ f_{2n-1} \\ f_{2n-2} \end{bmatrix},$$

and

$$\begin{bmatrix} f_1 \\ f_2 \\ \vdots \\ f_{2n} \end{bmatrix} = \begin{bmatrix} \frac{1}{8} & \frac{3}{4} & \frac{1}{8} & 0 & \cdots & 0 & 0 & 0 \\ 0 & \frac{1}{2} & \frac{1}{2} & 0 & \cdots & 0 & 0 & 0 \\ 0 & \frac{1}{8} & \frac{3}{4} & \frac{1}{8} & \cdots & 0 & 0 & 0 \\ \vdots & \vdots & \vdots & \vdots & \ddots & \vdots & \vdots & \vdots \\ 0 & 0 & 0 & 0 & \cdots & \frac{1}{8} & \frac{3}{4} & \frac{1}{8} \\ 0 & 0 & 0 & 0 & \cdots & 0 & \frac{1}{2} & \frac{1}{2} \end{bmatrix} \begin{bmatrix} c_2 \\ c_1 \\ c_2 \\ \vdots \\ c_n \\ c_n \end{bmatrix} + \begin{bmatrix} \frac{1}{4} & \frac{1}{4} & 0 & \cdots & 0 & 0 \\ 0 & 1 & 0 & \cdots & 0 & 0 \\ 0 & \frac{1}{4} & \frac{1}{4} & \cdots & 0 & 0 \\ \vdots & \vdots & \vdots & \ddots & \vdots & \vdots \\ 0 & 0 & 0 & \cdots & \frac{1}{4} & \frac{1}{4} \\ 0 & 0 & 0 & \vdots & 0 & 1 \end{bmatrix} \begin{bmatrix} d_1 \\ d_1 \\ d_2 \\ \vdots \\ d_n \end{bmatrix},$$

analogous to equations (2.6), (2.7), and (2.8), respectively.

Our last example uses the following multiresolution filter vectors containing the local regular filters of cubic B-spline from [SBO07]:

$$\begin{cases} \mathbf{a} = \begin{bmatrix} \frac{23}{196} & -\frac{23}{49} & \frac{9}{28} & \frac{52}{49} & \frac{9}{28} & -\frac{23}{49} & \frac{23}{196} \end{bmatrix}, \\ \mathbf{b} = \begin{bmatrix} \frac{13}{98} & -\frac{26}{49} & \frac{39}{49} & -\frac{26}{49} & \frac{13}{98} \end{bmatrix}, \\ \mathbf{p} = \begin{bmatrix} \frac{1}{8} & \frac{1}{2} & \frac{3}{4} & \frac{1}{2} & \frac{1}{8} \end{bmatrix}, \\ \mathbf{q} = \begin{bmatrix} -\frac{23}{208} & -\frac{23}{52} & -\frac{63}{208} & 1 & -\frac{63}{208} & -\frac{23}{52} & -\frac{23}{208} \end{bmatrix}. \end{cases} \tag{A.3}$$

The filter vectors in equation (A.3) are known as the *wide* and *optimal* filters of cubic B-spline. For these filter vectors, the matrix equations for a balanced multiresolution scheme we devised

using our method for $n \in \mathbb{Z}^+$ are

$$\begin{bmatrix} c_1 \\ c_2 \\ \vdots \\ c_n \end{bmatrix} = \begin{bmatrix} \frac{23}{196} & -\frac{23}{49} & \frac{9}{28} & \frac{52}{49} & \frac{9}{28} & -\frac{23}{49} & \frac{23}{196} & 0 & 0 & 0 & \cdots \\ 0 & 0 & \frac{23}{196} & -\frac{23}{49} & \frac{9}{28} & \frac{52}{49} & \frac{9}{28} & -\frac{23}{49} & \frac{23}{196} & 0 & \cdots \\ \vdots & \vdots & \vdots & \vdots & \vdots & \vdots & \vdots & \vdots & \vdots & \vdots & \ddots \end{bmatrix} \begin{bmatrix} f_3 \\ f_2 \\ f_1 \\ f_2 \\ \vdots \\ f_{2n-1} \\ f_{2n} \\ f_{2n-1} \\ f_{2n-2} \\ f_{2n-3} \end{bmatrix},$$

$$\begin{bmatrix} d_1 \\ d_2 \\ \vdots \\ d_n \end{bmatrix} = \begin{bmatrix} \frac{13}{98} & -\frac{26}{49} & \frac{39}{49} & -\frac{26}{49} & \frac{13}{98} & 0 & 0 & 0 & \cdots \\ 0 & 0 & \frac{13}{98} & -\frac{26}{49} & \frac{39}{49} & -\frac{26}{49} & \frac{13}{98} & 0 & \cdots \\ \vdots & \vdots & \vdots & \vdots & \vdots & \vdots & \vdots & \vdots & \ddots \end{bmatrix} \begin{bmatrix} f_3 \\ f_2 \\ f_1 \\ f_2 \\ \vdots \\ f_{2n-1} \\ f_{2n} \\ f_{2n-1} \end{bmatrix},$$

and

$$\begin{bmatrix} f_1 \\ f_2 \\ \vdots \\ f_{2n} \end{bmatrix} = \begin{bmatrix} \frac{1}{2} & \frac{1}{2} & 0 & \cdots & 0 & 0 & 0 & 0 & 0 \\ \frac{1}{8} & \frac{3}{4} & \frac{1}{8} & \cdots & 0 & 0 & 0 & 0 & 0 \\ \vdots & \vdots & \vdots & \ddots & \vdots & \vdots & \vdots & \vdots & \vdots \\ 0 & 0 & 0 & \cdots & 0 & \frac{1}{8} & \frac{3}{4} & \frac{1}{8} & 0 \\ 0 & 0 & 0 & \cdots & 0 & 0 & \frac{1}{2} & \frac{1}{2} & 0 \\ 0 & 0 & 0 & \cdots & 0 & 0 & \frac{1}{8} & \frac{3}{4} & \frac{1}{8} \end{bmatrix} \begin{bmatrix} c_1 \\ c_1 \\ c_2 \\ \vdots \\ c_{n-1} \\ c_n \\ c_{n-1} \end{bmatrix}$$

$$+ \begin{bmatrix} -\frac{23}{52} & 1 & -\frac{23}{52} & 0 & \cdots & 0 & 0 & 0 & 0 & 0 \\ -\frac{23}{208} & -\frac{63}{208} & -\frac{63}{208} & -\frac{23}{208} & \cdots & 0 & 0 & 0 & 0 & 0 \\ \vdots & \vdots & \vdots & \vdots & \ddots & \vdots & \vdots & \vdots & \vdots & \vdots \\ 0 & 0 & 0 & 0 & \cdots & -\frac{23}{208} & -\frac{63}{208} & -\frac{63}{208} & -\frac{23}{208} & 0 \\ 0 & 0 & 0 & 0 & \cdots & 0 & -\frac{23}{52} & 1 & -\frac{23}{52} & 0 \\ 0 & 0 & 0 & 0 & \cdots & 0 & -\frac{23}{208} & -\frac{63}{208} & -\frac{63}{208} & -\frac{23}{208} \end{bmatrix} \begin{bmatrix} d_2 \\ d_1 \\ d_2 \\ \vdots \\ d_{n-1} \\ d_n \\ d_n \\ d_{n-1} \end{bmatrix}, \tag{A.4}$$

analogous to equations (2.6), (2.7), and (2.8), respectively.

In Table A.1, we summarize all the balanced multiresolution schemes presented in this thesis so far, in addition to six other sets of symmetric/antisymmetric regular multiresolution filters. The biorthogonal and reverse biorthogonal filters [CDF92, Dau92] we referred to in the table are available in MATLAB [MAT14].

In the first column of In Table A.1, $\mathbf{q}^R$ denotes the reversed filter vector $\mathbf{q}$. The second through fifth columns specify the symmetric (S)/antisymmetric (A) structure of the $\mathbf{a}$, $\mathbf{b}$, $\mathbf{p}$, and $\mathbf{q}$ filter vectors, respectively, for each set of filters in the table. The next column mentions the parity of w_{a} and w_{b}, based on which we decide on the type of symmetric extension to use

for F.

For $n \in \mathbb{Z}^+$, the second-to-last column of Table A.1 illustrates the proposed extended vector of fine sample F' and the construction of the first coarse sample c_1 and detail sample d_1, applicable to one possible balanced multiresolution scheme for each set of filters in the table. Here, we only give the construction of c_1 and d_1 because the remaining pairs of coarse and detail samples can be obtained by subsequent shifts of the filter vectors $\mathbf{a}$ and $\mathbf{b}$ by two fine samples along F' (as shown in Fig. 3.6, for example). Finally, the last column shows the corresponding extended vectors of coarse samples C' and detail samples D', in addition to the reconstruction of the fine samples in F_l and F_r as defined in section 3.2.2. In this column, filter vectors of odd and even width are assumed to have formats similar to $\begin{bmatrix} \dots & v_{-2} & v_{-1} & v_0 & v_1 & v_2 & \dots \end{bmatrix}$ and $\begin{bmatrix} \dots & v_{-2} & v_{-1} & v_1 & v_2 & \dots \end{bmatrix}$, respectively.

Although providing a recipe for choosing the appropriate set of filters for a particular application is not the focus of this thesis, here we provide a high-level guideline. To decide which set of filters is more suitable for a particular application, a number factors such as smoothness of results, widths of filter vectors, the number of vanishing moments of the associated wavelet function, and the support of underlying basis function are taken into consideration. Firstly, when the visual quality of results is important, a set of filters that provides higher level of smoothness is preferred. Secondly, shorter widths of filter vectors imply faster implementation and if applicable, higher frame rate. An interactive focus+context visualization application like the one demonstrated in this thesis performs more efficiently if the filter vectors are not too wide. For instance, only one level of balanced decomposition of a $512 \times 512 \times 512$ image using a width-7 $\mathbf{a}$ filter vector in place of a width-4 $\mathbf{a}$ filter vector will take 21×256^3 more multiplications, incurring a 75% increase in the number of multiplications required. Next, higher number of vanishing moments of the associated wavelet function implies wider filter vectors and lesser smoothness of results. However, higher number of vanishing moments allows better approximation of scaling functions, which is desirable in

compression applications. Finally, filter vectors that provide compact support lead to better local effects, usually required for applications allowing multiresolution editing.

Daubechies proposed a family of orthogonal wavelets with the highest number of vanishing moments for some expected support but it does not allow for the best smoothness [Dau88]. The filter vectors resulting from this work are asymmetric (see equation (B.1), for example). Using a similar idea for construction, Cohen *el al.* proposed the first family of biorthogonal wavelets, which leads to filter vectors that are symmetric or antisymmetric about their centers [CDF92,

resulted from this work. On the other hand, the B-splines filters in Table A.1 are developed by Samavati *et al.* based on reverse subdivision [SB99, BS00, SBO07]. Filters of higher order B-spline produce smoother results. The associated construction procedure starts by setting the width of the decomposition filter vector $\mathbf{a}$, where wider $\mathbf{a}$ results in better coarse approximations. Constraints can be set in the construction procedure such that the resulting coarse approximations are smoother. For instance, Sadeghi and Samavati proposed smooth reverse subdivision for obtaining smooth coarse data through decomposition [SS09, SS11].

Table A.1: Balanced multiresolution schemes.

Filters	**a**	**b**	**p**	**q**	w_a, w_b	**Decomposition:** F', c_1, d_1	**Reconstruction:** $C', D', f_i \in \left[F_l^T \ F_r^T\right]^T$
Filters of second order B-spline (A.1) Biorthogonal 2.2 filters ($\mathbf{a}, \mathbf{b}, \mathbf{p}$, and $\mathbf{q}$ in [MAT14])	S	S	S	S	Odd	$F' = [f_2 \ f_1 \ \dots \ f_{2n} \ f_{2n-1} \ f_{2n-2}]^T$, $\begin{cases} c_1 = a_{-2}f_2 + a_{-1}f_1 + a_0 f_2 \\ \qquad + a_1 f_3 + a_2 f_4, \\ d_1 = b_{-1}f_2 + b_0 f_1 + b_1 f_2. \end{cases}$	$C' = [c_1 \ c_1 \ \dots \ c_n]^T$, $D' = [d_2 \ d_1 \ \dots \ d_n \ d_n]^T$, $\begin{cases} f_1 = p_1 c_1 + p_{-1} c_1 + q_2 d_2 + q_0 d_1 + q_{-2} d_2, \\ f_{2n-1} = p_1 c_{n-1} + p_{-1} c_n + q_2 d_{n-1} + q_0 d_n + q_{-2} d_n, \\ f_{2n} = p_0 c_n + q_1 d_n + q_{-1} d_n. \end{cases}$
Short filters of quadratic B-spline (3.1) Biorthogonal 3.1 filters ($\mathbf{a}, \mathbf{b}, \mathbf{p}$, and $\mathbf{q}^R$ in [MAT14]) Reverse biorthogonal 3.1 filters ($\mathbf{a}, \mathbf{b}, \mathbf{p}$, and $\mathbf{q}^R$ in [MAT14])	S	A	S	A	Even	$F' = [f_1 \ f_1 \ \dots \ f_{2n} \ f_{2n}]^T$, $\begin{cases} c_1 = a_{-2}f_1 + a_{-1}f_1 + a_1 f_2 + a_2 f_3, \\ d_1 = b_{-2}f_1 + b_{-1}f_1 + b_1 f_2 + b_2 f_3. \end{cases}$	$C' = [c_1 \ c_1 \ \dots \ c_n \ c_n]^T$, $D' = [-d_1 \ d_1 \ \dots \ d_n \ -d_n]^T$, $\begin{cases} f_1 = p_2 c_1 + p_{-1} c_1 + q_2(-d_1) + q_{-1} d_1, \\ f_{2n} = p_1 c_n + p_{-2} c_n + q_1 d_n + q_{-2}(-d_n). \end{cases}$
Wide filters of quadratic B-spline ($\mathbf{a}, \mathbf{b}, \mathbf{p}$, and $\mathbf{q}$ in [SBO07]) Biorthogonal 3.3 filters ($\mathbf{a}, \mathbf{b}, \mathbf{p}$, and $\mathbf{q}^R$ in [MAT14])	S	A	S	A	Even	$F' = [f_3 \ f_2 \ f_1 \ f_1 \ \dots \ f_{2n} \ f_{2n} \ f_{2n-1} \ f_{2n-2}]^T$, $\begin{cases} c_1 = a_{-4}f_3 + a_{-3}f_2 + a_{-2}f_1 + a_{-1}f_1 \\ \qquad + a_1 f_2 + a_2 f_3 + a_3 f_4 + d_4 f_5, \\ d_1 = b_{-2}f_1 + b_{-1}f_1 + b_1 f_2 + b_2 f_3. \end{cases}$	$C' = [c_1 \ c_1 \ \dots \ c_n \ c_n]^T$, $D' = [-d_2 \ -d_1 \ d_1 \ \dots \ d_n \ -d_n \ -d_{n-1}]^T$, $\begin{cases} f_1 = p_2 c_1 + p_{-1} c_1 + q_4(-d_2) + q_2(-d_1) + q_{-1} d_1 + q_{-3} d_2, \\ f_2 = p_1 c_1 + p_{-2} c_2 + q_3(-d_1) + q_1 d_1 + q_{-2} d_2 + q_{-4} d_3, \\ f_3 = p_2 c_1 + p_{-1} c_2 + q_4(-d_1) + q_2 d_1 + q_{-1} d_2 + q_{-3} d_3, \\ f_{2n-2} = p_1 c_{n-1} + p_{-2} c_n + q_3 d_{n-2} + q_1 d_{n-1} + q_{-2} d_n + q_{-4}(-d_n), \\ f_{2n-1} = p_2 c_{n-1} + p_{-1} c_n + q_4 d_{n-2} + q_2 d_{n-1} + q_{-1} d_n + q_{-3}(-d_n), \\ f_{2n} = p_1 c_n + p_{-2} c_n + q_3 d_{n-1} + q_1 d_n + q_{-2} - d_n + q_{-4}(-d_{n-1}). \end{cases}$
Short filters of cubic B-spline (A.2) Reverse biorthogonal 2.2 filters ($\mathbf{a}, \mathbf{b}, \mathbf{p}$, and $\mathbf{q}$ in [MAT14])	S	S	S	S	Odd	$F' = [f_2 \ f_1 \ \dots \ f_{2n} \ f_{2n-1} \ f_{2n-2}]^T$, $\begin{cases} c_1 = a_{-1}f_2 + a_0 f_1 + a_1 f_2, \\ d_1 = b_{-2}f_2 + b_{-1}f_1 + b_0 f_2 \\ \qquad + b_1 f_3 + b_2 f_4. \end{cases}$	$C' = [c_2 \ c_1 \ \dots \ c_n \ c_n]^T$, $D' = [d_1 \ d_1 \ \dots \ d_n]^T$, $\begin{cases} f_1 = p_2 c_2 + p_0 c_1 + p_{-2} c_2 + q_1 d_1 + q_{-1} d_1, \\ f_{2n-1} = p_2 c_{n-1} + p_0 c_n + p_{-2} c_n + q_1 d_{n-1} + q_{-1} d_n, \\ f_{2n} = p_1 c_n + p_{-1} c_n + q_0 d_n. \end{cases}$
Inverse powers of two filters of cubic B-spline (3.15) *Wide* and *optimal* filters of cubic B-spline (A.3)	S	S	S	S	Odd	$F' = [f_3 \ f_2 \ f_1 \ \dots \ f_{2n} \ f_{2n-1} \ f_{2n-2} \ f_{2n-3}]^T$, $\begin{cases} c_1 = a_{-3}f_3 + a_{-2}f_2 + a_{-1}f_1 + a_0 f_2 \\ \qquad + a_1 f_3 + a_2 f_4 + a_3 f_5, \\ d_1 = b_{-2}f_3 + b_{-1}f_2 + b_0 f_1 \\ \qquad + b_1 f_2 + b_2 f_3. \end{cases}$	$C' = [c_1 \ c_1 \ \dots \ c_n \ c_{n-1}]^T$, $D' = [d_2 \ d_1 \ \dots \ d_n \ d_n \ d_{n-1}]^T$, $\begin{cases} f_1 = p_1 c_1 + p_{-1} c_1 + q_2 d_2 + q_0 d_1 + q_{-2} d_2, \\ f_2 = p_2 c_1 + p_0 c_1 + p_{-2} c_2 + q_3 d_2 + q_1 d_1 + q_{-1} d_2 + q_{-3} d_3, \\ f_{2n-2} = p_2 c_{n-2} + p_0 c_{n-1} + p_{-2} c_n + q_3 d_{n-2} + q_1 d_{n-1} + q_{-1} d_n + q_{-3} d_n, \\ f_{2n-1} = p_1 c_{n-1} + p_{-1} c_n + q_2 d_{n-1} + q_0 d_n + q_{-2} d_n, \\ f_{2n} = p_2 c_{n-1} + p_0 c_n + p_{-2} c_{n-1} + q_3 d_{n-1} + q_1 d_n + q_{-1} d_n + q_{-3} d_{n-1}. \end{cases}$

Appendix B

Balanced Wavelet Transform using Asymmetric Filter Vectors: An Example

An attempt to apply our general approach for devising a balanced multiresolution scheme described in section 3.2 to Daubechies' asymmetric D4 filters [Dau88, SDS96],

$$\begin{cases} \mathbf{a} = \mathbf{p} = \left[\frac{1+\sqrt{3}}{4\sqrt{2}} \quad \frac{3+\sqrt{3}}{4\sqrt{2}} \quad \frac{3-\sqrt{3}}{4\sqrt{2}} \quad \frac{1-\sqrt{3}}{4\sqrt{2}} \right], \\ \mathbf{b} = \mathbf{q} = \left[\frac{1-\sqrt{3}}{4\sqrt{2}} \quad \frac{-3+\sqrt{3}}{4\sqrt{2}} \quad \frac{3+\sqrt{3}}{4\sqrt{2}} \quad \frac{-1-\sqrt{3}}{4\sqrt{2}} \right], \end{cases} \tag{B.1}$$

produces the balanced decomposition setup shown in Fig. B.1 and the perfect reconstruction setup shown in Fig. B.2. Note that it introduces two extraordinary boundary filter values, $\frac{-2+\sqrt{3}}{\sqrt{2}}$ and $\frac{2+\sqrt{3}}{\sqrt{2}}$ in the reconstruction of f_1 and f_8, respectively. Because the filter vectors in equation (B.1) are not symmetric/antisymmetric, the rewriting task suggested in step 2(c) and that of step 3 in our *general construction* given in section 3.2.2 were not entirely successful. Therefore, our approach could not ensure a perfect reconstruction using only the regular filters from equation (B.1).

As we observe in Fig. B.2, this particular example does not require any extraordinary boundary filters for the subdivision matrix $\mathbf{P}$. This may not always be the case while using other asymmetric filter vectors.

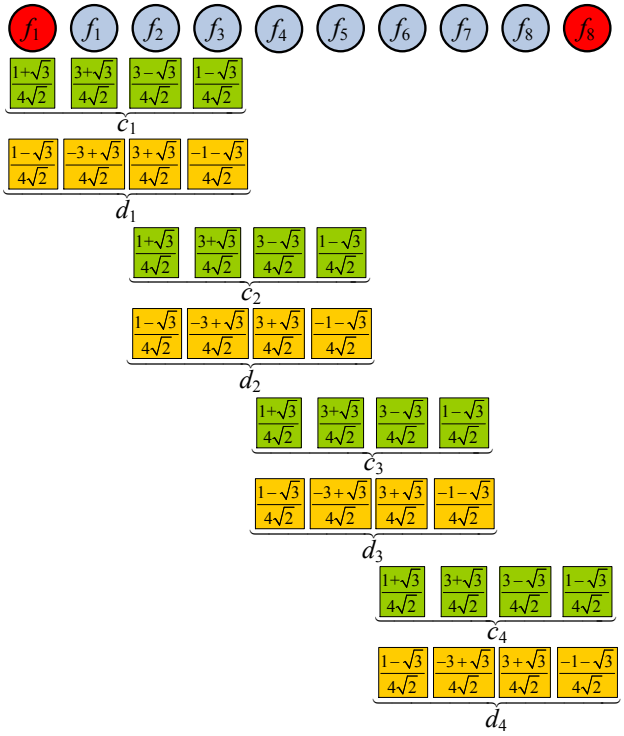

Figure B.1: Balanced decomposition of 8 fine samples using the decomposition filter vectors **a** and **b** from equation (B.1).

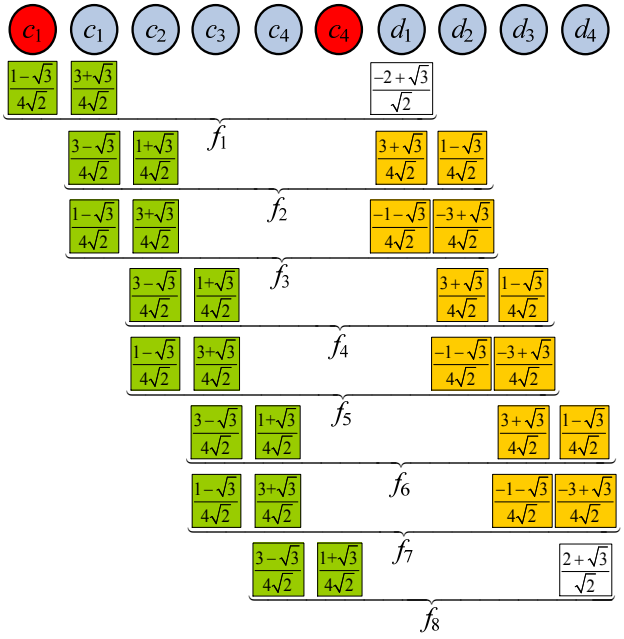

Figure B.2: Perfect reconstruction of 8 fine samples using the reconstruction filter vectors **p** and **q** from equation (B.1).

Appendix C

Balanced Integer Wavelet Transform Recipes

for Various Symmetric/Antisymmetric Decomposition Filter Vectors

Further to the examples in chapter 4, this appendix demonstrates our general approach for devising general recipes for balanced decomposition and perfect reconstruction described in section 4.2 by means of two more examples. As the first example, we present two possible general recipes in the second and third columns of table C.1 when the given decomposition filter vector

$$\mathbf{a} = \begin{bmatrix} \frac{1}{2} & \frac{1}{2} \end{bmatrix} \tag{C.1}$$

is of width two and a part of the Haar multiresolution filters [Haa10, SDS96].

Table C.1: Balanced multiresolution schemes for Haar filters

Process	**Our Recipe (i)**	**Our Recipe (ii)**	**Recipe from [SP96]**	**Recipe from [Haa10]**
Decomposition	$c_i = f_{2i} + \left\lfloor \frac{1}{2} \underbrace{(f_{2i-1} - f_{2i})}_{d_i} \right\rfloor.$	$c_i = f_{2i-1} + \left\lfloor \frac{1}{2} \underbrace{(f_{2i} - f_{2i-1})}_{d_i} \right\rfloor.$	$\begin{cases} c_i = \left\lfloor \frac{f_{2i-1}+f_{2i}}{2} \right\rfloor, \\ d_i = f_{2i-1} - f_{2i}. \end{cases}$	$\begin{cases} c_i^r = \frac{1}{2} f_{2i-1} + \frac{1}{2} f_{2i}. \\ d_i^r = \frac{1}{2} f_{2i-1} - \frac{1}{2} f_{2i}. \end{cases}$
Reconstruction	$\begin{cases} f_{2i-1} &= f_{2i} + d_i \\ &= c_i + d_i - \left\lfloor \frac{d_i}{2} \right\rfloor, \\ f_{2i} &= c_i - \left\lfloor \frac{d_i}{2} \right\rfloor. \end{cases}$	$\begin{cases} f_{2i-1} &= c_i - \left\lfloor \frac{d_i}{2} \right\rfloor, \\ f_{2i} &= f_{2i-1} + d_i \\ &= c_i + d_i - \left\lfloor \frac{d_i}{2} \right\rfloor. \end{cases}$	$\begin{cases} f_{2i-1} = c_i + \left\lfloor \frac{d_i+1}{2} \right\rfloor, \\ f_{2i} = f_{2i-1} - d_i. \end{cases}$	$\begin{cases} f_{2i-1} = c_i^r + d_i^r, \\ f_{2i} = c_i^r - d_i^r. \end{cases}$

For the sake of comparison, the fourth and fifth columns of table C.1 show preexisting general recipes for balanced multiresolution using Haar filters. In this table, f_{2i-1} and f_{2i} represent fine integer samples and c_i, d_i, c_i^r, and d_i^r represent a coarse integer sample, a detail integer sample, a coarse real sample, and a detail real sample, respectively, where $i \in \{1 \dots n\}$ for a suitably large $n \in \mathbb{Z}^+$. Note that because the given decomposition filter vector in equation (C.1) is of width two, the use of symmetric/antisymmetric extensions was not required for achieving a balanced decomposition and subsequent perfect reconstruction, and alternating definitions of detail integer samples were not required to ensure local perfect reconstruction.

The second example involves the following decomposition filter vector containing the local regular filters of cubic (fourth order) B-spline from [SBO07]:

$$\mathbf{a} = \begin{bmatrix} -\frac{1}{2} & 2 & -\frac{1}{2} \end{bmatrix}. \tag{C.2}$$

The decomposition filter vector in equation (A.2) is a part of the *short* multiresolution filters of cubic B-spline. Given this decomposition filter vector, following is a general recipe for balanced decomposition under our proposed framework:

$$\begin{cases} c_1 = f_2 + \left\lfloor \frac{1}{2} \underbrace{(-f_2 + 4f_1 - 3f_2)}_{d_1} \right\rfloor, \\ \vdots \\ c_i = f_{2i} + \left\lfloor \frac{1}{2} \underbrace{(-f_{2i-2} + 4f_{2i-1} - 3f_{2i})}_{d_i} \right\rfloor. \end{cases} \tag{C.3}$$

The corresponding general recipe for perfect reconstruction is

$$\begin{cases} f_1 = \frac{1}{2}c_1 + \frac{3}{4}c_1 + \frac{1}{4}d_1 - \frac{1}{4}\left\lfloor \frac{d_1}{2} \right\rfloor - \frac{3}{4}\left\lfloor \frac{d_1}{2} \right\rfloor, \\ f_2 = c_1 - \left\lfloor \frac{d_1}{2} \right\rfloor, \\ \vdots \\ f_{2i-1} = \frac{1}{2}c_{i-1} + \frac{3}{4}c_i + \frac{1}{4}d_i - \frac{1}{4}\left\lfloor \frac{d_{i-1}}{2} \right\rfloor - \frac{3}{4}\left\lfloor \frac{d_i}{2} \right\rfloor, \\ f_{2i} = c_i - \left\lfloor \frac{d_i}{2} \right\rfloor. \end{cases} \tag{C.4}$$

In (C.3) and (C.4), $i \in \{1 \ldots n\}$ for a suitably large $n \in \mathbb{Z}^+$. Note that because the given decomposition filter vector in equation (C.2) is of width three, the use of symmetric/antisymmetric extensions was required for achieving a balanced decomposition and subsequent perfect reconstruction, but alternating definitions of detail integer samples were not required to ensure local perfect reconstruction. However, the general recipes for balanced decomposition and perfect reconstruction presented for a given decomposition filter vector of width four in (4.26) and (4.52), respectively, as well as in (4.64) and (4.65), respectively, made use of symmetric/antisymmetric extensions for achieving a balanced decomposition and subsequent perfect reconstruction, and alternating definitions of detail integer samples to ensure local perfect reconstruction.

Appendix D

Balanced Integer Wavelet Transform using Reverse Chaikin Filters: An Example

In this example, we show a balanced decomposition and subsequent perfect reconstruction of a column vector of 16 fine integer samples

$$F = \begin{bmatrix} f_1 & f_2 & \dots & f_{15} & f_{16} \end{bmatrix}^T \tag{D.1}$$

for the given decomposition filter vector

$$\mathbf{a} = \begin{bmatrix} -\frac{1}{4} & \frac{3}{4} & \frac{3}{4} & -\frac{1}{4} \end{bmatrix}. \tag{D.2}$$

The decomposition filter vector $\mathbf{a}$ in equation (D.2), is a part of the *short*, local, regular multiresolution filters of quadratic (third order) B-spline [SBO07, SB04], obtained by reversing Chaikin subdivision [Cha74].

Following the general recipe for a balanced decomposition in equations (4.21) and (4.23) leading the generalization in (4.26), we obtain the column vector of 8 coarse integer samples

$$C = \begin{bmatrix} c_1 & c_2 & \dots & c_7 & c_8 \end{bmatrix}^T$$

and the column vector of 8 detail integer samples

$$D = \begin{bmatrix} d_1 & d_2 & \dots & d_7 & d_8 \end{bmatrix}^T$$

from an extended column vector of fine integer samples

$$F' = \begin{bmatrix} f_1 & f_1 & f_2 & \dots & f_{15} & f_{16} & f_{16} \end{bmatrix}^T$$

as follows:

$$\begin{cases} c_1 = (-f_1 + 2f_1) + \left\lfloor \frac{1}{4} \underbrace{(3f_1 - 5f_1 + 3f_2 - f_3)}_{d_1} \right\rfloor, \\ c_2 = (2f_4 - f_5) + \left\lfloor \frac{1}{4} \underbrace{(-f_2 + 3f_3 - 5f_4 + 3f_5)}_{d_2} \right\rfloor, \\ c_3 = (-f_4 + 2f_5) + \left\lfloor \frac{1}{4} \underbrace{(3f_4 - 5f_5 + 3f_6 - f_7)}_{d_3} \right\rfloor, \\ c_4 = (2f_8 - f_9) + \left\lfloor \frac{1}{4} \underbrace{(-f_6 + 3f_7 - 5f_8 + 3f_9)}_{d_4} \right\rfloor, \\ c_5 = (-f_8 + 2f_9) + \left\lfloor \frac{1}{4} \underbrace{(3f_8 - 5f_9 + 3f_{10} - f_{11})}_{d_5} \right\rfloor, \\ c_6 = (2f_{12} - f_{13}) + \left\lfloor \frac{1}{4} \underbrace{(-f_{10} + 3f_{11} - 5f_{12} + 3f_{13})}_{d_6} \right\rfloor, \\ c_7 = (-f_{12} + 2f_{13}) + \left\lfloor \frac{1}{4} \underbrace{(3f_{12} - 5f_{13} + 3f_{14} - f_{15})}_{d_7} \right\rfloor, \\ c_8 = (2f_{16} - f_{16}) + \left\lfloor \frac{1}{4} \underbrace{(-f_{14} + 3f_{15} - 5f_{16} + 3f_{16})}_{d_8} \right\rfloor. \end{cases} \tag{D.3}$$

Next, following the general recipe in (4.52), we perfectly reconstruct F from equation (D.1) from an extended column vector of coarse integer samples

$$C' = \begin{bmatrix} c_1 & c_1 & c_2 & \dots & c_7 & c_8 & c_8 \end{bmatrix}^T$$

and an extended column vector of detail integer samples

$$D' = \begin{bmatrix} d_1 & d_1 & d_2 & \dots & d_7 & d_8 & d_8 \end{bmatrix}^T$$

as follows:

$$
\begin{cases}
f_1 = \frac{1}{3}c_1 + \frac{2}{3}c_1 - \frac{1}{3}\left\lfloor \frac{d_1}{4} \right\rfloor - \frac{2}{3}\left\lfloor \frac{d_1}{4} \right\rfloor, \\
f_2 = -\frac{1}{8}c_1 + \frac{7}{8}c_1 + \frac{7}{24}c_2 - \frac{1}{24}c_3 + \frac{3}{8}d_1 + \frac{1}{8}d_2 + \frac{1}{8}\left\lfloor \frac{d_1}{4} \right\rfloor - \frac{7}{8}\left\lfloor \frac{d_1}{4} \right\rfloor - \frac{7}{24}\left\lfloor \frac{d_2}{4} \right\rfloor + \frac{1}{24}\left\lfloor \frac{d_3}{4} \right\rfloor, \\
f_3 = -\frac{1}{24}c_1 + \frac{7}{24}c_1 + \frac{7}{8}c_2 - \frac{1}{8}c_3 + \frac{1}{8}d_1 + \frac{3}{8}d_2 + \frac{1}{24}\left\lfloor \frac{d_1}{4} \right\rfloor - \frac{7}{24}\left\lfloor \frac{d_1}{4} \right\rfloor - \frac{7}{8}\left\lfloor \frac{d_2}{4} \right\rfloor + \frac{1}{8}\left\lfloor \frac{d_3}{4} \right\rfloor, \\
f_4 = \frac{2}{3}c_2 + \frac{1}{3}c_3 - \frac{2}{3}\left\lfloor \frac{d_2}{4} \right\rfloor - \frac{1}{3}\left\lfloor \frac{d_3}{4} \right\rfloor, \\
f_5 = \frac{1}{3}c_2 + \frac{2}{3}c_3 - \frac{1}{3}\left\lfloor \frac{d_2}{4} \right\rfloor - \frac{2}{3}\left\lfloor \frac{d_3}{4} \right\rfloor, \\
f_6 = -\frac{1}{8}c_2 + \frac{7}{8}c_3 + \frac{7}{24}c_4 - \frac{1}{24}c_5 + \frac{3}{8}d_3 + \frac{1}{8}d_4 + \frac{1}{8}\left\lfloor \frac{d_2}{4} \right\rfloor - \frac{7}{8}\left\lfloor \frac{d_3}{4} \right\rfloor - \frac{7}{24}\left\lfloor \frac{d_4}{4} \right\rfloor + \frac{1}{24}\left\lfloor \frac{d_5}{4} \right\rfloor, \\
f_7 = -\frac{1}{24}c_2 + \frac{7}{24}c_3 + \frac{7}{8}c_4 - \frac{1}{8}c_5 + \frac{1}{8}d_3 + \frac{3}{8}d_4 + \frac{1}{24}\left\lfloor \frac{d_2}{4} \right\rfloor - \frac{7}{24}\left\lfloor \frac{d_3}{4} \right\rfloor - \frac{7}{8}\left\lfloor \frac{d_4}{4} \right\rfloor + \frac{1}{8}\left\lfloor \frac{d_5}{4} \right\rfloor, \\
f_8 = \frac{2}{3}c_4 + \frac{1}{3}c_5 - \frac{2}{3}\left\lfloor \frac{d_4}{4} \right\rfloor - \frac{1}{3}\left\lfloor \frac{d_5}{4} \right\rfloor, \\
f_9 = \frac{1}{3}c_4 + \frac{2}{3}c_5 - \frac{1}{3}\left\lfloor \frac{d_4}{4} \right\rfloor - \frac{2}{3}\left\lfloor \frac{d_5}{4} \right\rfloor, \\
f_{10} = -\frac{1}{8}c_4 + \frac{7}{8}c_5 + \frac{7}{24}c_6 - \frac{1}{24}c_7 + \frac{3}{8}d_5 + \frac{1}{8}d_6 + \frac{1}{8}\left\lfloor \frac{d_4}{4} \right\rfloor - \frac{7}{8}\left\lfloor \frac{d_5}{4} \right\rfloor - \frac{7}{24}\left\lfloor \frac{d_6}{4} \right\rfloor + \frac{1}{24}\left\lfloor \frac{d_7}{4} \right\rfloor, \\
f_{11} = -\frac{1}{24}c_4 + \frac{7}{24}c_5 + \frac{7}{8}c_6 - \frac{1}{8}c_7 + \frac{1}{8}d_5 + \frac{3}{8}d_6 + \frac{1}{24}\left\lfloor \frac{d_4}{4} \right\rfloor - \frac{7}{24}\left\lfloor \frac{d_5}{4} \right\rfloor - \frac{7}{8}\left\lfloor \frac{d_6}{4} \right\rfloor + \frac{1}{8}\left\lfloor \frac{d_7}{4} \right\rfloor, \\
f_{12} = \frac{2}{3}c_6 + \frac{1}{3}c_7 - \frac{2}{3}\left\lfloor \frac{d_6}{4} \right\rfloor - \frac{1}{3}\left\lfloor \frac{d_7}{4} \right\rfloor, \\
f_{13} = \frac{1}{3}c_6 + \frac{2}{3}c_7 - \frac{1}{3}\left\lfloor \frac{d_6}{4} \right\rfloor - \frac{2}{3}\left\lfloor \frac{d_7}{4} \right\rfloor, \\
f_{14} = -\frac{1}{8}c_6 + \frac{7}{8}c_7 + \frac{7}{24}c_8 - \frac{1}{24}c_8 + \frac{3}{8}d_7 + \frac{1}{8}d_8 + \frac{1}{8}\left\lfloor \frac{d_6}{4} \right\rfloor - \frac{7}{8}\left\lfloor \frac{d_7}{4} \right\rfloor - \frac{7}{24}\left\lfloor \frac{d_8}{4} \right\rfloor + \frac{1}{24}\left\lfloor \frac{d_8}{4} \right\rfloor, \\
f_{15} = -\frac{1}{24}c_6 + \frac{7}{24}c_7 + \frac{7}{8}c_8 - \frac{1}{8}c_8 + \frac{1}{8}d_7 + \frac{3}{8}d_8 + \frac{1}{24}\left\lfloor \frac{d_6}{4} \right\rfloor - \frac{7}{24}\left\lfloor \frac{d_7}{4} \right\rfloor - \frac{7}{8}\left\lfloor \frac{d_8}{4} \right\rfloor + \frac{1}{8}\left\lfloor \frac{d_8}{4} \right\rfloor, \\
f_{16} = \frac{2}{3}c_8 + \frac{1}{3}c_8 - \frac{2}{3}\left\lfloor \frac{d_8}{4} \right\rfloor - \frac{1}{3}\left\lfloor \frac{d_8}{4} \right\rfloor.
\end{cases}
\tag{D.4}
$$

Note that as desired, no extraordinary boundary filters were used in (D.4) for the perfect reconstruction of fine boundary integer samples.

Appendix E

Copyright Transfer Agreements

Permitting Materials Inclusion in Dissertation

This appendix includes copies of copyright transfer agreements for one conference paper [HSJ14] and two journal articles [HSS15, HSJ15], first-authored by the author of this dissertation. These copyright transfer agreements permit the inclusion of materials in this dissertation from respective publications.

IEEE COPYRIGHT AND CONSENT FORM

To ensure uniformity of treatment among all contributors, other forms may not be substituted for this form, nor may any wording of the form be changed. This form is intended for original material submitted to the IEEE and must accompany any such material in order to be published by the IEEE.Please read the form carefully and keep a copy for your files.

TITLE OF PAPER/ARTICLE/REPORT, INCLUDING ALL CONTENT IN ANY FORM, FORMAT, OR MEDIA (hereinafter, "The Work"):**Multilevel Focus+Context Visualization using Balanced Multiresolution**

COMPLETE LIST OF AUTHORS:**Mahmudul Hasan**

IEEE PUBLICATION TITLE (Journal, Magazine, Conference, Book):**2014 International Conference on Cyberworlds**

COPYRIGHT TRANSFER

1. The undersigned hereby assigns to The Institute of Electrical and Electronics Engineers,Incorporated (the "IEEE") all rights under copyright that may exist in and to: (a) the above Work,including any revised or expanded derivative works submitted to the IEEE by the undersigned based on the Work; and (b) any associated written or multimedia components or other enhancements accompanying the Work.

CONSENT AND RELEASE

2. ln the event the undersigned makes a presentation based upon the Work at a conference hosted or sponsored in whole or in part by the IEEE, the undersigned, in consideration for his/her participation in the conference, hereby grants the IEEE the unlimited, worldwide, irrevocable permission to use, distribute, publish, license, exhibit, record, digitize, broadcast, reproduce and archive, in any format or medium, whether now known or hereafter developed: (a) his/her presentation and comments at the conference; (b) any written materials or multimedia files used in connection with his/her presentation; and (c) any recorded interviews of him/her (collectively, the "Presentation"). The permission granted includes the transcription and reproduction ofthe Presentation for inclusion in products sold or distributed by IEEE and live or recorded broadcast ofthe Presentation during or after the conference.

3. In connection with the permission granted in Section 2, the undersigned hereby grants IEEE the unlimited, worldwide, irrevocable right to use his/her name, picture, likeness, voice and biographical information as part of the advertisement, distribution and sale ofproducts incorporating the Work or Presentation, and releases IEEE from any claim based on right of privacy or publicity.

4. The undersigned hereby warrants that the Work and Presentation (collectively, the "Materials") are original and that he/she is the author of the Materials. To the extent the Materials incorporate text passages, figures, data or other material from the works of others, the undersigned has obtained any necessary permissions. Where necessary, the undersigned has obtained all third party permissions and consents to grant the license above and has provided copies of such permissions and consents to IEEE.

[X] Please check this box if you do not wish to have video/audio recordings made of your conference presentation.

See below for Retained Rights/Terms and Conditions, and Author Responsibilities.

AUTHOR RESPONSIBILITIES

The IEEE distributes its technical publications throughout the world and wants to ensure that the material submitted to its publications is properly available to the readership of those publications. Authors must ensure that their Work meets the requirements as stated in section 8.2.1 of the IEEE PSPB Operations Manual, including provisions covering originality, authorship, author responsibilities and author misconduct. More information on

IEEEs publishing policies may be found at http://www.ieee.org/publications_standards/publications/rights/authorrightsresponsibilities.html. Authors are advised especially of IEEE PSPB Operations Manual section 8.2.1.B12: "It is the responsibility of the authors, not the IEEE, to determine whether disclosure of their material requires the prior consent of other parties and, if so, to obtain it." Authors are also advised of IEEE PSPB Operations Manual section 8.1.1B: "Statements and opinions given in work published by the IEEE are the expression of the authors."

RETAINED RIGHTS/TERMS AND CONDITIONS

General

1. Authors/employers retain all proprietary rights in any process, procedure, or article of manufacture described in the Work.

2. Authors/employers may reproduce or authorize others to reproduce the Work, material extracted verbatim from the Work, or derivative works for the author's personal use or for company use, provided that the source and the IEEE copyright notice are indicated, the copies are not used in any way that implies IEEE endorsement of a product or service of any employer, and the copies themselves are not offered for sale.

3. In the case of a Work performed under a U.S. Government contract or grant, the IEEE recognizes that the U.S. Government has royalty-free permission to reproduce all or portions of the Work, and to authorize others to do so, for official U.S. Government purposes only, if the contract/grant so requires.

4. Although authors are permitted to re-use all or portions of the Work in other works, this does not include granting third-party requests for reprinting, republishing, or other types of re-use.The IEEE Intellectual Property Rights office must handle all such third-party requests.

5. Authors whose work was performed under a grant from a government funding agency are free to fulfill any deposit mandates from that funding agency.

Author Online Use

6. Personal Servers. Authors and/or their employers shall have the right to post the accepted version of IEEE-copyrighted articles on their own personal servers or the servers of their institutions or employers without permission from IEEE, provided that the posted version includes a prominently displayed IEEE copyright notice and, when published, a full citation to the original IEEE publication, including a link to the article abstract in IEEE Xplore.Authors shall not post the final, published versions of their papers.

7. Classroom or Internal Training Use. An author is expressly permitted to post any portion of the accepted version of his/her own IEEE-copyrighted articles on the authors personal web site or the servers of the authors institution or company in connection with the authors teaching, training, or work responsibilities, provided that the appropriate copyright, credit, and reuse notices appear prominently with the posted material. Examples of permitted uses are lecture materials, course packs, e-reserves, conference presentations, or in-house training courses.

8. Electronic Preprints. Before submitting an article to an IEEE publication, authors frequently post their manuscripts to their own web site, their employers site, or to another server that invites constructive comment from colleagues.Upon submission of an article to IEEE, an author is required to transfer copyright in the article to IEEE, and the author must update any previously posted version of the article with a prominently displayed IEEE copyright notice. Upon publication of an article by the IEEE, the author must replace any previously posted electronic versions of the article with either (1) the full citation to the IEEE work with a Digital Object Identifier (DOI) or link to the article abstract in IEEE Xplore, or (2) the accepted version only (not the IEEE-published version), including the IEEE copyright notice and full citation, with a link to the final, published article in IEEE Xplore.

INFORMATION FOR AUTHORS

IEEE Copyright Ownership

It is the formal policy of the IEEE to own the copyrights to all copyrightable material in its technical publications and to the individual contributions contained therein, in order to protect the interests of the IEEE, its authors and their employers, and, at the same time, to facilitate the appropriate re-

use of this material by others.The IEEE distributes its technical publications throughout the world and does so by various means such as hard copy, microfiche, microfilm, and electronic media.It also abstracts and may translate its publications, and articles contained therein, for inclusion in various compendiums, collective works, databases and similar publications.

Author/Employer Rights

If you are employed and prepared the Work on a subject within the scope of your employment, the copyright in the Work belongs to your employer as a work-for-hire. In that case, the IEEE assumes that when you sign this Form, you are authorized to do so by your employer and that your employer has consented to the transfer of copyright, to the representation and warranty of publication rights, and to all other terms and conditions of this Form. If such authorization and consent has not been given to you, an authorized representative of your employer should sign this Form as the Author.

GENERAL TERMS

1. The undersigned represents that he/she has the power and authority to make and execute this form.
2. The undersigned agrees to identify and hold harmless the IEEE from any damage or expense that may arise in the event of a breach of any of the warranties set forth above.
3. In the event the above work is not accepted and published by the IEEE or is withdrawn by the author(s) before acceptance by the IEEE, the foregoing grant of rights shall become null and void and all materials embodying the Work submitted to the IEEE will be destroyed.
4. For jointly authored Works, all joint authors should sign, or one of the authors should sign as authorized agent for the others.

Mahmudul Hasan	**18-07-2014**
Author/Authorized Agent For Joint Authors	**Date(dd-mm-yy)**

THIS FORM MUST ACCOMPANY THE SUBMISSION OF THE AUTHOR'S MANUSCRIPT.
Questions about the submission of the form or manuscript must be sent to the publication's editor.Please direct all questions about IEEE copyright policy to:
IEEE Intellectual Property Rights Office, [redacted](telephone)

RIGHTS & ACCESS

Elsevier Inc.

Article: Balanced Multiresolution for Symmetric/Antisymmetric Filters
Corresponding author: Mr. Mahmudul Hasan
E-mail address: [redacted]
Journal: Graphical Models
Our reference YGMOD913
PII: S1524-0703(15)00003-X
DOI: 10.1016/j.gmod.2015.01.001

YOUR STATUS

I am one author signing on behalf of all co-authors of the manuscript

ASSIGNMENT OF COPYRIGHT

I hereby assign to Elsevier Inc. the copyright in the manuscript identified above (where Crown Copyright is claimed, authors agree to grant an exclusive publishing and distribution license) and any tables, illustrations or other material submitted for publication as part of the manuscript (the "Article") in all forms and media (whether now known or later developed), throughout the world, in all languages, for the full term of copyright, effective when the Article is accepted for publication.

SUPPLEMENTAL MATERIALS

With respect to Supplemental Materials that I wish to make accessible through a link in the Article or through a service of Elsevier Inc. , Elsevier Inc. shall be entitled to publish, post, reformat, index, archive, make available and link to such Supplemental Materials on a non-exclusive basis in all forms and media (whether now known or hereafter developed) and to permit others to do so. "Supplemental Materials" shall mean additional materials that are not an intrinsic part of the Article, including but not limited to experimental data, e-components, encodings and software, and enhanced graphical, illustrative, video and audio material.

REVERSION OF RIGHTS

Articles may sometimes be accepted for publication but later rejected in the publication process, even in some cases after public posting in "Articles in Press" form, in which case all rights will revert to the author (see http://www.elsevier.com/locate/withdrawalpolicy).

REVISIONS AND ADDENDA

I understand that no revisions, additional terms or addenda to this Journal Publishing Agreement can be accepted without Elsevier Inc.'s express written consent. I understand that this Journal Publishing Agreement supersedes any previous agreements I have entered into with Elsevier Inc. in relation to the Article from the date hereof.

RETENTION OF RIGHTS FOR SCHOLARLY PURPOSES

I understand that I retain or am hereby granted (without the need to obtain further permission) the Retained Rights (see description below), and that no rights in patents, trademarks or other intellectual property rights are transferred to Elsevier Inc..

The Retained Rights include:

the right to use the Preprint or Accepted Author Manuscript for Personal Use, Internal Institutional Use and for Permitted Scholarly
the right to use the Published Journal Article for Personal Use ; and Internal Institutional Use.

but in each case as noted in the Definitions' clause excluding Commercial Use or Systematic Distribution (unless expressly agreed in writing by Elsevier Inc.).

AUTHOR REPRESENTATIONS / ETHICS AND DISCLOSURE

I affirm the Author Representations noted below, and confirm that I have reviewed and complied with the relevant Instructions to Authors, Ethics in Publishing policy, and Conflicts of Interest disclosure. Please note that some journals may require that all co-authors sign and submit Conflicts of Interest disclosure forms. I am also aware of the publisher's policies with respect to retractions and withdrawal (http://www.elsevier.com/locate/withdrawalpolicy).
For further information see the publishing ethics page at http://www.elsevier.com/publishingethics and the journal home page.

Author representations

The Article I have submitted to the journal for review is original, has been written by the stated authors and has not been publishe
The Article was not submitted for review to another journal while under review by this journal and will not be submitted to any oth
The Article and the Supplemental Materials contain no libellous or other unlawful statements and do not contain any materials that proprietary rights of any other person or entity.

I have obtained written permission from copyright owners for any excerpts from copyrighted works that are included and have cre
Article or the Supplemental Materials.
Except as expressly set out in this Journal Publishing Agreement, the Article is not subject to any prior rights or licenses and, if my
authors' institution has a policy that might restrict my ability to grant exclusive rights under this Journal Publishing Agreement, a w
policy has been obtained.
If I am using any personal details or images of patients, research subjects or other individuals, I have obtained all consents require
and complied with the publisher's policies relating to the use of such images or personal information. See http://www.elsevier.com
further information.
Any software contained in the Supplemental Materials is free from viruses, contaminants or worms.
If the Article or any of the Supplemental Materials were prepared jointly with other authors, I have informed the co-author(s) of th
Publishing Agreement and that I am signing on their behalf as their agent, and I am authorized to do so.

For information on the publisher's copyright and access policies, please see http://www.elsevier.com/copyright.
For more information about the definitions relating to this agreement click here.

☑ **I have read and agree to the terms of the Journal Publishing Agreement.**

18th February 2015 T-copyright-v19/2014

Personal use

Authors can use their articles, in full or in part, for a wide range of scholarly, non-commercial purposes as outlined below:

- Use by an author in the author's classroom teaching (including distribution of copies, paper or electronic)
- Distribution of copies (including through e-mail) to known research colleagues for their personal use (but not for Commercial Use)
- Inclusion in a thesis or dissertation (provided that this is not to be published commercially)
- Use in a subsequent compilation of the author's works
- Extending the Article to book-length form
- Preparation of other derivative works (but not for Commercial Use)
- Otherwise using or re-using portions or excerpts in other works

These rights apply for all Elsevier authors who publish their article as either a subscription article or an open access article. In all cases we require that all Elsevier authors always include a full acknowledgement and, if appropriate, a link to the final published version hosted on Science Direct.

Springer www.springer.com

MyPublication Home > Authors & Editors >

Affiliation Confirm | Open Choice | Copyright Transfer | Offprint / Color Order | Billing / Shipping

Welcome to MyPublication

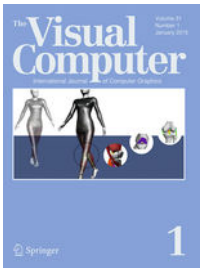

Dear Mahmudul Hasan,
Thank you for publishing your paper in one of Springer's journals.

Article Title: Interactive multilevel focus+context visualization framework
Journal: The Visual Computer
DOI: 10.1007/s00371-015-1180-1

Make Your Choice

In order to facilitate the production and publication of your article we need further information from you relating to:

- Please indicate if you would like to publish your article as open access with Springer's Open Choice option. If so, your article will become freely available online for anyone worldwide and you will be able to easily comply with open access mandates.
- Please transfer the copyright, if you do not publish your articles as open access.
- Please note: Springer has some agreements with institutions which cover the article processing charge for Open Choice articles of their affiliated corresponding authors. Please read the specific information when you indicate your affiliation.
- Please indicate if you would like to order offprints.

Answering the questions on the next few pages will take approximately 10 minutes of your time.

Please note: Be sure to complete the entire process until you get to the confirmation page. The subsequent production of your article depends on the finalization of the MyPublication process.

Please see our FAQ page if you have questions or problems completing the forms.

START NOW

SPRINGER SERVICES FOR MYPUBLICATION

Help

My Publication FAQs

11/11/2015 6:42 PM

Copyright Transfer Statement

BACK

The copyright to this article, including any graphic elements therein (e.g. illustrations, charts, moving images), is hereby assigned for good and valuable consideration to **Springer-Verlag Berlin Heidelberg** effective if and when the article is accepted for publication and to the extent assignable if assignability is restricted for by applicable law or regulations (e.g. for U.S. government or crown employees). Author warrants (i) that he/she is the sole owner or has been authorized by any additional copyright owner to assign the right, (ii) that the article does not infringe any third party rights and no license from or payments to a third party is required to publish the article, (iii) that the article has not been previously published or licensed and (iv) that in case the article contains excerpts from other copyrighted works (e.g. illustrations, tables, text quotations) Author obtained written permissions to the extent necessary from the copyright holder thereof and cited the sources of the excerpts correctly.

The copyright assignment includes without limitation the exclusive, assignable and sublicensable right, unlimited in time and territory, to reproduce, publish, distribute, transmit, make available and store the article, including abstracts thereof, in all forms and media of expression now known or developed in the future, including pre- and reprints, translations, photographic reproductions and microform. Springer may use the article in whole or in part in electronic form, such as use in databases or data networks (e.g. the Internet) for display, print or download to stationary or portable devices. This includes interactive and multimedia use as well as posting the article in full or in part or its abstract on social media accounts closely related to the Journal, and the right to alter the article to the extent necessary for such use.

Authors may self-archive the Author's accepted manuscript of their articles on their own websites. Authors may also deposit this version of the article in any repository, provided it is only made publicly available 12 months after official publication or later. He/she may not use the publisher's version (the final article), which is posted on SpringerLink and other Springer websites, for the purpose of self-archiving or deposit. Furthermore, the Author may only post his/her version provided acknowledgement is given to the original source of publication and a link is inserted to the published article on Springer's website. The link must be provided by inserting the DOI number of the article in the following sentence: "The final publication is available at Springer via http://dx.doi.org/[insert DOI]".

Prior versions of the article published on non-commercial pre-print servers like arXiv.org can remain on these servers and/or can be updated with Author's accepted version. The final published version (in pdf or html/xml format) cannot be used for this purpose. Acknowledgement needs to be given to the final publication and a link must be inserted to the published article on Springer's website, by inserting the DOI number of the article in the following sentence: "The final publication is available at Springer via http://dx.doi.org/[insert DOI]". Author retains the right to use his/her article for his/her further scientific career by including the final published journal article in other publications such as dissertations and postdoctoral qualifications provided acknowledgement is given to the original source of publication.

Articles disseminated via link.springer.com are indexed, abstracted and referenced by many abstracting and information services, bibliographic networks, subscription agencies, library

networks, and consortia.

After submission of the agreement signed by the corresponding author, changes of authorship or in the order of the authors listed will not be accepted by Springer.

I agree

☑ I have read and understood the Copyright Transfer Statement.*

CONTINUE

SPRINGER SERVICES FOR MYPUBLICATION

Help

My Publication FAQs

11/11/2015 6:53 PM

Bibliography

[Ada02] Adams M. D.: *Reversible Integer-to-Integer Wavelet Transforms for Image Coding*. PhD thesis, Department of Electrical and Computer Engineering, University of British Columbia, Vancouver, BC, Canada, Sep 2002.

[Ada03] Adams M. D.: Generalized reversible integer-to-integer transform framework. In *Proceedings of the 2003 IEEE Pacific Rim Conference on Communications Computers and Signal Processing (PACRIM 2003) (Cat. No.03CH37490)* (Aug 2003), vol. 2, pp. 569–572.

[AF98] Atsumi E., Farvardin N.: Lossy/lossless region-of-interest image coding based on set partitioning in hierarchical trees. In *Proceedings of the 1998 International Conference on Image Processing. ICIP98 (Cat. No.98CB36269)* (Oct 1998), vol. 1, pp. 87–91.

[AK00] Adams M. D., Kossentni F.: Reversible integer-to-integer wavelet transforms for image compression: Performance evaluation and analysis. *IEEE Transactions on Image Processing 9*, 6 (Jun 2000), 1010–1024.

[AW03] Adams M. D., Ward R. K.: Symmetric-extension-compatible reversible integer-to-integer wavelet transforms. *IEEE Transactions on Signal Processing 51*, 10 (Oct 2003), 2624–2636.

[BF89] Blume H., Fand A.: Reversible and irreversible image data compression using the S-transform and Lempel-Ziv coding. In *Proceedings of the SPIE, Medical Imaging III: Image Capture and Display* (May 1989), vol. 1091, pp. 2–18.

[BGS06] Bartels R. H., Golub G. H., Samavati F. F.: Some observations on local least squares. *BIT Numerical Mathematics 46*, 3 (Sep 2006), 455–477.

[BS00] Bartels R. H., Samavati F. F.: Reversing subdivision rules: local linear conditions and observations on inner products. *Journal of Computational and Applied Mathematics 119* (Jul 2000), 29–67.

[BS11] Bartels R., Samavati F.: Multiresolutions numerically from subdivisions. *Computers & Graphics 35*, 2 (2011), 185–197.

[BvdE92] Bruekers F. A. M. L., van den Enden A. W. M.: New networks for perfect inversion and perfect reconstruction. *IEEE Journal on Selected Areas in Communications 10*, 1 (Jan 1992), 129–137.

[CB04] Cohen M., Brodlie K.: Focus and context for volume visualization. In *Proceeding of the Theory and Practice of Computer Graphics Conference* (Jun 2004), IEEE, pp. 32–39.

[CDF92] Cohen A., Daubechies I., Feauveau J.-C.: Biorthogonal bases of compactly supported wavelets. *Communications on Pure and Applied Mathematics 45*, 5 (1992), 485–560.

[CDSY98] Calderbank A., Daubechies I., Sweldens W., Yeo B.-L.: Wavelet transforms that map integers to integers. *Applied and Computational Harmonic Analysis 5*, 3 (1998), 332–369.

[Cha74] Chaikin G. M.: An algorithm for high-speed curve generation. *Computer Graphics and Image Processing 3*, 4 (1974), 346–349.

[CK96] Cohen A., Kovacevic J.: Wavelets: the mathematical background. *Proceedings of the IEEE 84*, 4 (Apr 1996), 514–522.

[CMS13] Cossalter M., Mengshoel O. J., Selker T.: Multi-focus and multi-level techniques for visualization and analysis of networks with thematic data. In

Proceeding of the SPIE Conference on Visualization and Data Analysis (Feb 2013), vol. 8654, pp. 1–15. 865403.

[CN02] Card S. K., Nation D.: Degree-of-interest trees: A component of an attention-reactive user interface. In *Proceedings of the Working Conference on Advanced Visual Interfaces* (New York, USA, 2002), AVI '02, ACM, pp. 231–245.

[Dau88] Daubechies I.: Orthonormal bases of compactly supported wavelets. *Communications on Pure and Applied Mathematics 41*, 7 (1988), 909–996.

[Dau92] Daubechies I.: *Ten Lectures on Wavelets*. Society for Industrial and Applied Mathematics (SIAM), Philadelphia, PA, USA, 1992.

[DC97] Dewitte S., Cornelis J.: Lossless integer wavelet transform. *IEEE Signal Processing Letters 4*, 6 (Jun 1997), 158–160.

[Fab09] Faber G.: Über stetige Funktionen. *Mathematische Annalen 66* (1909), 81–94.

[FB88] Forsey D. R., Bartels R. H.: Hierarchical B-spline refinement. In *Proceedings of the 15th Annual Conference on Computer Graphics and Interactive Techniques* (New York, NY, USA, 1988), SIGGRAPH '88, ACM, pp. 205–212.

[GC95] Gortler S. J., Cohen M. F.: Hierarchical and variational geometric modeling with wavelets. In *Proceedings of the 1995 Symposium on Interactive 3D graphics* (Monterey, CA, Apr 9 1995), I3D '95, ACM, pp. 35–42.

[GSK*97] Gormish M. J., Schwartz E. L., Keith A. F., Boliek M. P., Zandi A.: Lossless and nearly lossless compression for high-quality images. In *Proceeding of the SPIE, Very High Resolution and Quality Imaging II* (Apr 1997), vol. 3025, pp. 62–70.

[Haa10] Haar A.: Zur Theorie der orthogonalen Funktionensysteme. *Mathematische Annalen 69* (1910), 331–371.

[Hau06] Hauser H.: Generalizing focus+context visualization. In *Scientific Visualization: The Visual Extraction of Knowledge from Data*, Bonneau G.-P., Ertl T., Nielson G., (Eds.), Mathematics and Visualization. Springer Berlin Heidelberg, 2006, pp. 305–327.

[HMC11] Hsu W.-H., Ma K.-L., Correa C.: A rendering framework for multiscale views of 3D models. In *Proceedings of the 2011 SIGGRAPH Asia Conference* (New York, NY, USA, 2011), SA '11, ACM, pp. 131:1–131:10.

[Hod03] Hodges E. R. S.: *The Guild handbook of scientific illustration.* John Wiley and Sons, Hoboken, NJ, USA, 2003.

[HSJ14] Hasan M., Samavati F. F., Jacob C.: Multilevel focus+context visualization using balanced multiresolution. In *Proceedings of the International Conference on Cyberworlds* (Oct 6-8 2014), CW, IEEE Computer Society, pp. 145–152.

[HSJ15] Hasan M., Samavati F. F., Jacob C.: Interactive multilevel focus+context visualization framework. *The Visual Computer 32*, 3 (2015), 323–334.

[HSS15] Hasan M., Samavati F. F., Sousa M. C.: Balanced multiresolution for symmetric/antisymmetric filters. *Graphical Models 78* (2015), 36–59.

[JP97] Jung H.-Y., Prost R.: Rounding transform based approach for lossless subband coding. In *Proceedings of International Conference on Image Processing* (Oct 1997), vol. 2, pp. 274–277.

[JP98a] Jung H.-Y., Prost R.: Lossless subband coding system based on rounding transform. *IEEE Transactions on Signal Processing 46*, 9 (Sep 1998), 2535–2540.

[JP98b] Jung H.-Y., Prost R.: Multi-port filtering system for lossless image compression. In *Proceedings of the 1998 International Conference on Image Processing.*

ICIP98 (Cat. No.98CB36269) (Oct 1998), vol. 3, pp. 861–865.

[KMS07] Kalkofen D., Mendez E., Schmalstieg D.: Interactive focus and context visualization for augmented reality. In *IEEE/ACM International Symposium on Mixed and Augmented Reality* (Nov 2007), ISMAR, IEEE, pp. 191–201.

[KNI94] Kiya H., Nishikawa K., Iwahashi M.: A development of symmetric extension method for subband image coding. *IEEE Transactions on Image Processing 3*, 1 (Jan 1994), 78–81.

[KZT02] Kharitonenko I., Zhang X., Twelves S.: A wavelet transform with point-symmetric extension at tile boundaries. *IEEE Transactions on Image Processing 11*, 12 (Dec 2002), 1357–1364.

[LH04] Losasso F., Hoppe H.: Geometry clipmaps: terrain rendering using nested regular grids. In *ACM SIGGRAPH 2004 Papers* (New York, NY, USA, 2004), SIGGRAPH '04, ACM, pp. 769–776.

[LHJ99] LaMar E., Hamann B., Joy K. I.: Multiresolution techniques for interactive texture-based volume visualization. In *Proceedings of the 1999 conference on Visualization* (Los Alamitos, CA, USA, 1999), VIS '99, IEEE Computer Society Press, pp. 355–361.

[LL00] Li S., Li W.: Shape-adaptive discrete wavelet transforms for arbitrarily shaped visual object coding. *IEEE Transactions on Circuits and Systems for Video Technology 10*, 5 (Aug 2000), 725–743.

[LS08] Lin J., Smith M. J. T.: New perspectives and improvements on the symmetric extension filter bank for subband/wavelet image compression. *IEEE Transactions on Image Processing 17*, 2 (Feb 2008), 177–189.

[LYK07] Lee S., Yoo C. D., Kalker T.: Reversible image watermarking based on integer-to-integer wavelet transform. *IEEE Transactions on Information Forensics and Security 2*, 3 (Sept 2007), 321–330.

[MAT14] MATLAB and Wavelet Toolbox Release 2014a. The MathWorks, Inc., Natick, MA, USA, 2014.

[Mey90] Meyer Y.: *Ondelettes et Opérateurs*. Hermann, 1990.

[MKS06] Mendez E., Kalkofen D., Schmalstieg D.: Interactive context-driven visualization tools for augmented reality. In *IEEE/ACM International Symposium on Mixed and Augmented Reality* (Oct 2006), ISMAR, IEEE, pp. 209–218.

[NC98] Nister D., Christopoulos C.: Lossless region of interest with a naturally progressive still image coding algorithm. In *Proceedings of the 1998 International Conference on Image Processing. ICIP98 (Cat. No.98CB36269)* (Oct 1998), vol. 3, pp. 856–860.

[OSB07] Olsen L., Samavati F., Bartels R.: Multiresolution for curves and surfaces based on constraining wavelets. *Computers & Graphics 31*, 3 (2007), 449–462.

[Pac13] Packer J. F.: *Focus+Context via Snaking Paths*. Master's thesis, Department of Computer Science, University of Calgary, Calgary, Alberta, Canada, Jun 2013.

[PHF07] Plate J., Holtkaemper T., Froehlich B.: A flexible multi-volume shader framework for arbitrarily intersecting multi-resolution datasets. *IEEE Transactions on Visualization and Computer Graphics 13*, 6 (Nov-Dec 2007), 1584–1591.

[PHS17] Packer J. F., Hasan M., Samavati F. F.: Illustrative multilevel focus+context visualization along snaking paths. *The Visual Computer 33*, 10

(Oct 2017), 1291–1306.

[PTCF02] Plate J., Tirtasana M., Carmona R., Fröhlich B.: Octreemizer: a hierarchical approach for interactive roaming through very large volumes. In *Proceedings of the symposium on Data Visualisation 2002* (Aire-la-Ville, Switzerland, 2002), VISSYM '02, Eurographics Association, pp. 53–60.

[RJ91] Rabbani M., Jones P. W.: *Digital Image Compression Techniques*, 1st ed. SPIE Optical Engineering Press, Bellingham, WA, USA, 1991.

[RVB*09] Ropinski T., Viola I., Biermann M., Hauser H., Hinrichs K.: Multimodal visualization with interactive closeups. In *Proceeding of the Theory and Practice of Computer Graphics Conference* (2009), Eurographics Association, pp. 17–24.

[Sad11] Sadeghi J.: Reversing Faber subdivision. Personal communication, 2011.

[SB99] Samavati F. F., Bartels R. H.: Multiresolution curve and surface representation: reversing subdivision rules by least-squares data fitting. *Computer Graphics Forum 18*, 2 (1999), 97–119.

[SB04] Samavati F. F., Bartels R. H.: Local filters of B-spline wavelets. In *Proceedings of the 2004 Intlernational Workshop on Biometric Technologies* (2004), BT '04, pp. 105–110.

[SBO07] Samavati F. F., Bartels R. H., Olsen L.: Local B-spline multiresolution with examples in iris synthesis and volumetric rendering. In *Image Pattern Recognition: Synthesis and Analysis in Biometrics*, Yanushkevich S. N., Gavrilova M. L., Wan P. S. P., Srihari S. N., (Eds.), vol. 67 of *Series in Machine Perception and Artificial Intelligence*. World Scientific Publishing, 2007, pp. 65–102.

[SDS96] Stollnitz E. J., Derose T. D., Salesin D. H.: *Wavelets for computer graphics: theory and applications*. Morgan Kaufmann Publishers Inc., San Francisco, CA, USA, 1996.

[SGM*11] Suter S., Guitian J. I., Marton F., Agus M., Elsener A., Zollikofer C., Gopi M., Gobbetti E., Pajarola R.: Interactive multiscale tensor reconstruction for multiresolution volume visualization. *IEEE Transactions on Visualization and Computer Graphics 17*, 12 (Dec 2011), 2135–2143.

[She17] Sherlock M. J.: *Visualizations on a Web-Based View-Aware Digital Earth*. Master's thesis, Department of Computer Science, University of Calgary, Calgary, Alberta, Canada, Jul 2017.

[SHS16] Sherlock M. J., Hasan M., Samavati F. F.: *A practical test for univariate and multivariate normality*. Tech. Rep. 2016-1091-10, Department of Computer Science, University of Calgary, Calgary, Alberta, Canada, Oct 2016.

[SP96] Said A., Pearlman W. A.: An image multiresolution representation for lossless and lossy compression. *IEEE Transactions on Image Processing 5*, 9 (Sep 1996), 1303–1310.

[SS09] Sadeghi J., Samavati F. F.: Smooth reverse subdivision. *Computers & Graphics 33*, 3 (2009), 217–225. IEEE International Conference on Shape Modelling and Applications 2009.

[SS11] Sadeghi J., Samavati F. F.: Smooth reverse Loop and Catmull-Clark subdivision. *Graphical Models 73*, 5 (2011), 202–217.

[Swe95] Sweldens W.: Lifting scheme: A new philosophy in biorthogonal wavelet constructions. In *Proceedings of the SPIE, Wavelet Applications in Signal and Image Processing III* (San Diego, CA, USA, Sep 1995), vol. 2569, pp. 68–79.

[Swe96] Sweldens W.: The lifting scheme: A custom-design construction of biorthogonal wavelets. *Applied and Computational Harmonic Analysis 3*, 2 (1996), 186–200.

[Swe98] Sweldens W.: The lifting scheme: A construction of second generation wavelets. *SIAM Journal on Mathematical Analysis 29*, 2 (1998), 511–546.

[TS08] Tu Y., Shen H.-W.: Balloon focus: A seamless multi-focus+context method for treemaps. *IEEE Transactions on Visualization and Computer Graphics 14*, 6 (2008), 1157–1164.

[TSS*06] Taerum T., Sousa M. C., Samavati F. F., Chan S., Mitchell J. R.: Real-time super resolution contextual close-up of clinical volumetric data. In *Proceedings of the Joint Eurographics - IEEE VGTC Symposium on Visualization (EuroVis06)* (May 8-10 2006), Eurographics Association, pp. 347–354.

[Wen87] Wendler T.: Verfahren für die hierarchische Codierung von Einzelbildern in medizinischen Bildinformationssystemen. Dr. Ing. thesis, Rheinisch-Westfälische Technische Hochschule Aachen, Germany, 1987.

[WS05] Wang C., Shen H.-W.: Hierarchical navigation interface: leveraging multiple coordinated views for level-of-detail multiresolution volume rendering of large scientific data sets. In *Proceedings of the Ninth International Conference on Information Visualisation* (Jul 2005), pp. 259–267.

[WSJ*12] Wong P. C., Shen H.-W., Johnson C., Chen C., Ross R. B.: The top 10 challenges in extreme-scale visual analytics. *IEEE Computer Graphics and Applications 32*, 4 (Jul 2012), 63–67.

[WWLM11] Wang Y.-S., Wang C., Lee T.-Y., Ma K.-L.: Feature-preserving volume data reduction and focus+context visualization. *IEEE Transactions on*

Visualization and Computer Graphics 17, 2 (Feb 2011), 171–181.

[XYZ*05] Xuan G., Yang C., Zhen Y., Shi Y. Q., Ni Z.: Reversible data hiding using integer wavelet transform and companding technique. In *Digital Watermarking* (Berlin, Heidelberg, 2005), Cox I. J., Kalker T., Lee H.-K., (Eds.), Springer Berlin Heidelberg, pp. 115–124.

[ZASB95] Zandi A., Allen J. D., Schwartz E. L., Boliek M.: Crew: Compression with reversible embedded wavelets. In *Data Compression Conference, 1995. DCC '95. Proceedings* (Mar 1995), pp. 212–221.

[ZSS97] Zorin D., Schröder P., Sweldens W.: Interactive multiresolution mesh editing. In *Proceedings of the 24th Annual Conference on Computer Graphics and Interactive Techniques* (New York, NY, USA, 1997), SIGGRAPH '97, ACM Press/Addison-Wesley Publishing Co., pp. 259–268.